The cellular basis of rhythmic activity patterns occurring in the CA1 region of the hippocampus

Ph.D. Dissertation

Rita Zemankovics

Semmelweis University

János Szentágothai School of Ph.D. Studies

Supervisor: Norbert Hájos Ph.D.
Institute of Experimental Medicine
Hungarian Academy of Sciences
Laboratory of Network Neurophysiology

Official Reviewers of the Ph.D. Dissertation:
Gábor Czéh Ph.D., D.Sc.
Gábor Gerber Ph.D.

Members of the Final Examination Board:
József Kiss Ph.D., D.Sc.- Chairman
József Takács Ph.D.
István Tarnawa Ph.D.

Budapest
2011

1. TABLE OF CONTENTS

2. LIST OF ABBREVIATIONS

ACh: acetylcholine

ACSF: artificial cerebrospinal fluid

AHP: afterhyperpolarization

AMPA: α-amino-3-hydroxy-5-methylisoxazole-4-propionic acid

AP: action potential

BIC: Bayesian information criterion

CA1-CA3: Cornu Ammonis fields

CA1 PC: CA1 pyramidal cell

CA1 IN: CA1 interneuron

CA3 PC: CA3 pyramidal cell

CA3 IN: CA3 interneuron

cAMP: cyclic adenosine monophosphate

CB1: cannabinoid receptor type 1

CCh: carbachol

CCK: cholecystokinin

cGMP: cyclic guanosine monophosphate

CNBD: cyclic-nucleotide binding domain

DG*:* dentate gyrus

EEG: electroencephalogram

EC: entorhinal cortex

eGFP: enhanced green fluorescent protein

EPSC: excitatory postsynaptic current

EPSP: excitatory postsynaptic potential

FFT: Fast Fourier Transform

FS PTI: fast spiking perisomatic region-targeting interneuron

GABA: γ-aminobutyric acid

HCN channel: hyperpolarization-activated cyclic nucleotide-gated channel

I_h: h-current; a current mediated by HCN channels

IN: interneuron

IPSC: inhibitory postsynaptic current

IPSP: inhibitory postsynaptic potential

ISI: interneuron-selective interneuron

KAR: kainate receptor

KCC2: K^+- Cl^- cotransporter

KW: Kruskal-Wallis test

M1-M5: muscarinic acetylcholine receptor subtypes

mAChR: muscarinic acetylcholine receptor

mGluR: metabotropic glutamate receptor

MP: membrane potential

MS-DBB: medial septum-diagonal band of Broca

nAChR: nicotinic ACh receptor

NMDA: N-methyl-D-aspartate

OA IN: oriens-alveus interneuron

OLM: oriens-lacunosum-moleculare cell

O-R: oriens-radiatum cell

PB: phosphate buffer

PC: pyramidal cell

PIP2: phosphatidylinositol 4,5-bisphosphate

PSC: postsynaptic current

PSD: power spectral density

PV: parvalbumin

PV+ IN : PV-eGFP positive interneuron

RAD IN: radiatum interneuron

REM: rapid eye movement sleep

Rp: Rayleigh probability

SCA : Schaffer collateral-associated interneuron

SOM: somatostatin

SPW: sharp wave

TTX: tetrodotoxin

ZD7288: 4-ethylphenylamino-1,2-dimethyl-6-methylaminopyrimidinium chloride

3. INTRODUCTION

The hippocampal formation is known to be involved in many higher order cognitive functions, such as encoding and retrieval of memory (Murray and Mishkin, 1984; Paulsen and Moser, 1998) or spatial navigation (O'Keefe and Recce, 1993). It is also well known that hippocampal circuitry exhibit a wide variety of population patterns, including oscillations at theta (4-7 Hz) or gamma (30-100 Hz) frequencies, or sharp-wave-ripple oscillations (100-200 Hz) under different behavioral states (Vanderwolf, 1969; Vanderwolf et al., 1977; Leung, 1980; Buzsáki et al., 1992; Chrobak and Buzsáki, 1994). Several lines of studies show that the occurrence of these special behavior-dependent activity patterns strongly correlates with different cognitive functions. There are many theories related to these observations that suggest that the complex dynamics presumably reflects specific information processing states of the networks. However, the exact role of these complex activity patterns in different operations of the brain remains elusive.

One way to get closer to understand the involvement of rhythmic oscillations occurring at different frequencies in certain brain functions is to reveal the underlying cellular mechanisms. Unfolding the contribution each component of the network makes to network oscillations will produce mechanistic as well as functional insights into their generation and role. In this thesis I would like to address the question what mechanisms tune the network to operate at certain frequencies in the hippocampus. To answer this we have to investigate the intrinsic properties of the individual elements of the network as well as the complex properties of the circuitry that makes the system being capable of generating or following rhythmic activity.

One theme in this thesis will be the intrinsic membrane properties of the different types of hippocampal CA1 neurons that can endow them with the capability of operating at certain preferred frequencies. I will review a study in which we showed that different cell classes in the CA1 region of the hippocampus have distinct types and degrees of frequency preference, and that these differences are partly due to variations in the quantity and biophysical properties of the voltage-gated ion channels, which mediate the so-called h-current.

The second theme of the thesis regards to the network properties of the hippocampal CA1 that can be important in defining the occurrence of rhythmic population patterns in this region. Here, I present a study that focuses on network oscillations occurring in the gamma frequency range in the hippocampus, and shows that under particular circumstances gamma oscillation in the CA1 region is driven by the activity of the CA3 region via a feed-forward inhibitory pathway.

3.1. Review of the literature

3.1.1. Anatomy of the hippocampus

In order to investigate network activity, a detailed knowledge not only of the components of the network, but also of how individual components are connected is required. The hippocampus in amongst the most intensively studied regions of the mammalian brain and thanks to the works of many outstanding researchers, its anatomy is known in great detail.

Although there are substantial differences in the architecture and in patterns of connectivity of the hippocampal formation between different species, the basic layout of cells and fiber pathway is phylogenetically conserved and much the same even in humans and rodents. Since the experimental work described in this thesis was carried out in rodents, the following description of the hippocampus is limited to the structure of the rodent hippocampus.

3.1.1.1. The cytoarchitecture of the hippocampus

3.1.1.1.1. Principal cells

The hippocampal formation includes the *dentate gyrus* (DG), the *Cornu Ammonis* fields (CA1-CA3), the *subiculum*, the *parasubiculum* and the *entorhinal cortex* (EC). In the narrow sense the hippocampus is defined as comprising the DG and the areas CA3-CA1.

Hippocampal neurons can be divided into two major categories based on their main neurotransmitters. Eighty five % of the cells are glutamatergic. These cells are called principal cells, since they form the major output pathways from hippocampal subregions. The remaining 15 % of the neurons are mainly GABAergic cells (i.e. releasing γ-aminobutyric acid as a main neurotransmitter). These cells are usually defined as interneurons, since they thought to be mainly local-circuit neurons, though certain classes of them establish commissural axon collaterals or even extrahippocampal projections.

The laminar structure of the hippocampus is basically defined in each subregion by the morphology of the principal cells and the main termination zones of their glutamatergic inputs arriving via distinct pathways.

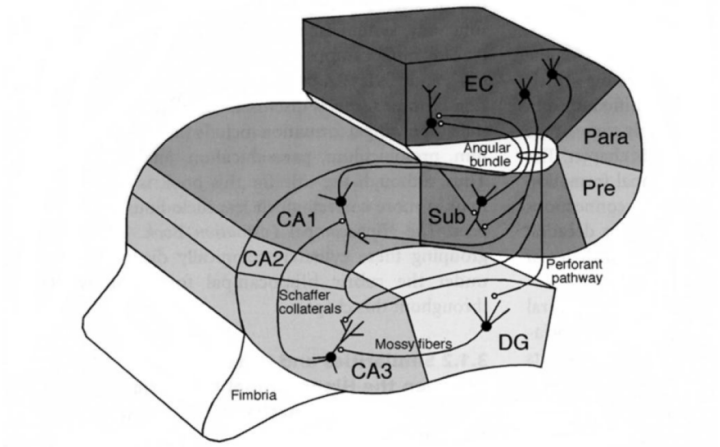

Figure 1. The information flow through the hippocampus. The hippocampus has bidirectional connections with the EC. Cells in the layer II of the EC project to the DG and the CA3 region of the hippocampus via the perforant path. Neurons in layer III of the EC project to the CA1 region of the hippocampus via the temporoammonic pathway. The axons of the granule cells in the DG form the mossy fibers and innervate the CA3 cells. Besides their dense local recurrent collaterals, CA3 pyramidal cells innervate the CA1 neurons via the Schaffer collaterals. CA3 neurons also innervate the contralateral hippocampus via the commissural afferents. Neurons in the CA1 field of the hippocampus and the subiculum project back to the layer V-VI of the EC. (Adapted from Andersen et al., 2007.)

The principal cells of the DG are the *granule cells* that are localized in one layer called the *granule cell layer*. Besides the granule cell layer, the DG has two other layers: the *molecular layer* and the *hilus*. The molecular layer is a largely acelullar layer

located above the granule cell layer, and consists the dendrites of the granule cells. The hilus is located below the granule cell layer and comprises different polymorphic cells. The axons of the granule cells innervate some of the neurons of the hilus, such as *mossy cells*, then exit the hilus and enter the stratum lucidum of CA3 as a bunch of fibers. These fibers are also called the *mossy fibers,* because of their special synaptic terminals formed on the CA3 neurons (Hamlyn, 1962) (Fig. 1).

The other excitatory (glutamatergic) cell type of the DG is the mossy cell (Amaral, 1978). Mossy cells project only to the molecular layer of the DG both ipsilaterally and contralaterally. These neurons tend not to project locally, but rather distant septotemporal levels of the DG.

The principal cells of the Cornu Ammonis field are the *pyramidal cells*. They are located also in one layer called *stratum pyramidale*. Unlike granule cells, pyramidal cells have dendritic trees extending perpendicularly to the cell layer in both directions. Based on the size of the pyramidal cells and their synaptic innervations, the Cornu Ammonis field is usually divided into three subfields; *CA1*, *CA2* and *CA3* (Lorente de Nó, 1934) (Fig. 1).

The CA3 region can be found near the DG and can be further subdivided into CA3c, b and a (from the hilus towards the CA1, respectively). CA3 contains pyramidal cells with relatively large somata. The apical dendrites of CA3 pyramidal cells traverse three strata: the *stratum lucidum*, the *stratum radiatum* and the *stratum lacunosum moleculare*. The basal dendrites extend into *stratum oriens* towards the *alveus*.

The stratum lucidum is unique to CA3 region. It contains the so-called *thorny excrescences* of the CA3 pyramidal cells, which are complex branched spines engulfed by a single large bouton of mossy fibers (Hamlyn, 1962). The other two regions of the Cornu Ammonis field receive no mossy fiber input, therefore they lack the stratum lucidum; otherwise they have the same laminar structure.

Besides giving rise to the *Schaffer collaterals* that project to the CA1 region, the axons of CA3 pyramidal cells also form a massive recurrent collateral system within the CA3 and give rise to commissural projections to the contralateral hippocampus.

The CA2 subfield is a very narrow zone of cells inserted between CA3 and CA1. CA2 pyramidal cells have large cell bodies like CA3 pyramidal cells, but receive no inputs from the DG, like CA1 cells. Like CA3 pyramidal cells, CA2 pyramidal cells

also have a recurrent collateral system as well as projections toward the CA1 and to the contralateral hippocampus.

The cell bodies of pyramidal cells in CA1 are smaller than in the other two Cornu Ammonis regions. CA1 pyramidal cells give rise to projections both to the subiculum and to the deep layers of the EC, without any prominent local collateral system (Fig. 1).

3.1.1.1.2. Interneurons

Compared to the relatively homogenous population of pyramidal neurons, interneurons of the hippocampus have been found to be much more diverse. For instance, just in the CA1 region at least 21 different types of GABAergic neuron have been described so far (Klausberger and Somogyi, 2008; Fig. 2). The morphological categorization of the interneurons is based on their dendritic and axonal arborization. The location of the dendritic tree can reveal the potential sources of inputs to these cells, while the location of the axonal arborization can disclose the possible postsynaptic targets of the interneurons. Therefore, this type of classification can be very useful, if we want to understand the function of the interneurons within the network.

The propensity for interneurons to express so-called neurochemical markers, such as different neuropeptides or Ca^{2+}-binding proteins allow us to refine their classification and can also help us in identifying them more precisely.

Depending on their axonal arborization, three main types of inhibitory cells can be distinguished: *perisomatic region targeting interneurons*; *dendritic region targeting interneurons*, and the so-called *interneuron-selective inhibitory neurons*.

Perisomatic region targeting interneurons innervate the perisomatic region of the pyramidal cells. These interneurons are in a good position to control the action potential generation of pyramidal cells. They are mainly located within or near the stratum pyramidale. Their dendrites project into stratum radiatum and stratum oriens and thus may receive excitatory inputs from Schaffer collaterals, commissural associational fibers and feedback synapses from local pyramidal neurons. There are also mutual inhibitory connections and dense gap junctional coupling among these interneurons (Freund and Buzsáki, 1996). Perisomatic region targeting interneurons can be further classified into *basket cells* and *axo-axonic cells*.

Each basket cell can make multiple contacts onto pyramidal neurons with its terminals forming a "basket" around pyramidal cell somata. The group of basket cells can be further subdivided based on their neurochemical markers. The cells expressing the neuropeptide cholecystokinin (CCK) have regular firing pattern and express various types of neuromodulatory receptors (Pawelzik et al., 2002; Freund and Katona, 2007). These cells require extensive integration of excitatory inputs to reach firing threshold (Glickfeld and Scanziani, 2006). In contrast, basket cells expressing the Ca^{2+} binding protein parvalbumin (PV) show fast spiking phenotype and have only few receptors for neuromodulatory molecules. These fast spiking PV-expressing basket cells can be quickly and easily recruited by excitation and provide an effective inhibition on pyramidal cells (Freund, 2003; Glickfeld and Scanziani, 2006; Freund and Katona, 2007). Based on these characteristic differences between the two basket cell-types, the PV- and CCK-containing basket cells have been suggested to play different roles in network oscillations. PV-expressing basket cells could operate as clockworks for oscillations, while CCK-expressing basket cells could function as a fine tuning device that modulate synchronous ensemble activities as a function of subcortical inputs, which carry information about emotions, motivation and the autonomic state of the animal (Freund, 2003; Freund and Katona, 2007).

Axo-axonic cells, as implied by the name, target the axon initial segment of the principal cells (Somogyi et al., 1985). These cells also express PV and tend to have fast spiking firing characteristics. An interesting feature of axo-axonic cells is that their postsynaptic effect can be, at least in some cases, excitatory, possibly due to low K^+- Cl^- cotransporter (KCC2) expression in the axon initial segment (Szabadics et al., 2006; but see Glickfeld et al., 2009).

Numerous types of interneurons target the dendrites of principal cells. Because their axonal arborization usually overlaps with the termination zone of the distinct excitatory pathways, they could control the efficacy of the different excitatory inputs in a very specific way.

Oriens-lacunosum-moleculare cells (OLM cells) are interneurons with somata and dendrites located in the stratum oriens and an axonal arbor in the stratum lacunosum moleculare (McBain et al., 1994; Sík et al., 1995; Maccaferri and McBain, 1996). They target the apical tufts of the pyramidal cell dendrites, thus their axonal

termination zone overlaps mostly with the EC inputs to pyramidal cells, though the presence of a few OLM axon collaterals has also been reported in the stratum oriens. (Sík et al., 1995). OLM cells express the neuropeptide somatostatin (SOM), high level of mGluR1α (Baude et al., 1993) and also some PV, though at lower levels compared to fast spiking perisomatic region targeting interneurons (Klausberger et al., 2003).

The apical dendritic tufts of the pyramidal cells are innervated also by the so-called *perforant path-associated cells*. The cell bodies of these cells are usually located at the border of the strata radiatum and lacunosum-moleculare, their dendrites can either cover all layers or remain in stratum lacunosum moleculare (Hájos and Mody, 1997; Klausberger et al., 2005).

The *Schaffer collateral-associated (SCA) cells* innervate the oblique dendrites and to a lesser extent also the basal dendrites of pyramidal cells, matching the excitatory input from CA3. The somata of this cell group is mainly located in the stratum radiatum, their dendrites can span all layers (Cope et al., 2002; Pawelzik et al., 2002). SCA cells tend to express CCK (Cope et al., 2002; Pawelzik et al., 2002).

The so-called *apical dendrite innervating cells* have very similar morphology to SCA cells, but they innervate preferentially the main apical shaft, not the oblique dendrites (Klausberger et al., 2005).

Bistratified cells usually have cell bodies within or close to the stratum pyramidale and make synaptic contacts onto oblique and basal dendrites of pyramidal cells (Buhl et al., 1994; Klausberger et al., 2004). Although there is little overlap among their target regions, bistratified cells and fast spiking perisomatic region targeting interneurons share several features. Both cell types express PV and show fast spiking phenotype (Klausberger et al., 2004). The dendritic morphology of these cells is also similar, however, in contrast to basket and axo-axonic cells, the dendrites of bistratified cells do not enter the stratum lacunosum-moleculare (Buhl et al., 1996; Halasy et al., 1996).

Some interneurons, such as *neurogliaform cells* and *ivy cells* have densely packed axon arborization and tend to evoke slow $GABA_A$ receptor and also $GABA_B$ receptor mediated responses (Price et al., 2005; Price et al., 2008). Neurogliaform cells are located mainly in the stratum lacunosum moleculare and target the apical tufts (Price et al., 2005; Price et al., 2008), while ivy cells are placed in the stratum pyramidale or

radiatum and innervate the oblique and basal dendrites of pyramidal cells (Fuentealba et al., 2008).

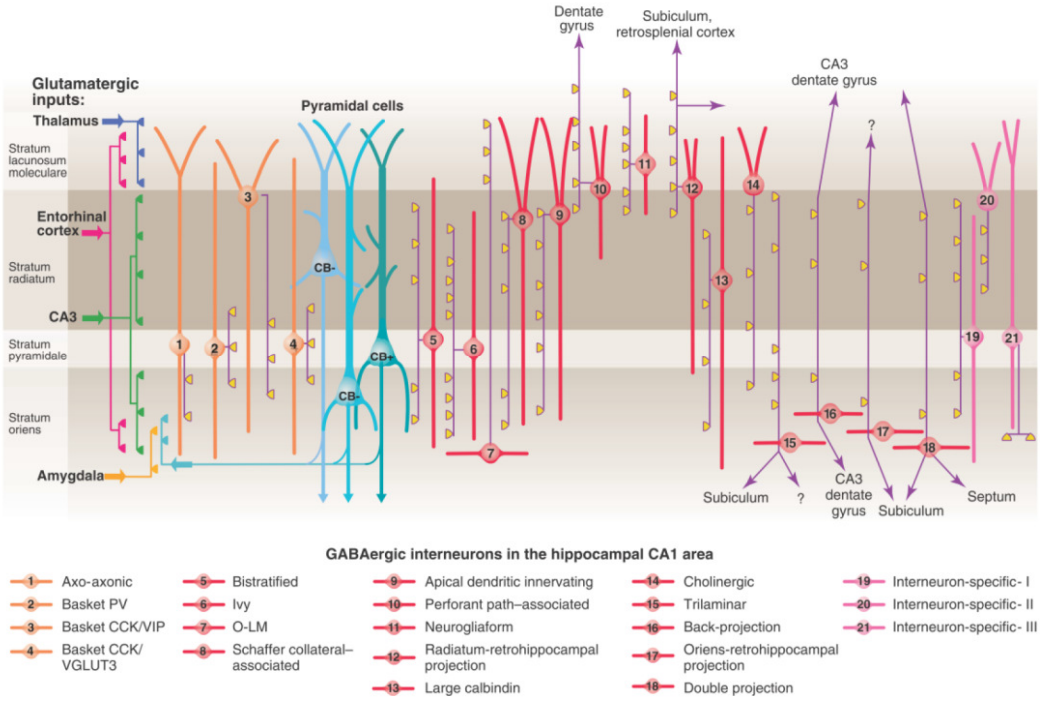

Figure 2. The diversity of cell types of the hippocampal CA1. According to the review of Klausberger and Somogyi (2008) there are at least 21 classes of interneuron in the hippocampal CA1 area. In this review the authors also distinguished at least 3 different types of CA1 pyramidal cells based on their somatic localization and their immuno-positivity for the Ca^{2+}-binding protein, calbindin. In the figure the main termination of the five glutamatergic inputs of CA1 are indicated on the left. The somata and dendrites of interneurons innervating pyramidal cells (blue) are orange, and those innervating mainly other interneurons are pink. Axons are purple; the main synaptic terminals are yellow. Note the association of the output synapses of different interneuron types with the perisomatic region (left) and either the Schaffer collateral/commissural or the entorhinal pathway termination zones (right), respectively. VIP, vasoactive intestinal polypeptide; VGLUT, vesicular glutamate transporter; O-LM, oriens lacunosum moleculare cell. (Adapted from Klausberger and Somogyi, 2008.)

There are several types of GABAergic neurons in the hippocampus that are not local interneurons, but send long range projections to other brain areas. Many of them are located in the stratum oriens and have horizontally running dendrites. *Trilaminar cells* have axonal arborization in three layers within the hippocampus (strata radiatum, pyramidale and oriens) and project to the subiculum (Sík et al., 1995; Ferraguti et al., 2005). *Backprojecting cells* in addition to innervating different layers of the CA1 area, project backwards to CA3 or DG (Sík et al., 1994). *Oriens retrohippocampal projection cells* send axons to the subiculum and retrohippocampal areas (Jinno et al., 2007), while

the so-called *double projection neurons* project to the medial septum and often also to the subiculum (Gulyás et al., 2003; Jinno et al., 2007; Takács et al., 2008). Retrohippocampal projection neurons can also be found in the stratum radiatum (Jinno et al., 2007)

Interneurons described so far target mainly pyramidal cells, but can also target other interneurons. The so-called *interneuron-selective interneurons* (ISI) target predominantly, if not exclusively other interneurons. ISIs also have at least three different subtypes and many of them can be identified based on their calretinin content (Acsády et al., 1996a,b; Freund and Buzsáki, 1996; Gulyás et al., 1996).

3.1.1.2. Hippocampal connectivity

Most of the sensory information reaches the hippocampus through the EC via the perforant path. The entorhinal projections to the DG and CA3/CA2 originate from cells in layer II. The synaptic contacts of this projection in DG and CA2/CA3 show a laminar organization; inputs from the lateral entorhinal area terminate superficially in the molecular layer/stratum lacunosum-moleculare, while inputs from the medial entorhinal area terminate in the middle third of the molecular layer or the deep half of the stratum lacunosum moleculare. The EC also project to the CA1, but this projection originates from layer III cells and the pattern of terminal distribution is organized in a topographical fashion; the lateral entorhinal area projects to the distal portion of the CA1 (close to the subiculum), while fibers originating in the medial entorhinal area terminate in the proximal portion (close to CA2). In a recent study of Chevaleyre and Siegelbaum (2010) the authors showed that CA2 neurons are also innervated by layer III EC cells, which means that CA2 pyramidal cells receive convergent excitatory inputs from layer II and layer III EC neurons on their distal dendrites.

Within the hippocampus the progression of excitatory pathways is largely unidirectional. This special chain of excitatory synaptic connections is also known as the *trisynaptic loop*, and can be summarized as follows: Granule cells of the DG receive their major input from the layer II of the EC via the perforant pathway (1st synapse). The axons of the granule cells form the mossy fibers and innervate CA3 pyramidal cells (2nd synapse). Besides their dense local recurrent collaterals (associated connections),

CA3 pyramidal cells innervate CA1 pyramidal cells via the Schaffer collaterals (3rd synapse). CA1 pyramidal cells project to the subiculum and back to the layer V-VI of the EC (Fig. 1). The mossy fiber projections do not appear to have topographical organization (Paxinos, 2004).

The recurrent collaterals of CA3/CA2 pyramidal cells form dense associational connections in the stratum radiatum and stratum oriens of the CA3 and CA2. All portions of the CA3 and CA2 project to the CA1. The CA3 projections to the CA1 are typically called the Schaffer collaterals and organized in a three-dimensional, topographical manner. CA3 pyramidal cells located close to the DG, i.e. within the CA3c region, are more likely to contact CA1 cells near the subicular border, and project more heavily to levels of CA1 located septal to their location. In contrast, pyramidal cells near the CA3/CA2 border, i.e. within CA3a, are more likely to target CA1 cells near the CA2/CA1 border, and project more heavily to the levels of CA1 located temporally compared to their septotemporal position (Li et al., 1994; Paxinos, 2004; Ropireddy et al., 2011).

Axons of the CA3 pyramidal cells distribute fibers to the same fields also in the contralateral hippocampus (commissural connections). CA3 pyramidal cells do not project to the subiculum or EC, however, they project subcortically to the lateral septal nucleus.

Unlike CA3 and CA2, CA1 has much more limited associational and commissural connections, and gives rise to projections to the subiculum and EC. The axons of CA1 pyramidal cells travel in the stratum oriens or alveus and give rise to occasional collaterals, preferentially contacting local interneurons in CA1 (Tamamaki et al., 1987; Amaral et al., 1991). The projection to the subiculum is also organized topographically in the transverse plane. Cells located near the CA3 project to the distal third of the subiculum, while CA1 cells located near the subicular border tend to contact cells in the subiculum near the CA1 border. Both CA1 and subicular pyramidal cells give rise to projections to the EC, targeting the deep layers of the EC. Septal regions of the CA1 and subiculum project to the more lateral parts of the EC, while the more temporal regions project to the medial parts (Tamamaki and Nojyo, 1995; Witter et al., 2000; Naber et al., 2001).

Interneurons of the hippocampus can be recruited into network activities as sources of feedback or feed-forward inhibition. Those interneurons that receive their excitatory drive in parallel to the principal cells they innervate participate in feed-forward inhibition. Interneurons that are activated by the recurrent collaterals of the principal cells can contribute to feedback inhibition.

As it was already mentioned, the localization of the soma and dendritic arborization of the interneurons can determine their possible excitatory drives. For instance, perisomatic region targeting interneurons having dendrites spreading to all layers can be involved both in feedback and feed-forward circuitries (Wierenga and Wadman, 2003a,b; Pouille and Scanziani, 2001). Some perforant path associated interneurons innervating the apical tufts of the pyramidal cells have dendrites located mainly in the stratum lacunosum moleculare. Hence, these cells are likely to be excited by the EC input in a feed-forward manner (Lacaille and Schwartzkroin, 1988a,b). On the other hand, OLM cells that target the same dendritic region of pyramidal cells, but have horizontal dendrites in the stratum oriens have been shown to take part rather in feedback than in feed-forward inhibition. (Blasco-Ibanez and Freund, 1995; Sík et al., 1995). Therefore, inhibition arriving at a certain region of the pyramidal cell might be controlled by different ways depending on the network state.

The approximately 10:1 ratio of pyramidal cells to interneurons within the hippocampal circuitry (Vizi and Kiss, 1998) implies that many pyramidal cells converge onto a single interneuron, while a single interneuron contacts many pyramidal cells (Sík et al., 1995). Therefore, one single interneuron can have a widespread effect on the network (Cobb et al., 1995).

As it was mentioned above, the main neocortical input-output structure of the hippocampal formation is the EC. Besides its reciprocal connections with the EC, CA1 gives rise to projections to the perirhinal and postrhinal cortices as well as to prefrontal cortex, and also to the amygdaloid complex. These areas all project back to CA1 (Andersen et al., 2007).

The most dominant subcortical input to the hippocampus arises from the medial septum-diagonal band of Broca (MS-DBB), which has been shown to play a crucial role in the generation and modulation of certain rhythmic activity patterns of the hippocampus (Petsche et al., 1962; Lee et al., 1994). Projections from the MS-DBB

terminate most heavily in the stratum oriens and, to a lesser extent in the stratum radiatum (Nyakas et al., 1987; Gaykema et al., 1990). GABAergic fibers of the MS-DBB innervate selectively interneurons of the hippocampus (Freund and Antal, 1988), and some GABAergic cells also project back to the septum (Tóth and Freund, 1992; Tóth et al., 1993; Gulyás et al., 2003; Jinno et al., 2007). Pyramidal cells of the CA3 region give rise to projections both to the ipsi- and contralateral lateral septal nucleus (Swanson and Cowan, 1977; Swanson et al., 1980).

In addition to the septal connections, the hippocampus receives a variety of neuromodulatory signals from other subcortical areas as well, including noradrenergic inputs from the locus coeruleus (Jones and Moore, 1977), serotoninergic inputs from the medial and dorsal raphe nuclei (Freund et al., 1990; Freund, 1992), or dopaminergic inputs from the ventral tegmental area (Scatton et al., 1980). The CA2 area and the DG also receives inputs from the tuberomammillaris and supramammillaris nuclei of the hypothalamus (Panula et al., 1989; Maglóczky et al., 1994). Projections from the nucleus reuniens target mainly CA1 pyramidal cells and interneurons (Wouterlood et al., 1990).

As the cholinergic input has a particular relevance to this thesis, I will review the cholinergic neuromodulation of the hippocampus in the next section.

3.1.1.2.1. Cholinergic neuromodulation in the hippocampus

The majority of the cholinergic fibers from the MS-DBB shows numerous varicosities and do not associate with a distinct postsynaptic element (Umbriaco et al., 1995). The minority of the fibers may contact either pyramidal cells or interneurons (Frotscher and Léránth, 1985; Léránth and Frotscher, 1987). Few cholinergic interneurons can be found also locally within the hippocampus (Frotscher et al., 2000).

The direct action of cholinergic modulation on hippocampal pyramidal cells is excitatory, though biphasic responses of CA1 pyramidal cells upon transient cholinergic activation have been reported (Gulledge and Kawaguchi, 2007). The responses of pyramidal cells are mediated primarily by activation of M1/M3 muscarinic receptors (Levey et al., 1995; Dasari and Gulledge, 2011). The M1/M3 receptor activation initiates secondary messenger cascades that will lead to reduction of various types of potassium conductances, such as K^+ conductance mediated by the so-called M-current;

Ca^{2+}-activated K^+ conductance; a delayed rectifier K^+ conductance; or the leak conductance (Krnjevic et al., 1971; Halliwell and Adams, 1982; Nakajima et al., 1986; Madison et al., 1987; Halliwell, 1990; Guerineau et al., 1994). As an end effect, acetylcholine (ACh) depolarizes PCs, increases the input resistance of the cells, and so increases their excitability. ACh has also been shown to modulate some other conductances, such as voltage-gated Ca^{2+}, or Na^+ conductances (Toselli and Lux, 1989; Cantrell et al., 1996), and it might potentiate the response to N-methyl-D-aspartate (NMDA) receptor activation (Markram and Segal, 1990).

Interneurons of the hippocampus show various responses upon cholinergic receptor activation (McQuiston and Madison, 1999a,b,c). Some interneurons in the hippocampus, such as OLM cells or CCK-expressing basket cells have been shown to be activated by application of cholinergic receptor agonists via M1/M3 receptors (Lawrence et al., 2006b; Cea-del Rio et al., 2010; Cea-del Rio et al., 2011). In contrast to M1/M3 receptor activation, activation of M2/M4 receptors induces different secondary messenger cascades, which results in hyperpolarization of the cells. M2 receptors have been shown to be expressed at the axon terminals of perisomatic region targeting interneurons (Hájos et al., 1998), where they can effectively reduce transmitter release (Fukudome et al., 2004; Szabó et al., 2010). The transmitter release can also be reduced via M4 receptors at the axon terminals of the Schaffer collaterals (Shirey et al., 2008; Dasari and Gulledge, 2011). In addition, M1/M3 receptor activation can induce synthesis of endocannabinoids in the postsynaptic cell, which in turn might reduce the transmitter release at the presynaptic terminals of CB1 cannabinoid receptor expressing cells (Fukudome et al., 2004; Neu et al., 2007). Some interneurons also express M2 receptors on their somato-dendritic compartments (Hájos et al., 1998; Ferraguti et al., 2005).

ACh can also activate ionotropic receptors, at which nicotine act as a full agonist (nAChR). The precise expression pattern of nAChR subunits in the hippocampus has not been fully established. The α7- nAChR subtype is highly expressed at multiple loci including somata, dendrites, spines and axon fibers of different cell types (Fabian-Fine et al., 2001), and can produce cell-type specific responses. Nicotinic ACh receptor activation has been shown to cause membrane depolarization in dendritic region targeting interneurons, while it appears to have no direct effect on the somata of

pyramidal cells or perisomatic region targeting interneurons (Frazier et al., 1998; McQuiston and Madison, 1999a). On the other hand, it can affect transmitter release both at glutamatergic and GABAergic axon terminals (Wonnacott et al., 2006).

3.1.2. Behavior related activity patterns of the hippocampus

Several patterns of electrical activity can be recorded from the hippocampus, and these patterns are usually correlated with certain behavioral states. In the hippocampus of the freely moving rat four prominent rhythmical EEG patterns have been identified: theta rhythm (occurring at 4-10 Hz); beta waves (between 12 and 30 Hz); gamma oscillations (in the range of 30-100 Hz); and sharp wave (SPW) associated ripple oscillations (from 100 up to 300 Hz) (Andersen et al., 2007) (Fig. 3).

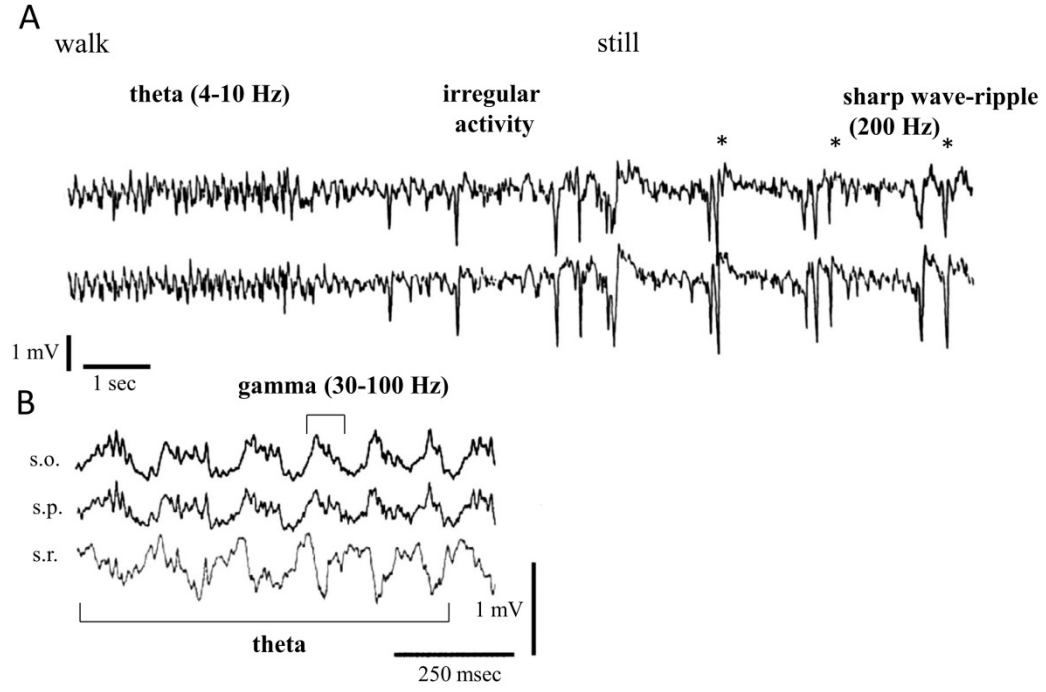

Figure 3. Behavior-dependent rhythmic activity patterns of the rodent hippocampus**. (A)** Field recordings from the stratum radiatum of the left (upper trace) and the right (lower trace) CA1 region of the hippocampus of a rat during walk-immobility (still) transition. Note regular theta waves during walk and large monophasic SPWs during immobility. **(B)** Hippocampal field activity in the mouse recorded during wheel-running. Note that high frequency (30-100 Hz) gamma oscillation is embedded in the 4-10 Hz theta oscillation. (Adapted from Buzsáki, 1989. and Buzsáki et al., 2003)

Theta oscillation occurs primarily during translational movements that change the location of the animal's head with respect to the environment. For instance: walking,

running, exploratory head movements or struggling. Theta also occurs during rapid eye movement sleep (REM) and occasionally during immobile attention or arousal (Vanderwolf, 1969; Buzsáki et al., 1983; Andersen et al., 2007).

The full range of behavioral correlates of gamma and beta waves are less well characterized. Gamma oscillations are often embedded in theta rhythms, but can also be observed during non-theta epochs, during behaviors, such as immobility and slow wave sleep (Csicsvári et al., 2003; Senior et al., 2008). In rodents beta waves have been observed for instance during sniffing of odors associated with predators (Vanderwolf, 2001).

Sharp waves are large amplitude population events, lasting between 40-100 ms. Sharp waves are associated with high-frequency oscillations of 100-300 Hz (ripples) and can be seen during drinking, eating, grooming, drowsiness, and slow wave sleep (Buzsáki et al., 1983; Ylinen et al., 1995b).

Although the behavioral correlates of certain oscillatory patterns have been known for a long time, it is still unresolved what the exact function of oscillatory activity is in different cognitive operations. There are many theories regarding the computational roles of rhythmic activity patterns in different brain operations.

Network oscillations have been suggested to provide a clock signal against which action potential of the individual cells can be timed. This feature of oscillations has been proposed to play a crucial role in the representation of sensory signals. For instance it can synchronize the firing of many cells and therefore can determine how the different sensory inputs can be bound into a coherent cognitive percept (Gray and Singer, 1989; Sejnowski and Paulsen, 2006). The information could also be represented by the firing phase of the cells compared to the ongoing oscillation. Phase-precession of hippocampal place cells is a well-known phenomenon that could be a good example for phase-encoding of the information (O'Keefe and Recce, 1993). Place cells are hippocampal pyramidal cells that fire preferentially, when an animal is in a specific location in an environment, also referred to as the cell's place field. When the animal enters the cell’s place field, the given place cell increases its firing rate and as the animal traverses the place field, the cell fires progressively earlier relative to the theta oscillation.

An important requirement for both synchronization and phase codes to work is the reliable spike timing of the cells. Synchronized membrane potential oscillations of the cells provided either by intrinsic membrane properties or rhythmic synaptic inputs could promote the temporal precision of spike generation of the cells (Kamondi et al., 1998; Penttonen et al., 1998; Pike et al., 2000).

Another possible function of oscillations could be to regulate the flow of information in neural circuits. By changing the balance between the different excitatory and inhibitory inputs, oscillations could work as a filter capable of selecting the relevant and important inputs to the network (Salinas and Sejnowski, 2000; Sejnowski and Paulsen, 2006).

By regulating the strength and the exact timing of the input signals, oscillations could set the optimal circumstances for the induction of synaptic plasticity (Bliss and Lomo, 1973; Markram et al., 1997; Song et al., 2000), and so they can assist in the storage and retrieval of information in neural circuits.

Within the hippocampus theta and gamma oscillations have been proposed to work together to form a neural code based on the EC inputs (memory acquisition) (Jensen and Lisman, 2000; Hasselmo, 2005), while sharp waves have been suggested to play a crucial role in memory consolidation and in the transfer of information from hippocampus to neocortex (Skaggs and McNaughton, 1996; Siapas and Wilson, 1998; Nádasdy et al., 1999).

Since the mechanisms investigated in this thesis are more likely to contribute to the genesis of theta and gamma frequency oscillations, in the next sections I will review the *in vivo* data according to these two types of rhythmic activity patterns of the hippocampus. I will focus primarily on the potential rhythm-generating mechanisms involved in these oscillations.

3.1.2.1. Theta oscillations in the hippocampus

Besides hippocampus, theta oscillations can be observed also in other brain areas, such as subiculum, entorhinal, perirhinal, cingulated cortices and amygdala (Adey, 1967; Buzsáki, 2002; Leung and Borst, 1987; Pare and Collins, 2000). In addition, several subcortical structures show theta frequency activity. The MS-DBB

and the supramammillary nucleus exhibit prominent theta oscillations. These areas are reciprocally connected to each other and are thought to play a critical role in the generation of theta oscillation in cortical regions (Petsche et al., 1962; Kocsis and Vertes, 1994; Borhegyi and Freund, 1998; Borhegyi et al., 1998). Neurons of other subcortical structures, such as the dorsal raphe nucleus, the ventral tegmental nucleus of Gudden and the anterior thalamic nuclei also tend to show phase-locked firing to the hippocampal theta (Buzsáki, 2002; Kocsis et al., 2001; Kocsis and Vertes, 1992; Vertes et al., 2001).

Within the hippocampus the largest theta activity can be recorded in the stratum lacunosum moleculare of CA1, but it can be seen in areas CA3 and DG as well (Bragin et al., 1995; Buzsáki, 2002). The phase of the oscillation shifts gradually between stratum oriens and stratum lacunosum moleculare (Winson, 1974; Bragin et al., 1995). Phase is further shifted by approximately 90° in the granule cell layer (Buzsáki et al., 1983). The current-source density analysis suggests that during theta oscillation there are rhythmic sources in the pyramidal cell layer that couple with sinks in the stratum lacunosum moleculare representing a putative inhibitory source and excitation by the perforant path input. In the stratum radiatum, an additional sink can be observed presumably mediated by the Schaffer collaterals of the CA3 pyramidal cells (Kamondi et al., 1998; Buzsáki, 2002).

On the basis of pharmacological sensitivity, two components of theta oscillation can be distinguished: an atropine-sensitive and an atropine-resistant component (Kramis et al., 1975). Theta oscillations in the anesthetized animal can be abolished by muscarinic receptor blockers (atropine sensitive theta), while in the awake walking animal muscarinic receptor antagonists change only the shape and depth profile of theta oscillation, whereas the amplitude and the frequency remains stable (atropine resistant theta) (Buzsáki et al., 1986). The pharmacological characteristics of atropine resistant theta have not been precisely identified, but it appears to depend on glutamate and serotonin (Leung et al., 1994; Buzsáki, 2002) and probably involves the activation of NMDA receptors (Soltész and Deschenes, 1993). Different types of surgical lesions and inactivation experiments showed that both components of theta activity are dependent on MS-DBB input, but only the atropine resistant theta is dependent on the EC input (Petsche et al., 1962; Buzsáki et al., 1983).

The septo-hippocampal projection has both cholinergic and GABAergic component. Selective lesion of cholinergic cells only reduces, but does not abolish hippocampal theta oscillations (Lee et al., 1994). Hence, GABAergic input from the MS-DBB may be sufficient for the generation of hippocampal theta rhythms. The GABAergic septo-hippocampal connections have been shown to innervate selectively the interneurons of the hippocampus; therefore this input might control pyramidal cell firing through disinhibition (Freund and Antal, 1988; Tóth et al., 1997). Moreover, the majority of the hippocampal output to the neurons of the MS-DBB is also GABAergic (Tóth et al., 1993).

Combining these data proposes a model for hippocampal theta generation, whereby cholinergic neurons of the MS-DBB provide slow depolarization of their target pyramidal cells and basket interneurons. Meanwhile the GABAergic neurons of the MS-DBB rhythmically hyperpolarize the hippocampal interneurons, which evoke rhythmic inhibitory postsynaptic potentials (IPSPs) in pyramidal cells (sources). Rhythmic excitatory postsynaptic potentials (EPSPs) evoked by the EC input are responsible for the sink in the stratum lacunosum moleculare (Buzsáki et al., 1983; Leung, 1984; Stewart and Fox, 1990;Lee et al., 1994).

This model gives back many features of hippocampal theta oscillations, but there are still many unresolved details according to the underlying cellular mechanisms. We still do not know what determines the firing phase of hippocampal pyramidal cells. If their firing was driven by the EC input, they would be expected to fire at the peak of the theta oscillation recorded in the stratum pyramidale. However, they fire with the highest probability at the trough of the oscillation (Buzsáki and Eidelberg, 1983; Fox et al., 1986; Csicsvári et al., 1999). Although, we have to be aware of that in the behaving animal the theta phase relationship of PCs is not fixed, but changes as a function of behavior (O'Keefe and Recce, 1993, Skaggs et al., 1996).

The involvement of different types of interneurons also has to be revealed. Extracellular recordings from freely moving animals suggest that the activity of most of the hippocampal interneurons is phase locked to the ongoing theta oscillation (Klausberger et al., 2003, 2004, 2005; Czurkó et al., 2011). Klausberger and colleagues recorded the firing activity of various types of interneurons of the CA1 during theta oscillations under urethane-ketamine-xylazine anesthesia by using the so called

juxtacellular method (Pinault 1996.). This technique allows labeling and post-hoc identification of the *in vivo* extracellularly recorded cells. The authors found that different classes of interneurons tend to fire at different phases of theta oscillation. Among perisomatic region targeting interneurons PV-expressing basket cells fired mostly at the descending phase of theta, while CCK-immunopositive basket cells fired rather slightly before the peak. Axo-axonic cells also fired close to the peak, but slightly later than CCK-containing basket cells. The dendritic targeting OLM and bistratified cells were most active at the trough of the oscillation, in the same phase as pyramidal cells (Klausberger et al., 2003, 2004, 2005).

In vivo intracellular recordings showed that pyramidal cells display prominent membrane potential oscillations during theta activity of the network (Ylinen et al., 1995a; Kamondi et al., 1998) and some studies suggest that intrinsic resonance properties of these cells might have an important role in producing these membrane potential oscillations (Hu et al., 2002). Some interneurons might also be capable of resonating at theta frequencies (Ylinen et al., 1995a; Pike et al., 2000). The exact role of intrinsic membrane oscillations in the generation or maintenance of theta has to be revealed.

Computational modeling and *in vitro* data suggest that reciprocal connections between MS-DBB and the hippocampus/EC also play a critical role in the generation of hippocampal theta (Wang, 2002; Manseau et al., 2008). Moreover, the hippocampus was also suggested to function as a theta oscillator in itself (Gillies et al., 2002; Gloveli et al., 2005a; Rotstein et al., 2005; Manseau et al., 2008; Goutagny et al., 2009).

3.1.2.2. Gamma oscillations in the hippocampus

Gamma oscillations are most commonly seen during epochs of theta oscillation, but can also be observed in the absence of theta activity in both the awake and anesthetized animal (Bragin et al., 1995, Penttonen et al., 1998; Csicsvári et al., 2003).

When gamma rhythm is embedded in the theta activity, its frequency strongly correlates with the frequency of the ongoing theta oscillation (Bragin et al., 1995), and also its amplitude is modulated by the theta rhythm, with the largest amplitude gamma activity occurring around the positive peak of the theta cycle (Csicsvári et al., 2003).

Gamma oscillations in the hippocampus are thought to be generated in two largely independent ways. Gamma oscillations occurring in the DG are mainly driven by the EC input. Lesion of the EC practically abolishes this type of gamma oscillation (Bragin et al., 1995). The other gamma generator is thought to be intrinsic to the hippocampus and involves the CA3-CA1 system. A recent study by Colgin et al. suggests that these two types of gamma oscillation are likely to occur at different frequencies and at different defined phases of theta oscillation (Colgin et al., 2009).

Current source density analysis of the intrinsically generated gamma rhythm shows alternating pairs of sinks and sources in the stratum pyramidale and the stratum radiatum of both CA3 and CA1 (Csicsvári et al., 2003). The appearance of sink-source pairs in the CA3 precedes that in the CA1. These data suggest that this type of gamma oscillation is generated in CA3, and propagates somehow to CA1. A current source in the soma associated with a corresponding current sink in the dendrites, could reflect either somatic inhibition or dendritic excitation or both. Single unit recordings in the behaving animal from putative pyramidal cells and perisomatic region targeting interneurons suggest that in the CA3 region the recurrent excitation of perisomatic region targeting interneurons by CA3 pyramidal cells could give rise to synchronization of the local neuronal network (Csicsvári et al., 2003). This hypothesis was also strengthened by *in vitro* models of gamma oscillation (Hájos et al., 2004; Mann et al., 2005; Oren et al., 2006; see also later in this chapter).

The gamma oscillation generated in CA3 entrains the CA1 circuitry, but the way of propagation is still unclear. Both CA1 pyramidal cells and interneurons could be activated by the Schaffer collaterals or commissural projections of CA3 pyramidal cells, therefore the oscillation could propagate from CA3 to CA1 region via either feed-forward excitation or feed-forward inhibition. The “feed-forward excitation” would mean that CA3 pyramidal cells directly discharge CA1 pyramidal cells and then a recurrent network between CA1 pyramidal cells and local interneurons produce the local field potential oscillation in CA1, similarly to CA3. In the “feed-forward inhibition” scenario CA3 pyramidal cells excite predominantly CA1 interneurons instead of CA1 pyramidal cells, and the local field potential oscillation arise from the rhythmic activity of interneurons driven by the excitation via the Schaffer-collaterals/commissural projections of CA3 pyramidal cells (see also Fig. 4).

In the above mentioned study of Csicsvári et al. (2003) the authors found that during CA3 driven gamma oscillation CA1 interneurons fired at the same time or somewhat later than CA3 interneurons, while CA1 pyramidal cells fired earlier than CA3 pyramidal cells within a gamma cycle. The time lag between the discharge of CA1 pyramidal cells and CA1 interneurons was too long to be taken as a monosynaptic excitation, which suggests that CA1 interneurons were discharged rather by CA3 pyramidal cells than CA1 pyramidal cells. Hence, these results propose that the feed-forward inhibition model is more likely to be valid.

Nevertheless, it is difficult to create a detailed model of gamma oscillations, since we know very little about the pattern and kinetics of synaptic currents in the different cell types during these network states. Another limitation of the *in vivo* multielectrode techniques is that the identification of different cell types is rather difficult under these circumstances and therefore, the technique does not allow studying the differential contribution of distinct interneuronal subclasses to the network oscillations.

In vivo intracellular recordings under urethane anesthesia revealed gamma-frequency membrane potential oscillations and phase-coupled firing of CA1 pyramidal cells during gamma oscillations. The phase and amplitude of intracellular membrane potential oscillations were voltage dependent with a phase reversal at the Cl^- equilibrium potential (Penttonen et al., 1998), suggesting that they were produced by rhythmically generated IPSPs.

Juxtacellular recordings of various types of interneurons of the CA1 during spontaneously occurring gamma oscillations under anesthesia revealed that the firing activity of many different interneuron types is modulated by the ongoing gamma oscillation. PV expressing interneurons, and especially bistratified cells showed strong gamma-modulation and tended to fire at the ascending phase of the field potential oscillation recorded in the stratum pyramidale. CCK-containing basket cells also tended to fire phase locked, however, these cells preferred firing at the trough of the oscillation. In contrast no phase-preference of OLM cells could be detected in this study (Tukker et al., 2007).

The above mentioned techniques are undisputedly helpful in understanding the functional connectivity behind certain activity patterns of the circuitry. However, we

still do not know how the different cell types are recruited to the network; what are the cellular and synaptic mechanisms that synchronize their activity during special behavioral or cognitive states.

Although *in vitro* techniques obviously have their own limitations, they allow recording synaptic currents from identified cell types in parallel with pharmacological modification of the network. Therefore, physiologically relevant *in vitro* models of network oscillations could definitely help understanding at least some aspects of rhythm generating mechanisms of the brain.

3.1.3. Possible models of rhythm generation within a network

Theoretically there are three principal ways in which oscillatory activity could be generated in a neuronal network (Mann and Paulsen, 2005): (1) The simplest way is the so-called "extrinsic pacemaker model" in which the network activity is driven by a rhythmic external input (Green and Arduini, 1954; Stewart and Fox, 1990). (2) The second model is the intrinsic model, where individual elements of the network have the capability of firing at certain frequencies, and the rhythmic firing of a subset of the neuronal population could entrain the network intrinsically (McCormick and Pape, 1990). The synchronized firing of rhythm-generating cells might be promoted by electrical coupling (Draguhn et al., 1998). (3) The "synaptic loop model" actually includes three scenarios. In the "synaptic feedback model" the oscillation emerges from synaptic recurrent feedback loops between excitatory and inhibitory cells (Freeman, 1968). Synaptic synchronization is, however, possible also through "mutual inhibitory" as well as "mutual excitatory loops" (Whittington et al., 1995; Wilson and Bower, 1992). Yet, during mutual inhibition the network probably requires a tonic excitatory drive, while during mutual excitation an inhibitory coupling is needed to prevent runaway excitation.

Network oscillations occurring at the same frequencies might be generated by multifarious ways, and certainly the above mentioned models are not mutually exclusive. These scenarios might occur at the same time and can reinforce each other's effect.

In order to understand the cellular and synaptic mechanisms that may underlie rhythmic activity patterns of a network, we have to investigate both the intrinsic properties of the single elements of the network and the possible synaptic synchronization mechanisms that are encoded in the connectivity of the network.

3.1.4. *In vitro* methods to study rhythm-generating mechanisms of the brain

3.1.4.1. Investigating the resonance properties of single cells

Intrinsic membrane potential oscillations in single neurons can serve as a basis for oscillatory behavior of the network (Lampl and Yarom, 1997). The ability of neurons to generate intrinsic membrane potential oscillations strongly correlates with their resonance properties (Lampl and Yarom, 1997). The easiest way to reveal the resonance properties of the neuronal membrane is to record the so-called *impedance magnitude profile* of the cell. To measure the impedance properties of the cells, we have to inject sinusoidal current inputs to the cell at different frequencies and record its voltage responses. The impedance values at each frequency (Z) can be calculated by dividing the Fast Fourier Transform (FFT) of the voltage response of the cell by that of the input current. The impedance magnitude profile is obtained by plotting the impedance values against the frequency of the input current (see Methods and Fig. 5A).

In modeling studies the neuronal membrane is represented by electrical equivalent circuits. The simplest circuitry that can be used to describe the behavior of a membrane is composed of a resistor and a capacitor (RC circuit). In response to sinusoidal current injections a simple passive neuronal membrane would behave as an RC circuit: the higher the input frequency is, the lower voltage response of the cell can be detected. Thus, the "passive cell" acts as a low-pass filter. However, if a voltage-gated conductance is activated in the cellular membrane (which can be modeled by introducing an inductive element to the original RC circuit, i.e. creating an RLC circuit), the cell starts to behave as a band-pass filter. Depending on the properties of the voltage-gated conductance, the cell will produce larger amplitude responses to inputs at defined frequencies. This phenomenon is called resonance and will appear as a "hump" in the impedance magnitude profile of the neuron (Fig. 5A).

Besides the magnitude profile, impedance can also be characterized by the so-called *impedance phase profile*. The impedance phase profile illustrates the temporal relationship between the injected current and the steady-state voltage response of the cell. In the case of an RC circuit (and a passive cell membrane) the phase of the impedance is always negative at any frequencies, which means that there is a lag in the voltage response with respect to the current injected. However, the presence of an inductive element in the circuit (an active conductance in the cell membrane) causes a positive shift in the impedance phase profile. Depending on the interaction of the passive membrane properties and the active conductance the impedance phase can be positive at certain frequencies even in real neurons, which means that the voltage response of the cell could lead the current input (Fig. 5B). Therefore, the operation of voltage-gated ion channels in the cell membrane may change both the amplitude and the timing of the neuronal response in a frequency-dependent manner.

In the hippocampus, pyramidal cells are known to express subthreshold resonance at frequencies within the theta range (4-7 Hz) (Leung and Yu, 1998; Pike et al., 2000; Hu et al., 2002; Narayanan and Johnston, 2007), which might contribute to their membrane potential oscillations *in vivo* (Ylinen et al., 1995a; Kamondi et al., 1998) as well as to their discharge properties (Pike et al., 2000). Recent studies have revealed that subthreshold resonance in pyramidal cells is predominantly mediated by the hyperpolarization-activated cyclic nucleotide-gated channels (HCN channels), which generate a non-selective cation current – termed I_h (Hu et al., 2002). Besides I_h the so-called M-current, a muscarinic receptor controlled K^+ current was also shown to create resonance in pyramidal cells at membrane potentials closer to the firing threshold. (Hu et al 2002).

Some hippocampal interneurons also have been shown to have frequency tuning properties (Gloveli et al., 2005b; Lawrence et al., 2006a) and can also resonate at certain frequencies (Pike et al., 2000). However, it is still unclear which GABAergic cell types show resonance at which frequencies, and what cellular mechanisms are involved.

3.1.4.1.1. I_h (h-current)

The hyperpolarization-activated cation current (I_h, but also know as I_f or I_Q) was initially discovered in the sinoatrial node of the heart over 30 years ago (Noma and

Irisawa, 1976). So far I_h has also been described in many types of neurons and gained enormous attention in the recent years, because of its potential contribution to rhythmic activity patterns of the brain (Pape, 1996; Lüthi and McCormick, 1998). In addition to having a key role in producing resonance in distinct types of neurons (Hu et al., 2002; Heys et al., 2010) and its vital function in pacemaker activities as well as in network oscillations (Lüthi and McCormick, 1998; Kocsis and Li, 2004), this conductance has been suggested to contribute to synaptic waveform normalization (Magee, 1999) and even to learning processes (Nolan et al., 2003).

HCN channels mediating I_h can be activated by hyperpolarizing the cell to membrane potentials negative to -50 mV. I_h is a mixed monovalent cation current. HCN channels are permeable for both K^+ and Na^+ ions. The ratio of K^+ to Na^+ permeability ranges from 3:1 to 5:1, which will result in a reversal potential of the current between -25 and -40 mV. Therefore, activation of the channel at typical resting potentials results in a net inward current largely carried by Na^+ ions (Robinson and Siegelbaum, 2003). In current clamp experiments, in the voltage response of the HCN-channel expressing cells to negative current steps of appropriate magnitude, a depolarizing *sag* can be seen due to the activation of I_h (Fig. 6, 7). Following the end of the current pulse, there is a rebound depolarization caused by the extra inward Na^+ flux through HCN channels that were activated by hyperpolarization. In some cells this rebound depolarization can even trigger an action potential.

The activation kinetics of I_h are complex. The onset of I_h is usually preceded by a significant delay. After this delay, channel opening can be described by either a single or double exponential function, depending on the cell type. The time course of activation varies widely among the different cell types in the range of few ten milliseconds to several seconds (Robinson and Siegelbaum, 2003).

Another interesting feature of HCN channels is that they can be directly modulated by cyclic nucleotides. The C-terminal fragment of each subunit contains a so-called cyclic-nucleotide binding domain (CNBD), which can bind cyclic nucleotides. CNBD has the highest affinity to bind cAMP (Wainger et al., 2001; Wang et al., 2001), but cGMP has also been reported as an effective modulator of HCN channel activity (Pape and Mager, 1992). Binding of cyclic nucleotides usually shift the activation curve of the channel to a more depolarized range.

So far, four HCN pore-forming α-subunits were identified (HCN1-4). Each channel is composed of four of these subunits. The subunits can form either homo- or heterotetramers, which have been described in both heterologous expression systems and real neurons (Lewis et al., 2010; Santoro et al., 2000). There are differences in the kinetic properties, in the voltage-dependence, as well as in the affinity to bind cyclic nucleotides between the distinct isoforms. For instance, HCN1 shows the more positive threshold for activation, the fastest activation kinetics, and the lowest sensitivity to cAMP, while HCN4 channels have very slow time constants and high sensitivity to cAMP. HCN2 and HCN3 have intermediate properties (Santoro et al., 2000; Franz et al., 2000; Ishii et al., 2001; Wahl-Schott and Biel, 2009). The expression pattern of the different subunits is cell type dependent, and correlates well with the properties of I_h found in the given cell types (Santoro et al., 2000). Thus, the functional heterogeneity of I_h found in the different cell types is likely to result, at least in part, from the molecular heterogeneity of isoform expression and subunit composition.

All four HCN isoforms are expressed in the mammalian brain (Santoro et al., 2000, Moosmang et al., 1999). Within the hippocampus HCN1 can be found both in CA1 and CA3 pyramidal cells, with somewhat higher levels of expression in CA1 neurons compared with that in CA3 neurons. HCN2, in contrast, is expressed at somewhat higher levels in CA3 than in CA1 pyramidal cells (Bender et al., 2001; Notomi and Shigemoto, 2004; Brewster et al., 2002, 2007). It was also revealed that in CA1 pyramidal cells HCN1 tends to have a graded distribution with showing 60-fold increase from somatic to distal apical dendritic membranes (Lőrincz et al., 2002). HCN1 and HCN2 are also expressed in neurons with cell bodies located in the stratum oriens and stratum lucidum (Bender et al., 2001; Notomi and Shigemoto, 2004; Brewster et al., 2007). Such cells most likely represent inhibitory interneurons, which have been shown to contain I_h (Maccaferri and McBain, 1996, Santoro et al., 2000). Expression of HCN1 in the DG is quite low. HCN4 is also expressed in the hippocampus, though at much lower levels than HCN1 or HCN2. HCN4 shows a similar distribution as HCN2 (Robinson and Siegelbaum, 2003; Notomi and Shigemoto, 2004; Brewster et al., 2007). Some HCN channels are probably also expressed on presynaptic terminals and regulate transmitter release (Aponte et al., 2006).

Besides the actual cAMP level, the activity of I_h may also be regulated by protein phosphorilation or dephosphorilation (Yu et al., 1993), binding of special auxiliary subunits to the HCN tetramers (Wahl-Schott and Biel, 2009), or allosteric modulators, such as phosphatidylinositol 4,5-bisphosphate (PIP2) (Zolles et al., 2006; Pian et al., 2007). Therefore, the activity of I_h can be finely and precisely tuned in each cell individually.

3.1.4.2. Introducing *in vitro* network oscillation models

Although synchronized network activities apparently require intact connectivity within the circuitry, under certain circumstances rhythmic population activity can be induced also in brain slices. Due to the approximately lamellar organization of the Cornu Ammonis field, hippocampal slices can be cut in a manner, in which much of the intrahippocampal connectivity is maintained, and thus, certain network properties can be studied in the absence of external inputs.

Oscillatory activity can be induced in hippocampal slices by cholinergic receptor activation (Fisahn et al., 1998; Buhl et al., 1998), ionotropic and metabotropic glutamate receptor activation (Buhl et al., 1998; Gloveli et al., 2005a,b, Gillies et al., 2002; Pálhalmi et al., 2004), increased level of potassium (LeBeau et al., 2002; Towers et al., 2002) or tetanic stimulation (Whittington et al., 1997).

Many of the *in vitro* models were originally developed in interface-type recording chambers, where the slice preparations are positioned in the interface of the liquid and the gaseous phase, and the oxygenation of the slice is provided directly from the moisturized gas mixture at the gas-fluid interface. In this set-up the diffusion of O_2 and CO_2 between the tissue and the gaseous phase is very efficient. Unfortunately, visually guided whole cell patch clamp recordings are available only in the submerged-type recording chamber, where the preparations are fully submerged in the superfusing solution. Though the superfusing solution is oxygenated, in many cases this set-up does not provide sufficient oxygenation for high energy consuming population events, such as network oscillations. Therefore, to be able to reproduce the oscillation models under submerged conditions some technical modifications might be required; e.g.

modification of the recording chamber or the perfusion system (see Results and also Hájos et al., 2004, 2009).

In vitro models have been used to gain insight into the cellular and synaptic mechanisms of synchronized population activities of the hippocampus occurring at different frequencies, including theta (Fellous and Sejnowski, 2000; Gillies et al., 2002; Gloveli et al., 2005a), gamma (Whittington et al., 1995; Fisahn et al., 1998; Gloveli et al., 2005a;b) and sharp wave associated ripple oscillations (Behrens et al., 2005; Ellender et al., 2010). Since in the study presented in this thesis we investigated the network activities underlying gamma frequency oscillations by using an *in vitro* model, in the next section I will review the *in vitro* models of gamma oscillations.

3.1.4.2.1. *In vitro* gamma oscillation models

Two forms of gamma oscillations can be induced in hippocampal slices: transient and persistent gamma oscillations. Transient gamma last for few seconds and can be initiated by puffing glutamate (Pöschel et al., 2002), high molarities of kainate (Gloveli et al., 2005a,b) or potassium (LeBeau et al., 2002; Towers et al., 2002) on the slices or by tetanic stimulation in the CA1 region (Whittington et al., 1997). Persistent gamma oscillations may last for hours and can be induced by bath application of agonists of muscarinic acetylcholine receptors (mAChR) (Fisahn et al., 1998; Fellous and Sejnowski, 2000), kainate receptors (KAR) (Fisahn et al., 2004, Gloveli et al., 2005a) and metabotropic glutamate receptors (mGluR) (Pálhalmi et al., 2004).

Gamma oscillations evoked by different drug-applications can differ in their peak frequencies, maximal power or spectral width (Pálhalmi et al., 2004) and also in their dependence on excitation and inhibition (Whittington et al., 1995; Fisahn et al., 1998; Fisahn et al., 2004; Pálhalmi et al., 2004; Boddeke et al., 1997). The various properties of gamma oscillations induced by different methods suggest that different cellular and network mechanisms can be involved in the generation of rhythmic activities occurring at gamma frequencies in hippocampal slices. For instance, oscillations occurring in response to mGluR activation have been suggested to depend primarily on mutual inhibition between interneurons in CA1 (Whittington et al., 1995), but gamma frequency rhythmic network activities have been shown to be generated also by a reciprocal pyramidal-interneuronal cell interaction in CA3 (Oren et al., 2006)

One of the most widely used *in vitro* models for studying gamma oscillations in the hippocampus is the carbachol (CCh) induced persistent oscillation model (Hájos et al., 2004; Mann et al., 2005; Oren et al., 2006). The validity of this model is also supported by the fact that the hippocampus receives a dense cholinergic projection from the MS-DBB that appears to play an important role in the generation of rhythmic hippocampal activities (Petsche et al., 1962). Moreover, CCh-induced gamma oscillations in hippocampal slices share many features of the hippocampal gamma rhythms occurring *in vivo* (Hájos and Paulsen, 2009). In the CA3 region the phase of the oscillation reverses in both cases in the stratum lucidum (Csicsvári et al., 2003; Mann et al., 2005) and current-source-density analysis reveals current sink-source pairs in the stratum pyramidale and the apical dendritic region of the pyramidal cells in both situations (Csicsvári et al., 2003; Mann et al., 2005). The firing properties of the different cell types of the CA3 region are also comparable. Pyramidal cells tend to fire at low frequencies (< 5 Hz) close to the trough of the oscillation, while interneurons usually fire at higher frequencies at the ascending phase of the oscillation (Csicsvári et al., 2003; Hájos et al., 2004). Finally, under both conditions the gamma oscillations are generated in the CA3 region, and then propagate to the CA1 (Bragin et al., 1995; Fisahn et al., 1998; Csicsvári et al., 2003).

These similarities suggest that the same mechanisms could underlie *in vitro* cholinergically induced gamma frequency oscillations and hippocampal gamma oscillations occurring *in vivo*. Therefore, the CCh-induced *in vitro* model can be an appropriate tool to study the precise cellular mechanisms of hippocampal gamma oscillations of the behaving animal.

The mechanisms of the generation of gamma oscillation in the CA3 region have been studied thoroughly by using the CCh-induced *in vitro* model. Gamma oscillations have been shown to be produced by a monosynaptic feedback loop between CA3 pyramidal cells and perisomatic region targeting interneurons (Hájos et al., 2004; Mann et al., 2005; Oren et al., 2006). Very little is known, however, about the properties of gamma oscillations in the CA1 region.

4. AIMS OF THESIS

The main goal of this thesis was to reveal cellular mechanisms that may underlie rhythmic activity patterns in the CA1 region of the hippocampus. To this end, two objectives were identified.

The first objective was to identify intrinsic properties of the single neurons of the network that might contribute to rhythmic activity patterns occurring at population levels. We wanted to determine the subthreshold resonance properties of different types of hippocampal neurons and the underlying mechanisms. We investigated the impedance profiles of distinct types of anatomically identified neurons in the CA1 region of rat hippocampal slices. We focused on the dissimilarities in the voltage response of the cells to sinusoidal current inputs and wanted to determine the role of I_h in producing these differences. We also tried to give a quantitative account for the observed differences by using a computational model.

The second objective was to reveal the synaptic mechanisms within the network that may underlie oscillatory activity in the CA1 region, particularly in the gamma frequency range. We were primarily interested in the mechanisms of propagation of intrinsically generated gamma oscillation from the CA3 to the CA1 area of the hippocampus. We presumed two possible mechanisms (Fig. 4):

- The feed-forward excitation model: whereby CA3 pyramidal cells directly discharge CA1 pyramidal cells and then a recurrent network between CA1 pyramidal cells and local interneurons produce the local field potential oscillation in CA1, similarly to CA3.
- The feed-forward inhibition model: whereby CA3 pyramidal cells excite primarily CA1 interneurons instead of CA1 pyramidal cells, and the local field potential oscillation arise from the rhythmic activity of interneurons driven by the rhythmic excitation via the Schaffer-collaterals of CA3 pyramidal cells.

To be able to decide which model is valid, we aimed to reveal what determines the behavior of the different cell types during gamma oscillation in CA1. To this end, we investigated the relationship between firing activity and synaptic inputs of different

hippocampal cell types during cholinergically induced fast network oscillations in hippocampal slices.

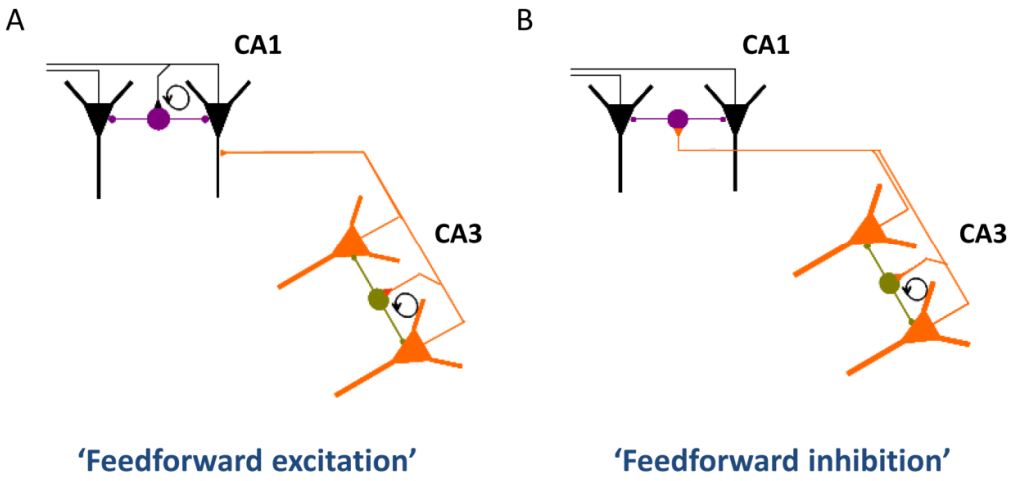

Figure 4. Possible mechanisms of propagation of gamma oscillations from the CA3 to the CA1 area of the hippocampus. We hypothesized two possible mechanisms for the propagation of the gamma frequency oscillation from the CA3 to the CA1 region: **(A)** The feed-forward excitation model, whereby CA3 pyramidal cells directly discharge CA1 pyramidal cells and then a recurrent network between CA1 pyramidal cells and local interneurons produce the local field potential oscillation in CA1, similarly to CA3. **(B)** The feed-forward inhibition model, whereby CA3 pyramidal cells excite the CA1 interneurons instead of the CA1 pyramidal cells, and the local field potential oscillation arise from the rhythmic activity of interneurons driven by the excitation via the Schaffer collaterals of the CA3 pyramidal cells. Orange triangles: CA3 pyramidal cell; black triangles: CA1 pyramidal cell; dark yellow circles: CA3 interneuron; purple circles: CA1 interneuron.

5. METHODS

5.1. Ethical approval

Animals were kept and used according to the regulations of the European Community's Council Directive of 24 November 1986 (86/609/EEC), and experimental procedures were reviewed and approved by the Animal Welfare Committee of the Institute of Experimental Medicine, Hungarian Academy of Sciences, Budapest. (Permission number: 2301/003.)

5.2. Tissue preparations

For studying the intrinsic membrane properties of hippocampal CA1 neurons male Wistar rats (postnatal day 14-26) were used. The pups were decapitated under deep isoflurane anesthesia. The brain was removed into ice cold cutting solution, which had been bubbled with 95% O_2-5% CO_2 (carbogen gas) for at least 30 minutes before use. Both hemispheres were glued to a vibratome plate for cutting using cyanoacrylate adhesive. Horizontal slices of 400 μm thickness were cut using a vibratome (Leica VT1000S). The slices were transferred to a Petri dish containing room temperature artificial cerebrospinal fluid (ACSF) and trimmed of most extrahippocampal areas before being transferred to a storage chamber.

For studying the propagation of CCh-induced gamma oscillation from the CA3 region to CA1, CD1 mice of both sexes (postnatal day 15-23) were used. To measure selectively from cells expressing the Ca^{2+} binding protein parvalbumin (PV) transgenic mice expressing enhanced green fluorescent protein (eGFP) controlled by PV promoter (Meyer et al., 2002) were also used in this study (postnatal day 15-21). The methods of acute slice preparation were the same as described in rats, except that the thickness of the slices were 450 μm here and exceptional care was taken to remove the entorhinal cortical parts from the slices.

5.3. Tissue storage

After acute slice preparation the slices were placed into an interface-type holding chamber for recovery. This chamber contained standard ACSF at 35ºC that gradually cooled down to room temperature. After incubation for a minimum of one hour, slices were transferred individually to a submerged-style recording chamber. In study I a commercially available recording chamber was used. During recordings slices were kept submerged in a chamber perfused with ACSF at a flow rate of 3-4 ml/min. These recordings were made at 34-37 ^{o}C.

In the case of experiments studying *in vitro* oscillations (study II) a modified custom made recording chamber was used with dual superfusion system for providing better metabolic supply for the slices (for details see also Results, Fig13.). In this design, the slices were placed on a mesh and two separate fluid inlets allowed ACSF to flow both above and below the slices with a rate of 3-3.5 ml/min for each channel at 30-32 ^{o}C.

In both types of recording chambers, slices were held in position by a nylon grid stretched across a U-shaped platinum harp.

5.4. Solutions

The cutting solution contained (in mM): 252 sucrose, 2.5 KCl, 26 $NaHCO_3$, 0.5 $CaCl_2$, 5 $MgCl_2$, 1.25 NaH_2PO_4, 10 glucose, saturated with 95% O_2-5% CO_2). The ACSF had the following composition (in mM): 126 NaCl, 2.5 KCl, 26 $NaHCO_3$, 2 $CaCl_2$, 2 $MgCl_2$, 1.25 NaH_2PO_4, 10 glucose, saturated with 95% O_2-5% CO_2.

The intrapipette solution used in study I contained (in mM): 125 K-gluconate, 6 KCl, 4 NaCl, 10 HEPES, 10 disodium creatine phosphate, 4 Mg-ATP, 0.3 Tris-GTP (pH: 7.38; 284-290 $mOsm \cdot l^{-1}$). For the voltage-clamp experiments in study II another intrapipette solution was used with different composition (containing in mM: 138 K-gluconate , 3 CsCl, 10 disodium creatine phosphate, 4 Mg-ATP, 0.4 Tris-GTP, 10 HEPES, 0.2 QX 314; pH: 7.38; 285 $mOsm \cdot l^{-1}$). All intrapipette solutions were stored in frozen aliquots. For later morphological identification of the recorded cells 5 mg/ml biocytin was added to the pipette solution freshly before use in both studies.

In voltage-clamp experiments of study I 50-100 μM picrotoxin and 2-3 mM kynurenic acid (Sigma-Aldrich, St Louis, MO) were added to abolish synaptic events, and 0.5 μM tetrodotoxin (TTX) (Alomone Labs, Jerusalem, Israel) was added to block voltage-gated Na^+ channels. Blocking the h-current was accomplished by adding 10 μM ZD7288 (4-ethylphenylamino-1,2-dimethyl-6-methylaminopyrimidinium chloride, Tocris Bioscience Ltd, Bristol, UK) to the bath solution. To induce persistent oscillations in study II, the cholinergic receptor agonist CCh (10 μM) was added to the bath. Drugs used in experiments were stored in concentrated stock solutions in the freezer (-20 °C) or fridge (4 °C) and were added to the ACSF during the course of the experiments.

5.5. Electrode preparation

Standard patch electrodes were used in all recording configurations (i.e. whole-cell patch-clamp, loose patch and field potential recordings). These electrodes were pulled from thin-wall borosilicate glass capillaries with an inner filament (outer diameter: 1.5 mm; inner diameter: 1.12 mm) using a vertical DMZ-Universal Puller (Zeitz Instruments, München, Germany). Pipette resistances were 3-6 MΩ when filled either with the intrapipette solution or with ACSF.

5.6. Electrophysiological recordings and data analysis in study I

5.6.1. Data acquisition

Whole-cell patch-clamp experiments were performed under visual guidance using a Versascope (E Marton Electronics, Canoga Park, CA) or an infrared differential interference contrast microscope (Olympus BX61WI). Recordings were made from pyramidal cells and interneurons in the stratum oriens of the CA1 region using an Axopatch 200B or a Multiclamp 700B amplifier (Molecular Devices, Foster City, CA). Data were digitized using a PCI-MIO-16-4E board (National Instruments, Austin, TX). Traces were filtered at 2 kHz and digitised at 8 kHz in the current-clamp experiments and 6 kHz in the voltage-clamp experiments.

Data for current-clamp experiments were acquired and analyzed with Igor Pro 4.0 software. For voltage-clamp experiments data acquisition was done using the EVAN program (courtesy of Prof. I. Mody; UCLA, CA) or the Stimulog software (courtesy of Prof. Z. Nusser; Institute of Experimental Medicine, Hungarian Academy of Sciences, Budapest, Hungary), and analyzed with Origin 7.0 software (OriginLab Corp. Northamton, MA).

In voltage-clamp experiments, series resistance was compensated and was between 5 and 15 MΩ. Only cells with stable series resistance (± 20%) were included in the study. In current-clamp experiments resting membrane potential was measured in bridge mode (I=0) immediately after obtaining whole-cell access. Only cells with stable resting membrane potential and overshooting action potentials with stable amplitude were included in the study. Reported values for membrane potential were not corrected for the liquid junction potential.

From perisomatic region-targeting interneurons only those cells were included in this study which could be identified unequivocally as fast-spiking interneurons based on their action potential phenotype. These cells were characterized by a fast-decaying afterhyperpolarization (AHP) measured at 25 % of the AHP amplitude (less than 3.2 ms) and by the small width of action potentials determined at half peak amplitude of the first and the last action potentials of the train (less than 0.5 ms; for 800 ms, 0.2 nA pulses) (Han, 1994; Pawelzik et al., 2002; Lien and Jonas, 2003).

5.6.2. Characterization of the passive membrane properties of the cells

The basic physiological characteristics of the cells were determined from the voltage responses to a series of hyperpolarizing and depolarizing square current pulses of 800 ms duration and amplitudes between -200 and 200 pA, at 20 pA intervals from a holding potential of -60 mV. To estimate the membrane time constant and the total membrane capacitance at -60 mV, single exponential functions with a common decay time constant were fitted simultaneously to the voltage responses to the five smallest amplitude hyperpolarizing current steps (-20 - -100 pA) between 5 and 37.5 ms after the onset of the pulse. The median value of the membrane capacitance estimated from these fits was used. In order to estimate the input resistance of the cell, double exponential

functions were fitted to the voltage traces during the current step, and the minimum and steady-state voltage values were determined (this procedure also allowed us to characterize the voltage sag; see below). Estimated steady-state voltage responses were then plotted against current amplitude for the five smallest amplitude hyperpolarizing current steps (-20 to -100 pA), and the input resistance at -60 mV was estimated from the slope of the linear regression through these points (Fig. 7A).

5.6.3. Characterization of the "sag" potential

In many cells, a voltage sag was observed in response to a hyperpolarizing current pulse. We characterized this voltage sag by fitting the difference of two exponential functions to the membrane potential during the pulse (see above). The sag responses were described quite accurately by this class of function; our choice of functional description was further motivated by the fact that the response of a simple model of I_h-containing neurons (the linearized I_h-model, described below) can be calculated analytically, and also predicts a sag shaped as a difference of exponential functions. Fitting a continuous function to the data allowed us to robustly estimate the relative sag amplitude, defined as the ratio of two differences in membrane potential: the difference between the minimum voltage during the sag and the steady-state voltage later in the pulse, and the difference between the steady-state voltage and the membrane potential measured immediately after the beginning of the step (see Fig. 7B). We also determined the peak delay, defined as the time of the negative peak of the membrane potential relative to the beginning of the current pulse. Both the relative sag amplitude and the peak delay were calculated for the five largest amplitudes of the negative current steps (-120 - -200 pA), and their median values were used to characterize the sag in each cell.

5.6.4. Characterization of neuronal impedance profiles and resonance properties

To determine the impedance profile and subthreshold resonance properties of each cell, 3-second-long sinusoidal currents were injected into the cells with a peak-to-peak amplitude of 120 pA at fixed frequencies (0.5, 1, 2, 3, 4, 5, 6, 7, 8, 9, 10, 15, 20, 40

Hz). Since the neuronal impedance is in general voltage-dependent, measurements were repeated at different subthreshold membrane potentials (-60, -70, -80, and in some cases at -90 mV). These baseline potentials were manually adjusted by direct current (DC) injection through the recording electrode. The complex impedance value (Z) at a given frequency (f) was determined by calculating the Fast Fourier Transform (FFT) of the voltage response and dividing the FFT component corresponding to the input frequency by the analogous FFT component of the input current (Fig 5A).

The magnitude of the impedance was plotted against input frequency to give the impedance magnitude profile (Fig 5A). In order to facilitate the comparison of multiple impedance magnitude profiles, we characterized the impedance magnitude curves by four summary statistics (Fig. 5C). First, we measured the impedance value at the lowest input frequency (0.5 Hz), $Z_{(0.5Hz)}$. Cutoff frequency (f_{cutoff}) was defined as the input frequency at which the magnitude of the impedance first dipped below $\frac{1}{\sqrt{2}} \cdot Z_{(0.5Hz)}$ (this definition returns the classic cutoff frequency $\frac{1}{2\Pi RC}$ for a passive linear cell, where $R \approx Z_{(0.5Hz)}$). Since many of our cells displayed a clear peak in the impedance magnitude profile at some nonzero frequency, we also defined the resonance magnitude (Q) as the impedance magnitude at the resonance peak (maximal impedance value) divided by the impedance magnitude at the lowest input frequency (0.5 Hz), i.e. $Q = Z_{max} / Z_{(0.5\ Hz)}$ (Hutcheon et al., 1996a). Finally, the frequency of maximal impedance (f_{max}) was determined as the frequency at which the maximum impedance magnitude value was detected. In those cells that showed no peak in their impedance profile (Q = 1), f_{max} is equal to 0.5 Hz.

The phase of the impedance (which equals the difference between the phases of the voltage and current oscillations) was also determined and plotted as a function of frequency to define the phase profile of the neuron (Fig 5B). Since positive values of this quantity (i.e., the response leading the input) indicate a membrane with nonlinear properties with potential computational significance (see Results and Discussion), following Narayanan and Johnston (2008) we defined Φ_L as the area under the positive part of the phase profile (Fig. 5C). This is a robust measure of the resonance properties of the membrane. Finally, we combined the magnitude and phase of the impedance to obtain the complex-valued impedance of the neuron. A plot of the complex impedance

for all frequencies (i.e., a plot of the imaginary part of the impedance against the real part as frequency varies, known as a Nyquist plot) is a useful indicator of the basic properties of a system, and is widely used in engineering applications.

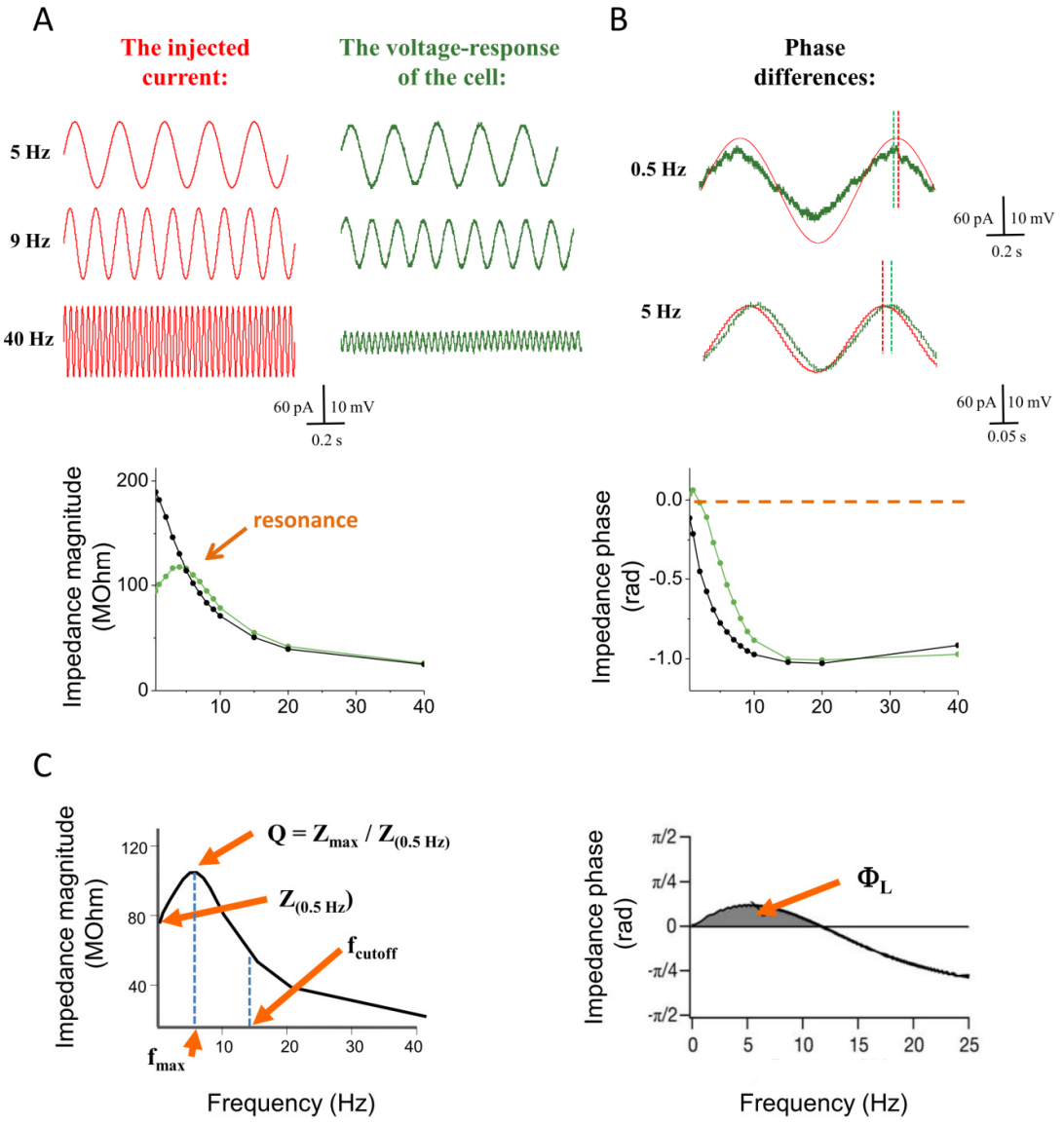

Figure 5. Methods to define the impedance properties of the cells. **(A)** To reveal the impedance properties of the neurons 3 s long sinusoidal currents were injected into the cells with different frequencies (between 0.5 and 40 Hz) at different membrane potentials (-60, -70 and -80 mV; upper panel, red traces) and the voltage responses of the cells were recorded (upper panel, green traces). Note that the magnitude of the voltage response changes with the frequency. The impedance values were calculated by dividing the FFT of the voltage response of the cell by that of the input current. The impedance magnitude profile was obtained by plotting the impedance values against the input frequency (lower panel). When "resonating-currents" are present in the cell, a hump can be observed in the impedance magnitude profile of the cell (lower panel, green trace), while there is no hump in the case of a "passive membrane" (lower panel, black trace). **(B)** Not only the magnitude but also the phase of the response changes with the input frequency both in the case of "active" and "passive membranes" (lower panel, green and black traces

respectively). However, while in the case of a "passive membrane" the voltage response of the cell always follows the input current in time; active conductances can enable the voltage response to precede the input current, which is reflected in the impedance phase profile as a positive value. The impedance phase profile is generated by plotting the phase differences between the input current and the voltage trace against the input frequency (lower panel). The upper panel shows the phase differences between the input current (red trace) and the voltage response of the cell (green trace) at 0.5 Hz and 5 Hz in a resonating cell. Dotted lines indicate the peak of the sinusoidal traces. Note that at 0.5 Hz the voltage leads the current, while at 5 Hz this order reverses, and the voltage follows the current. (All panels in A and B are from recordings from the same cell. "Active traces" were recorded under control conditions, while "passive traces" are from recordings taken in the presence of the h-current blocker, ZD7288 (10 μM.)) **(C)** Impedance curves were characterized by five different parameters. The impedance magnitude profile was described by: impedance at 0.5 Hz ($Z_{(0.5\ Hz)}$), cutoff frequency (f_{cutoff}), resonance magnitude (Q) and the frequency of maximal impedance (f_{max}) (left panel). Impedance phase profile was characterized by the total inductive phase (Φ_L), which is defined as the area under the positive part of the phase profile (right panel). (The right panel of part C was adapted from Narayanan and Johnston, 2008.)

5.6.5. Characterization of I_h in different cell types

In order to determine the properties of I_h, 800-ms-long voltage-clamp steps were given in -10 mV increments up to -120 mV from a holding potential of -40 mV. Since I_h has quite slow activation kinetics, rather long voltage steps are needed to activate the current fully at a given membrane potential. However, most of the interneurons proved to be sensitive to prolonged hyperpolarizing pulses, and therefore we adjusted our protocol to have the shortest possible voltage step that still enabled us to measure the current. Nevertheless, it has to be noted that the shortness of the steps, in combination with the voltage-dependent kinetics of I_h, may cause some negative shift (up to a few mV) of the estimated activation curves.

I_h was obtained by subtracting the current traces before and after the application of 10 μM ZD7288, a specific blocker of HCN channels (Harris and Constanti, 1995). This current difference trace during the voltage step was used to determine the time constant(s) of I_h activation as well as the steady-state current, while the tail current recorded immediately after the end of the step was used to estimate the steady-state activation function. To determine the time constant(s) of I_h activation, either a single- or a double-exponential model was fitted to the difference current recorded from 20 ms after the beginning of the voltage step to the end of the step. The steady-state current was determined concurrently for all step potentials by fitting exponential functions with a common time constant to the current traces during the late phase (last 500 ms) of the

voltage step. The I_h activation curve was calculated by fitting single exponential functions to the tail current between 2 and 20 ms after the end of the voltage step (the first 2 ms were excluded to ignore fast transients), and extrapolating back to the end of the step to determine the instantaneous tail current. We then plotted the tail current as a function of the step potential, and fitted a sigmoidal function,

$$I(V) = \frac{I_{\max}}{1+\exp\left(-\left(V - V_{1/2}\right)/m\right)}, \qquad (1)$$

where $I_{\max}$ is the asymptotic maximum of the sigmoid, $V_{1/2}$ is the potential of half-maximal I_h activation, and $\frac{1}{4m}$ is the slope of the activation function at $V_{1/2}$. The measured tail current values at each voltage were then divided by $I_{\max}$ to arrive at the activation function for each cell.

The I_h reversal potential for each cell type was calculated for a subset of our cells from the open-channel I-V relationship, which was obtained by the following protocol: I_h was activated with an 800-ms-long pulse to -120 mV and this was followed by steps to different test potentials (from -110 to -40 mV in +10 mV increments). The instantaneous I-V plot was constructed from the tail current amplitudes measured at each test potential in the same way as described above, and a straight line was fitted through the data points. The reversal potential of I_h was defined as the voltage at which the fitted line crossed the V-axis.

Once the I_h reversal potential was known, the maximal conductance of I_h in each cell could be determined from the steady-state I-V relationship. Assuming a sigmoidal form for the activation function, the steady-state current can be written as

$$I_{ss} = \bar{g}_h \frac{1}{1+\exp\left(-\left(V - V_{1/2}\right)/m\right)}\left(V - E_h\right) \qquad (2)$$

where $\bar{g}_h$ is the maximal I_h conductance, and E_h is the I_h reversal potential. Three parameters of this function ($\bar{g}_h$, $V_{1/2}$ and m) were optimized to fit the measured I-V relationship, resulting in an estimate of the maximal conductance value for each cell.

5.6.6. Statistical analyses

Since, in many cases, data were not normally distributed (according to a Lilliefors test), nonparametric statistical tests were used whenever possible. We employed Wilcoxon's signed rank test to compare medians from two groups. When comparing more than two groups, a Kruskal-Wallis test was used, often followed by post hoc comparisons based on average ranks using Tukey-Kramer critical values to account for multiple comparisons. However, in a few cases for which no appropriate nonparametric test has been established (such as in a three-way design, or a two-way design combining between- and within-subject factors), conventional parametric tests (such as ANOVA) were used. Summary statistics are also displayed in a form appropriate for non-Gaussian distributions; including box plots, which indicate the median of the data as well as its interquartile range, with whiskers showing the full range of the data, and extreme outliers (data points outside 2.5 times the interquartile range) marked by crosses outside the whiskers. The notch around the median value indicates a robust estimate of the confidence of the median, such that non-overlapping notches for two groups mean that the two medians are significantly different at the 5% level.

Comparisons of the goodness of fit between models with a different number of free parameters were performed using the Bayesian information criterion (BIC) (Bishop, 2006). The BIC attempts to compensate for the fact that better fits are more easily achieved with more complex models by penalizing models according to the number of free parameters. For each model we calculate the quantity

$$BIC = n\ln\left(\frac{RSS}{n}\right) + k\ln(n) \qquad (3)$$

where RSS is the residual sum of squares for the model, n is the number of data points, and k is the number of free parameters. Then, out of two or more models of the same data set, the best model is the one for which the quantity defined by Equation (3) is the smallest.

5.7. Computational model used in study I

The computational modeling part of study I was performed by Dr. Szabolcs Káli (Laboratory of Cerebral Cortex Research, Institute of Experimental Medicine, Budapest). The aim of the model was to capture quantitatively the experimentally measured impedance profiles of single hippocampal neurons. Single-compartment models of varying complexity were constructed and their parameters were optimized. The simplest model, which will be referred to as the passive model, contained only the membrane capacitance (C) and a (voltage-independent) leak conductance (g_l). In this model the impedance of the neuron (Z) can be expressed by the following formula:

$$Z = \frac{1}{g_l + i\omega C} \tag{4}$$

where $\omega = 2\pi f$, and f is the frequency of the oscillating input.

The second model (called the I_h-model) also contained, in addition to the membrane capacitance and the leak conductance, a voltage-gated hyperpolarization-activated conductance, which was described by a Hodgkin-Huxley-type formalism with a single gating variable, and whose parameters matched the properties of I_h in different cell types as determined in our experiments. The (complex) impedance of this model was described as:

$$Z = \frac{1}{g_l + i\omega C + \bar{g}_h m_\infty^{(h)}(V_0) + \frac{\bar{g}_h b(V_0 - E_h)}{1 + i\omega\tau_h}} \tag{5}$$

where $\bar{g}_h$ is the maximal conductance of I_h, $m_\infty^{(h)}(V_m)$ is the steady-state value of the gating variable for the activation of I_h as a function of the membrane potential (V_m), V_0 is the actual membrane potential in the absence of the oscillating input, b is the slope of the function $m_\infty^{(h)}(V_m)$ at V_0, E_h is the I_h reversal potential and τ_h is the time constant of I_h activation.

A detailed description of both models can be found in the Appendix.

5.8. Electrophysiological recordings and data analysis in study II

5.8.1. Data acquisition

Data were recorded with a Multiclamp 700B amplifier (Molecular Devices, Sunnyvale, CA.) As a first step, two pipettes filled with ACSF were placed into the hippocampal slice preparation; one to the stratum pyramidale of the CA1 area, and another to the stratum pyramidale of the CA3b area. After approximately 10-15 minutes of bath application of 10 μM CCh, which was usually enough time to induce stable persistent oscillations in the slices (Hájos and Mody, 2009), the field potentials were recorded simultaneously on two channels for at least 120 s, with the aim to compare the local field potential oscillations between the two regions. Then the electrode was removed from the CA3 area, while the CA1-electrode was left in the same position. As a next step besides recording the local field potential in CA1, action potentials were detected extracellularly from individual neurons of CA1 or CA3 with the second pipette filled with ACSF. The loose patch recordings were visually guided using differential interference contrast microscopy (Olympus BX61W), and action potentials were detected for 60-120 s, depending on the firing frequency of the cell. This pipette was then withdrawn from the slice, and whole-cell patch-clamp recordings were performed on the same cells with a new pipette filled with intracellular solution. Access resistance was in the range of 5-20 MOhm and was compensated (65-75%). Only recordings, where it did not change substantially (more than 25%) were included in the study. Reported values of voltage measurements were not corrected for the junction potential. To record excitatory postsynaptic currents (EPSCs) and inhibitory postsynaptic currents (IPSCs) cells were voltage clamped at a nominal holding potential of the estimated reversal potential for IPSCs (~ -70 mV) and EPSCs (~ 0 mV), respectively. Both field and unit recordings were low-pass filtered at 2 kHz using the built-in Bessel filter of the amplifier. Data were digitized at 6 kHz with a PCI-6042E board (National instruments, Austin, Texas) and EVAN 1.3 software, and were analyzed offline with Igor Pro 5.01 software (Wavemetrics, Oregon) using either standard or custom-made Igor Pro procedures. The custom-made Igor procedures were written by Dr. Iris Oren

(Department of Clinical and Experimental Epilepsy, Institute of Neurology, University College London, London).

5.8.2. Event detection and analysis

Recordings were further filtered offline using a digital, bidirectional, phase-conserving filter. Field recordings were low-pass filtered at 1 kHz, extracellular unit recordings were high-pass filtered at 40 Hz to isolate spikes, while whole-cell recordings of postsynaptic currents (PSCs) were high-pass filtered at 1 Hz to filter out slow fluctuations in holding current.

The power of the field oscillation was calculated with power spectral density (PSD) analysis of ~ 60 s long field recordings. Before the FFT was performed, time windows of ~ 1.5 s with 50 % overlap were multiplied by a Hanning window to minimize end-effects. The area under the power spectral density curve between 10 and 45 Hz was taken as the power of the gamma-frequency oscillation.

To extract the magnitude and the phase of the different frequency-components of the field oscillation and to get information on changes in frequency and amplitude of the periodic signal with time, wavelet analysis using a Morlet-wavelet basis was used. The wavelet transform of the field recording was examined between 10 and 45 Hz with scales chosen to reflect the equivalent Fourier frequency (Torrence and Compo, 1998; Le Van Quyen et al., 2001). For each time point, the maximum of the wavelet transform magnitude was found, and the corresponding dominant frequency identified. The phase of the time point was defined in terms of the dominant frequency. Phase was defined in radians such that $-\pi$ was associated with the minimum of the oscillation, and a full cycle ran from $-\pi$ to π. Cells for which the wavelet magnitude of the field oscillation changed by > 2 SDs between spike train and PSC recordings were excluded from the study.

Event times for action potentials were defined as the time of crossing a voltage threshold set by visual inspection to exceed the noise level. Mean firing rate for cells was calculated as the total number of events during the recording epoch divided by the length of the epoch. Normalized spiking frequency was calculated by dividing the mean firing rate by the frequency of the oscillation. Event phases were defined as the wavelet phase of the dominant frequency at the time of the event. To calculate the probability of

discharge of a given cell group, the event number vs. phase histograms of each cell in the group were normalized, summed and divided by the number of cells in the given cell group. This averaged phase histogram was then multiplied by the mean of the normalized spiking frequency for the given cell group. Event times for PSCs were defined as time of peak current per cycle of the oscillation, and these were converted to wavelet phases of the dominant frequency.

The cycle-averaged events (Fig. 18/1-2) (as well as the cycle averaged field) were obtained by summing recordings over cycles, between - π and π and dividing by the number of cycles. Each cycle was linearly scaled to span 2π radians regardless of the number of data points.

Phasic charge transfer was calculated in the following way: an initial baseline estimate was obtained by taking the maximum (for EPSCs) or minimum (for IPSCs) of the cycle-averaged events. Then for each 0.2 s epoch the mean of all current values exceeding this initial baseline estimate was calculated. This mean was used as the baseline for the epoch. If no current value was found to exceed the initial baseline estimate during the epoch, the baseline estimate would increment negatively for EPSCs and positively for IPSCs until such current values were found. This calculation was repeated for all epochs of the entire recording. The integral from this baseline value was calculated over each cycle, and the mean of these integrals was taken as the phasic charge transfer.

The cycle-averaged PSCs were converted to excitatory (g_e) and inhibitory (g_i) conductances using

$$g_{e/i} = \frac{I_{e/i}}{(V_h - E_{e/i}^{rev})} \tag{6}$$

where $I_{e/i}$ is the phasic excitatory/inhibitory current, V_h is the holding potential, and $E_{e/i}^{rev}$ is the reversal potential for the conductance of interest. The conductances were used to estimate the net apparent reversal potential (E_{syn}^{rev}) by solving

$$I_{syn} = g_e (E_{syn}^{rev} - E_e^{rev}) + g_i (E_{syn}^{rev} - E_i^{rev}) = 0$$

$$\Rightarrow E_{syn}^{rev} = \frac{I_{syn} + g_e E_e^{rev} + g_i E_i^{rev}}{g_e + g_i} \tag{7}$$

5.8.3. Statistical analyses

The phase coupling of the events was determined by using circular statistics. The strength of phase coupling was calculated by summing all event phases within an epoch as unity vectors and then dividing the resulting vector sum ($\vec{R}$) by the number of events (Zar, 1999). The length of this normalized vector ("r") was taken as the strength of the phase-coupling. If the phases of all unity vectors are identical then r is equal to 1, while it is 0 in a case of uniform distribution. The mean event phase was defined as the direction of the resultant vector (ϕ).

The Rayleigh probability of $\vec{R}$ was used to determine the significance of the phase-coupling. It was calculated by the following equation:

$$p = e^{-z} \cdot \left(1 + \frac{2Z - Z^2}{4n} - \frac{24Z - 132Z^2 + 76Z^3 - 9Z^4}{288n^2}\right) \qquad (8)$$

where n is the number of spikes, and $Z = n\ r^2$. Events were considered to be phase coupled, if the Rayleigh test indicated that they were not distributed randomly around the gamma cycle ($p < 0.01$) (Zar, 1999).

The circular standard deviation was taken as

$$\sigma = \sqrt{-2 \ln r} \qquad (9)$$

where r is the phase-coupling strength (Zar, 1999).

Linear data were all normally distributed according to the Kolmogorov-Smirnov test ($p > 0.05$), therefore to test the equality of means of the measured variables of the different cell groups ANOVA was performed and the Bonferroni post-hoc test was used to find significant differences between group means. To test equality of means of angular variables the multi-sample Watson-Williams test was used.

To correlate linear-linear variables the Pearson's correlation coefficient was used. To correlate angular variables (a) with linear variables (X), the parametric angular-linear correlation coefficient r_{al} was used, which was defined as:

$$r_{al} = \sqrt{\frac{r_{Xc}^2 + r_{Xs}^2 - 2 r_{Xc} r_{Xs} r_{cs}}{1 - r_{cs}^2}}, \qquad (10)$$

where r_{XC} is a coefficient for correlation between X and cosα, r_{XS} is a coefficient for correlation between X and sinα, and r_{CS} is a coefficient for correlation between the cosine and sine of α. The methods for determining these coefficients are described in Zar (1999).

All correlation coefficients are quoted as r in the text. Values are given as mean ± standard error of the mean (SEM).

5.9. Anatomical identification of the neurons

The recorded cells were filled with biocytin during the recordings in both studies. After the recording the slices were fixed in 4 % paraformaldehyde in 0.1 M phosphate buffer (PB; pH=7.4) for at least 1 hour, followed by washout with PB several times and incubation in 30 % sucrose in 0.01 M PB for at least 2 hours. Then slices were freeze-thawed three times above liquid nitrogen and treated with 1 % H_2O_2 in PB for 15 minutes to reduce the endogenous peroxidase activity. Recorded cells were visualized using avidin-biotinylated horseradish peroxidase complex reaction (Vector Laboratories Inc., Burlingame, CA) with nickel-intensified 3,3'- diaminobenzidine as chromogen giving a dark reaction product. After dehydration and embedding in Durcupan cells were morphologically identified on the basis of their dendritic and axonal arborization. Representative neurons were reconstructed using a drawing tube.

6. RESULTS

6.1. Part I.: Single cell resonances in hippocampal CA1 neurons produced by intrinsic membrane characteristics

In this chapter I address the question what kind of intrinsic membrane properties the CA1 hippocampal neurons have that can endow them with the capability of producing membrane potential oscillations and resonance at different frequencies (Hutcheon and Yarom, 2000). These frequency tuning properties enable the cells to respond preferentially to inputs at certain frequencies (Pike et al., 2000), and they can influence the precise spike timing of the cell relative to the ongoing network activity (Lengyel et al., 2005; McLelland and Paulsen, 2009). As a net effect these features of the cells may play a significant role in setting network dynamics (Hutcheon and Yarom, 2000). Moreover these built-in membrane characteristics of a cell shape the amplitude and the temporal dynamics of the neuronal response, influence the integration of synaptic inputs, and contribute to controlling the precise timing of the action potential output (Magee, 1998; Magee, 1999; Richardson et al., 2003; McLelland and Paulsen, 2009).

The intrinsic membrane properties arise from the interaction of passive membrane properties and active conductances, i.e., the operation of voltage-gated ion channels. Therefore, to describe the intrinsic membrane properties of the cells both the passive and active properties of the membranes were studied in the following experiments. We characterized the impedance profiles of distinct types of anatomically identified neurons in the CA1 region of the rat hippocampus. We focused on the dissimilarities in the voltage response of the cells to sinusoidal current inputs and wanted to determine the role of I_h in producing these differences. To give a quantitative explanation of how the voltage-gated conductances interacted with the passive membrane properties in the different cell types, we also introduced a computational model to our study.

6.1.1. The different cell types investigated in this study

Four anatomically identified cell types of the CA1 region of the hippocampus were investigated in this study using the whole-cell patch-clamp method. During the measurements the cells were filled with biocytin and were identified post hoc on the basis of their dendritic and axonal arborization. In addition to pyramidal cells (PC, n=27, Fig. 6A), three interneuron types were recognized. Those interneurons that could not be unambiguously classified as belonging to any one of these categories were excluded from this study.

One group of interneuron (n=24) had cell bodies and smooth or sparsely spiny horizontal dendrites restricted to the stratum oriens. Their axon, which predominantly originated from the soma, ramified sparsely in strata radiatum and oriens and carried en passant and often drumstick-like boutons, which were distributed irregularly along them (Fig. 6A). Some of the axon collaterals could be followed to the subiculum or to the CA3 region. The overall appearance of their axon cloud was spread out longitudinally compared to the other two interneuron types (see below). These neurons resembled those cells that were earlier characterized by Gulyás et al. (2003), Hájos et al. (2004), and Goldin et al. (2007) in slice preparations, and by Jinno et al. (2007) in intact brain. Although these neurons may represent a heterogeneous population of inhibitory cells including local interneurons as well as GABAergic cells with long-range projections (such as backprojecting cells, oriens retrohippocampal projection cells, or double projection cells based on the review of Maccaferri (2005), Klausberger and Somogyi (2008) and Klausberger (2009)), their physiological features were rather comparable; therefore the data obtained in neurons with this type of morphology were pooled under the name of oriens-radiatum (O-R) cells. This name only refers to the fact that the axon collaterals of these neurons were restricted to the strata oriens and radiatum in hippocampal slices, and may not correspond to a functional category.

Another group of interneurons also had both the cell body and dendritic tree in the stratum oriens, but their horizontally running dendrites were often densely decorated with long spines. Their axon frequently originated from a proximal dendrite, and after ramification the main axon without boutons could be followed into the stratum lacunosum-moleculare. In this layer the axon ramified extensively bearing heavily

packed varicosities. Some axon collaterals with boutons were also observed in the stratum oriens. These neurons were identified as oriens-lacunosum-moleculare (OLM) cells (n=26) (Fig. 6A; McBain et al., 1994).

The somata of the third group of interneurons were also found in the stratum oriens, sometimes in the close vicinity of the stratum pyramidale. Their aspiny or sparsely spiny dendritic tree had either horizontal or vertical orientation, and the axonal arbour was predominantly located in the stratum pyramidale (Fig. 6A). Thus, these interneurons belonged to the perisomatic region-targeting inhibitory cells, which comprise both basket cells and axo-axonic cells (Freund and Buzsáki, 1996). Since the light microscopic examination of these interneurons did not allow us to unequivocally distinguish them from each other, data from all perisomatic region-targeting interneurons were pooled. However, only those neurons were included in this study that could be classified as fast spiking interneurons based on their action potential phenotype (see Methods for details). We refer to this group of cells as fast-spiking perisomatic region-targeting interneurons (FS PTI).

6.1.2. Basic electrophysiological characteristics

We first determined the apparent passive membrane properties (i.e. input resistance and time constant) of the neuronal classes included in our study by injecting small-amplitude hyperpolarizing current steps (see Methods). Both input resistance and membrane time constant varied significantly among the different cell types (Kruskal-Wallis (KW) test, $p<0.001$). Multiple post hoc comparisons (see Methods) indicated that OLM cells (n=12) had a significantly higher input resistance than PCs ($p<0.01$, n=19) and FS PTIs ($p<0.05$, n=7) (Table 1). OLM cells also had a significantly slower membrane time constant at rest than any other cell type studied (OLM vs. PC: $p<0.001$; OLM vs. O-R: $p<0.05$; OLM vs. FS PTI: $p<0.001$) (Table 1). In order to facilitate later comparisons with models that directly include capacitance as a parameter, we also estimated the membrane capacitance from the small-amplitude transient responses. Capacitance varied significantly between cell types (KW test, $p<0.01$); in particular, OLM cells had a significantly larger capacitance than O-R cells (n=11) and FS PTIs (both $p<0.05$) (Table 1). The resting membrane potentials were estimated to be -62.4 ±

2.4 mV for PCs (n=21), -55.4 ± 9.5 mV for O-Rs (n=17), -55.7 ± 6.5 mV for OLM cells (n=19) and -50.4 ± 8.1 mV for FS PTIs (n=7) (data presented here as mean ± S.D.).

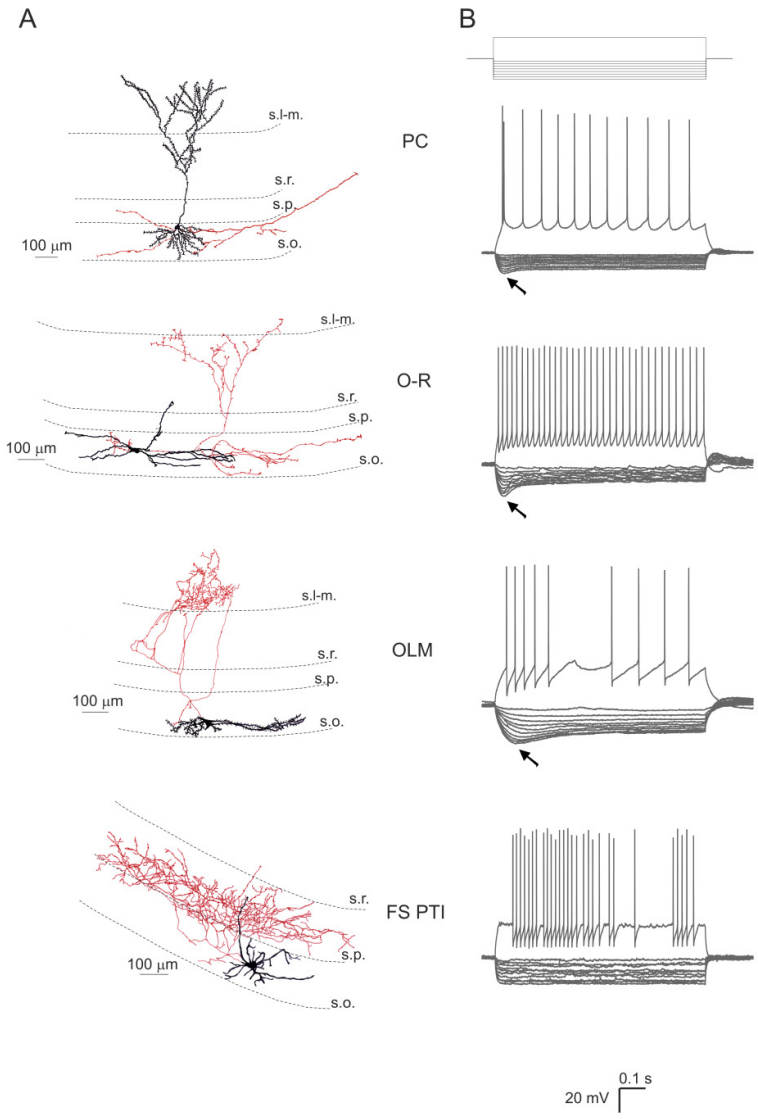

Figure 6. Light microscopic reconstructions and voltage responses to current steps of the investigated cell types recorded in the stratum oriens of hippocampal CA1 region. **(A)** Example artistic renderings of light microscopic reconstructions of a pyramidal cell (PC), an oriens-radiatum cell (O-R), an OLM cell (OLM), and a fast spiking perisomatic region-targeting interneuron (FS PTI). Dendrites are represented in black and axons in red. Dendritic spines are enhanced for visibility. **(B)** Voltage responses to depolarizing (200 pA) and hyperpolarizing current steps (from -20 to -200 pA in increments of 20 pA). A sag (marked with arrows) indicating the presence of I_h can be seen in pyramidal cells (PC), oriens-radiatum cells (O-R) and OLM cells. Fast spiking interneurons (FS PTI) had a small or no sag. s.l-m., stratum lacunosum-moleculare; s.r., stratum radiatum; s.p., stratum pyramidale; s.o., stratum oriens.

	PC (n=19)	O-R (n=11)	OLM (n=12)	FS PTI (n=7)
Input resistance (MOhm)	101 (91 - 131)	144 (116 - 199)	197 (169 - 211)	117 (112 - 219)
Membrane capacitance (pF)	155 (121 - 195)	97 (84 - 110)	181 (136 - 255)	106 (91 - 132)
Membrane time constant (ms)	16.6 (13.4 - 19.6)	18.5 (15.4 - 25.5)	37.7 (31.9 - 46.9)	8.7 (8.3 - 16.2)
Passive cutoff frequency (Hz)	9.6 (8.1 - 11.9)	8.6 (6.2 - 10.3)	4.2 (3.4 - 5.0)	18.4 (10.6 - 19.3)
Relative sag amplitude	0.175 (0.160 - 0.216)	0.687 (0.560 - 0.695)	0.445 (0.382 - 0.644)	0.074 (0.021 - 0.138)
Peak delay (ms)	44.7 (39.9 - 49.2)	36.8 (32.0 - 60.2)	92.3 (69.5 - 107.0)	74.0 (67.6 - 80.4) *

Table 1. Passive membrane properties and sag characteristics of the investigated cell types. Data are presented as median with interquartile range in parentheses. * n=2 (only cells with a relative sag amplitude > 0.1)

6.1.3. Distinct features of depolarizing *sag* in hippocampal neuron types

We observed a *sag* in the voltage response of PCs, O-Rs and OLM cells to negative current steps of suitable magnitudes (Fig. 6B and 7A). In these cells a rebound depolarizing hump could also be detected after the offset of the current step and in a few interneurons some rebound spikes could be observed as well (in 5 out of 17 O-R cells and in 4 out of 19 OLM cells). Both the sag and rebound depolarization were eliminated by bath application of the specific I_h blocker, ZD7288 (10 μM; data not shown). The properties of the sag varied substantially between the cell types (Fig. 7C, D). In particular, the cell types differed significantly in the relative sag amplitude ($p < 0.001$, KW test), and post hoc multiple comparisons indicated that O-Rs and OLM cells had a significantly larger relative sag amplitude than PCs (O-R vs. PC: $p < 0.001$; OLM vs. PC: $p<0.01$) and FS PTIs (both $p<0.001$) (Fig. 7C). The time taken to reach the negative peak amplitude of membrane potential during the current step (i.e., peak delay) also varied significantly between cell types ($p < 0.001$, KW test). OLM cells, in particular,

had a significantly slower sag than PCs and O-Rs (both $p < 0.001$, post hoc multiple comparisons as detailed above) (Fig. 7D).

Qualitatively, PCs (n=18 out of 19) displayed a small but rather fast sag, O-Rs (n=11) had the largest and fastest sag, while OLM cells (n=12) usually showed a large but relatively slow sag. In 2 out of 7 fast-spiking cells some I_h-mediated sag could be observed, but even in these particular neurons the sag was rather small and tended to appear only at very negative potentials (more negative than -90 mV).

These data suggest that, in addition to passive membrane characteristics, the properties of some active conductances such as the non-selective cation conductance mediating I_h, might be different between these cell types.

6.1.4. The impedance profiles and resonance properties of four types of hippocampal neuron

The differences in sag characteristics among cell types suggest that the I_h-dependent resonance could also be dissimilar. In order to characterize the subthreshold impedance profiles and possible resonance properties of the cells, a 3-s-long sinusoidal current was injected into the cells at different membrane potentials negative to the firing threshold (Fig. 8). Impedance magnitude and phase curves were characterized by the five summary statistics (Table 2): impedance at 0.5 Hz ($Z_{(0.5\ Hz)}$; this quantity can also be used as an estimate of the input resistance of the cell, which, by definition, is the same as the impedance at 0 Hz), cutoff frequency (f_{cutoff}), resonance magnitude (Q), the frequency of maximal impedance (f_{max}) and total inductive phase (Φ_L), as described in the Methods section. These quantities were then compared statistically between the different cell types and experimental conditions.

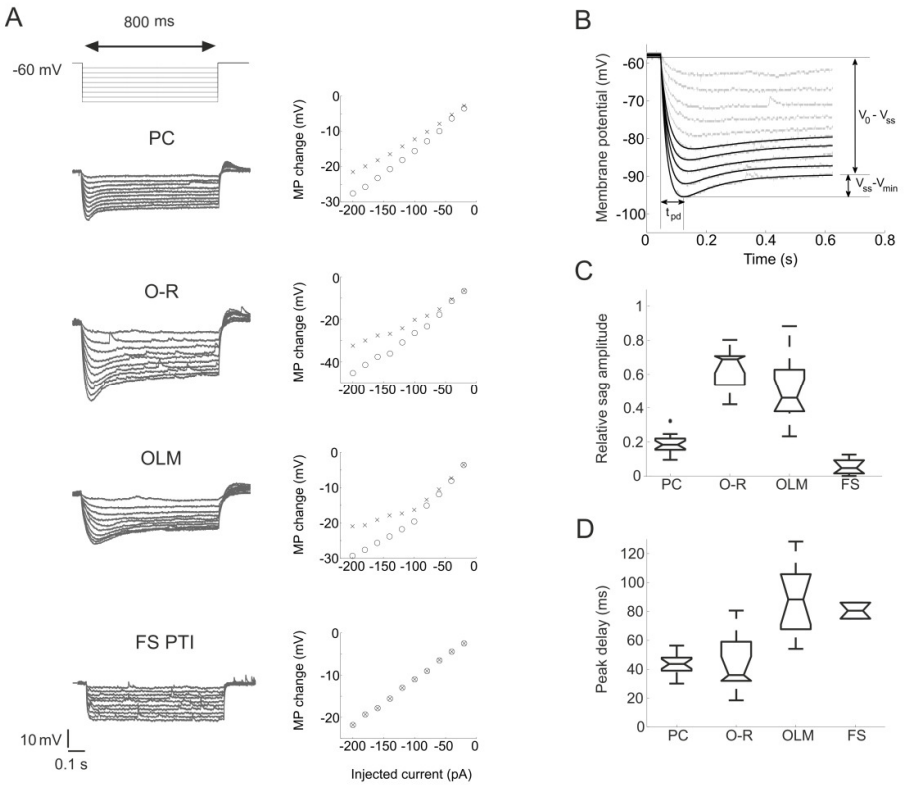

Figure 7. Properties of the sag in the investigated cell types. (A) Representative voltage responses of the investigated cell types to hyperpolarizing current pulses (800 ms long steps from -20 to -200 pA, at 20 pA intervals from a holding potential of -60 mV), and the corresponding IV plots of the peak (open circles) and the steady state membrane potential (MP) changes of the same cells (crosses). **(B)** Sag parameters were determined from the voltage response of the cell to the five largest amplitudes of the negative current steps (from -120 pA to - 200 pA, in 20 pA steps). Relative sag amplitude is the ratio of the difference between the steady state voltage at the end of the pulse and the minimum voltage during the sag (Vss-Vmin), and the difference between the holding potential and the steady-state voltage (Vo-Vss). The holding potential was approximately -60 mV in each cell. The peak delay (t_{pd}) was defined as the time of the negative peak of the membrane potential relative to the beginning of the current pulse. **(C, D)** Relative sag amplitudes and peak delays in the different cell types. Note that PCs (n=19) displayed small but rather fast sag, O-Rs (n=11) had a large and fast sag, while OLM cells (n=12) usually showed a rather large but relatively slow sag. Two out of seven FS PTI cells also showed a sag but it was rather small and could be observed only at membrane potentials negative to -90 mV.

We found that cell type had a significant effect on all five of the derived statistics: $Z_{(0.5\ Hz)}$, f_{cutoff}, Q, f_{max} and Φ_L ($p<0.001$ in each case, KW test; Fig. 8B-D). Multiple comparisons indicated that PCs had a significantly smaller $Z_{(0.5\ Hz)}$ than OLM cells and O-Rs (both $p<0.001$) and FS PTIs also had a smaller $Z_{(0.5\ Hz)}$ than OLM cells ($p<0.01$); f_{cutoff} was significantly lower in OLM cells than in any other cell type studied

(all $p<0.001$); Q was significantly larger in PCs, O-Rs and OLM cells than in FS PTIs ($p<0.001$ for PCs and O-Rs, and $p<0.05$ for OLM cells) and it was significantly larger in PCs than in OLM cells ($p<0.01$); PCs had a significantly higher f_{max} than any other cell type (all $p<0.001$), and f_{max} was also significantly higher in O-Rs than in OLM cells ($p<0.01$) and FS PTIs ($p<0.01$). Φ_L was significantly smaller in FS PTIs than in O-Rs ($p<0.001$) and in PCs ($p<0.05$) (Fig. 8D). In addition, the shape of the impedance profiles changed with variations in baseline membrane potential (Fig. 8). In particular, a two-way analysis of variance (ANOVA) using cell type as between-subject factor and membrane potential as within-subject factor showed that three of the summary statistics varied significantly with membrane potential ($Z_{(0.5\ Hz)}$: $p<0.001$; f_{cutoff}: $p<0.001$; Φ_L: $p<0.05$).

To separate cells with a monotonically decreasing impedance profile from those with resonance, resonating cells were defined as cells with a Q value greater than 1.05 at any of the investigated membrane potentials. We found that all PCs showed resonance (n=9), indicated as a clear peak in the impedance curve. Resonance was most prominent at hyperpolarized potentials (at -70 and -80 mV), but was also apparent (though weaker) at depolarized potentials (Fig. 8B, D). The f_{max} values fell into the theta range (4-6 Hz) (Fig. 8D). Almost all O-Rs also exhibited resonance (n=15 out of 16), although a rather large variance could be seen in Q values; f_{max} was between 2 and 6 Hz. Ten out of 15 OLM cells also showed resonance, however, the resonance frequency fell in the range of 1 to 3 Hz. An obvious resonance peak could be observed in only one out of seven FS PTI cells at the investigated membrane potentials (Fig. 8B, D).

In line with the prediction based on the sag characteristics, both the impedance profiles and the resonance properties were found to vary substantially between the cell types. Therefore, we next investigated the contribution of I_h to their impedance profiles.

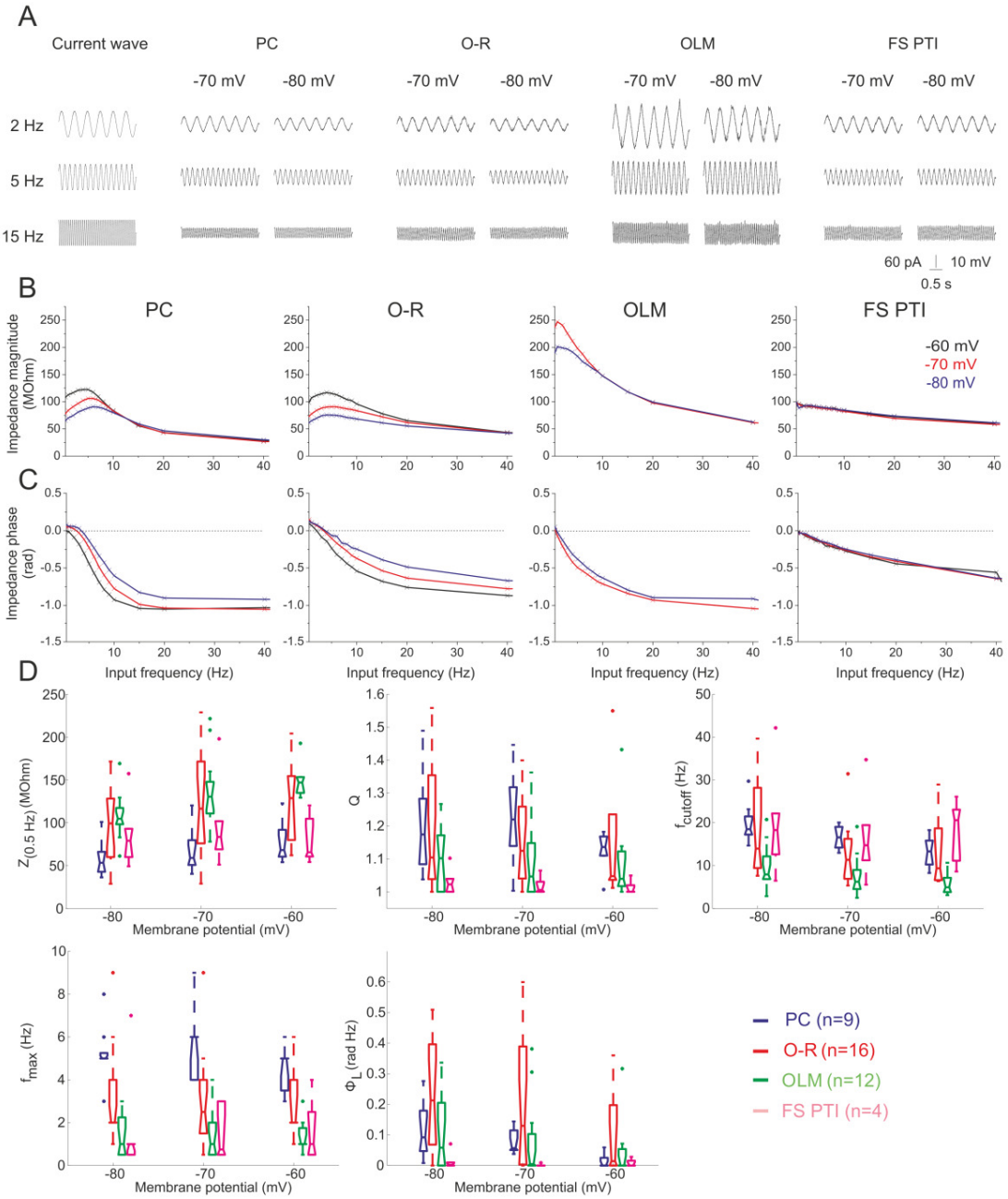

Figure 8. Characterization of the impedance profile in the different cell types. **(A)** Voltage responses of sample cells of the investigated cell types to 3 s long sinusoidal current inputs at 2, 5 and 15 Hz at a holding potential of -70 and -80 mV. **(B)** The impedance-frequency relationship of the same cells as in A at different membrane potentials. PCs and O-Rs showed a clear resonance peak in the theta frequency range. Most of the OLM cells also showed resonance, although it was less apparent and occurred at lower frequencies. Fast spiking interneurons (FS PTI) showed no subthreshold resonance. **(C)** The impedance phase profile of the different cell types at the investigated potentials. Note that the amplitude and frequency extent of positive phase values increased with membrane hyperpolarization in PCs, O-Rs and OLM cells. Colors identify corresponding membrane potentials. **(D)** Five parameters were used to quantitatively characterize the properties of the impedance curves. $Z_{(0.5\ Hz)}$ is the impedance

value at the lowest input frequency (0.5 Hz). The Q value (Z_{max}/ $Z_{(0.5\ Hz)}$) was used to quantify the magnitude of the resonance. f_{max} means the input frequency at which the maximal impedance value was detected. Cutoff frequency (f_{cutoff}) is the input frequency where the magnitude of the impedance first dipped below $\frac{1}{\sqrt{2}} \cdot Z_{(0.5\ Hz)}$. Φ_L is the total inductive phase defined as the area under the positive segment of the impedance phase profile. PCs are shown in blue, O-Rs in red, OLM cells in green and FS PTIs in magenta (See also Table 2).

	PC			O-R			OLM			FS PTI		
	-80	**-70**	**-60**	**-80**	**-70**	**-60**	**-80**	**-70**	**-60**	**-80**	**-70**	**-60**
$Z_{(0.5Hz)}$ (MOhm)	53 (43-66)	59 (51-80)	68 (60-92)	99 (60-128)	117 (76-172)	129 (80-154)	105 (98-117)	130 (111-148)	147 (135-153)	79 (60-93)	83 (69-102)	66 (61-105)
Q	1.17 (1.08-1.28)	1.22 (1.14-1.32)	1.14 (1.11-1.17)	1.10 (1.04-1.35)	1.12 (1.04-1.26)	1.05 (1.04-1.24)	1.10 (1.00-1.17)	1.05 (1.00-1.15)	1.04 (1.02-1.12)	1.02 (1.00-1.04)	1.01 (1.00-1.03)	1.00 (1.00-1.02)
f_{cutoff} (Hz)	18.5 (17.2-21.5)	16.6 (14.2-19.0)	13.3 (10.3-15.8)	14.0 (9.4-28.2)	11.3 (6.9-16.2)	9.4 (6.6-18.7)	7.9 (6.8-12.1)	6.2 (4.5-9.0)	4.9 (3.8-7.1)	18.3 (12.6-22.2)	14.7 (11.2-19.4)	20.6 (11.1-23.1)
f_{max} (Hz)	5.0 (5.0-5.3)	6.0 (4.0-6.0)	5.0 (3.5-5.0)	2.0 (2.0-4.0)	2.5 (1.5-4.0)	2.0 (2.0-4.0)	1.0 (0.5-2.3)	1.0 (0.5-2.0)	1.0 (1.0-1.8)	1.0 (0.5-1.0)	0.8 (0.5-3.0)	1.0 (0.5-2.5)
Φ_L (rad Hz)	0.09 (0.05-0.18)	0.06 (0.05-0.11)	0.00 (0.00-0.03)	0.21 (0.07-0.40)	0.13 (0.00-0.39)	0.01 (0.00-0.20)	0.06 (0.00-0.20)	0.00 (0.00-0.10)	0.00 (0.00-0.05)	0.00 (0.00-0.01)	0.00 (0.00-0.00)	0.00 (0.00-0.02)

Table 2. Properties of the impedance curves. Data are presented as median with interquartile range in parentheses.

6.1.5. The involvement of I_h in impedance profiles and resonance

I_h is an active conductance, which was shown to be essential for the emergence of resonance behavior in some neurons (Hutcheon et al., 1996a; Lüthi and McCormick, 1998; Hu et al., 2002; Narayanan and Johnston, 2007). In our experiments only those cells that showed an I_h-dependent sag showed subthreshold resonance. Furthermore, the application of 10 μM ZD7288, a blocker of HCN channels, strongly reduced or eliminated the sag in all cell types ($p<0.001$ overall, and $p< 0.05$ in each individual cell

type except FS PTIs). ZD7288 also had a moderate effect on passive membrane properties at -60 mV, increasing both the input resistance ($p<0.05$ overall) and the apparent membrane capacitance ($p<0.001$ overall) (Table 3).Therefore, the effect of ZD7288 on the impedance profile was tested in each of the investigated cell types. A three-way ANOVA, with cell type as a between-subject factor, and membrane potential and ZD7288 treatment as within-subject factors, indicated that ZD7288 had a significant effect on all five of our summary measures ($Z_{(0.5\ Hz)}$, f_{cutoff}, Q, f_{max}, and Φ_L; Fig. 9). In particular, the blockade of HCN channels significantly increased $Z_{(0.5\ Hz)}$ in PCs ($n=9$, $p<0.001$), O-Rs ($n=6$, $p<0.01$) and OLM cells ($n=7$, $p<0.01$) and significantly decreased f_{cutoff} in the same three cell types (PCs: $p<0.001$; O-Rs: $p<0.01$; OLM cells: $p<0.001$). Most importantly, ZD7288 completely abolished the resonance, resulting in a significant reduction in the Q value in PCs ($p<0.001$), O-Rs ($p<0.01$) and in OLM cells ($p<0.05$) (Fig. 9). The elimination of resonance by ZD7288 was also evident in the change in f_{max}, which was significant in PCs ($p<0.001$), O-Rs ($p<0.01$) and in OLM cells ($p<0.01$), and in Φ_L, which was reduced significantly in the same three cell types (PCs: $p<0.001$; O-Rs: $p<0.01$; OLM cells: $p<0.05$). However, ZD7288 had no effect on the shape of the impedance profile (as characterized by these five quantities) at any of the investigated membrane potentials in FS PTIs ($n=4$) (Fig. 9).

	PC (n=7)	O-R (n=8)	OLM (n=6)	FS PTI (n=5)
Input resistance (MOhm)	125 (112 - 159)	211 (186 - 235)	233 (182 - 245)	119 (109 - 190)
Membrane capacitance (pF)	220 (199 - 256)	160 (104 - 190)	208 (149 - 275)	135 (111 - 219)
Membrane time constant (ms)	25.3 (19.3 - 27.9)	23.5 (20.0 - 30.8)	26.0 (23.7 - 33.0)	8.9 (7.5 - 20.0)
Passive cutoff frequency (Hz)	6.3 (5.7 - 8.3)	6.8 (5.2 - 8.0)	6.1 (4.8 - 6.7)	17.9 (8.5 - 21.4)
Relative sag amplitude	0.066 (0.050 - 0.084)	0.099 (0.036 - 0.155)	0.076 (0.004 - 0.086)	0.0 (0.0 - 0.029)

Table 3. Passive membrane properties and sag amplitude after the application of ZD7288. Data are presented as median with interquartile range in parentheses.

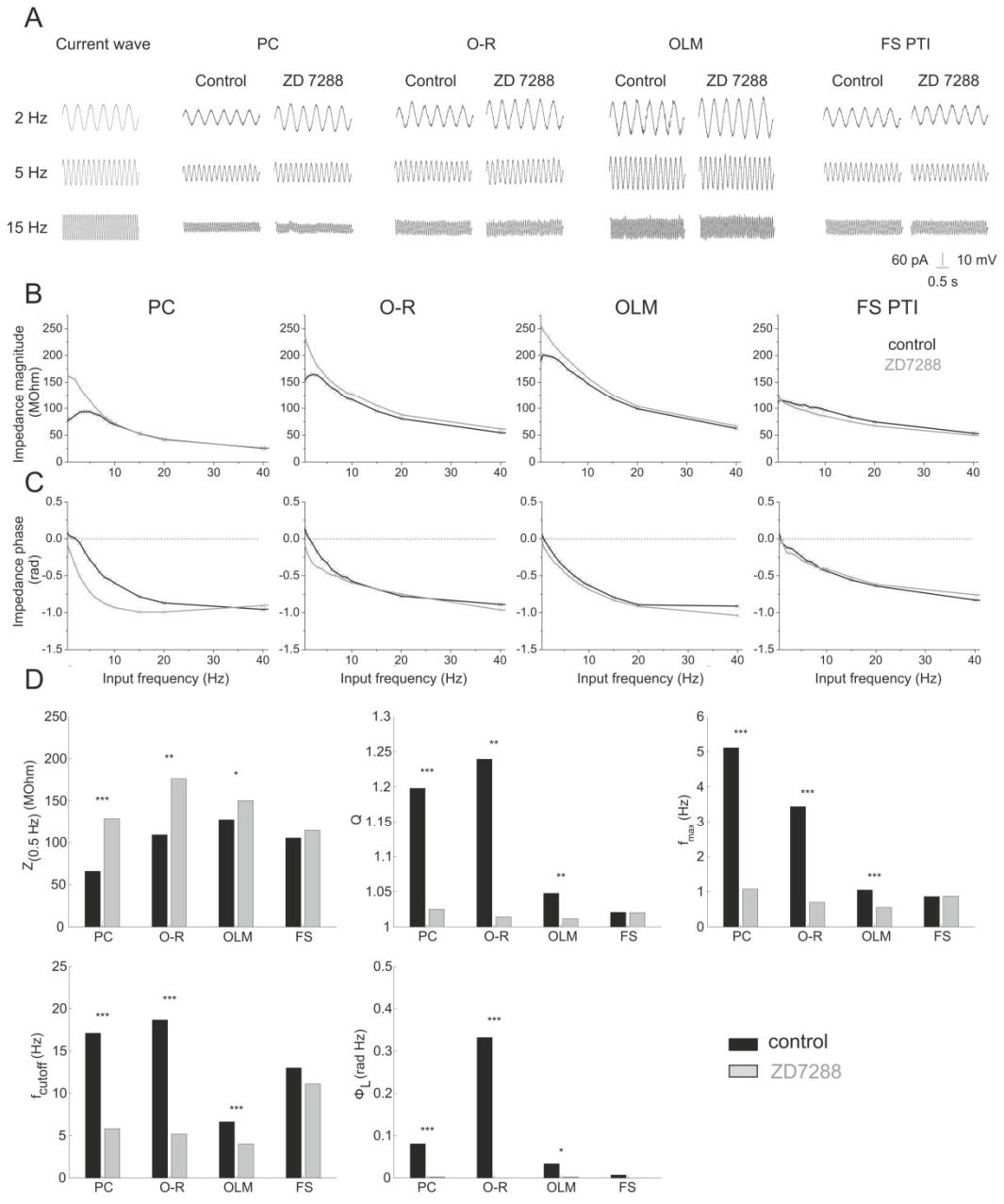

Figure 9. The effect of blocking I_h on the impedance profile of the investigated cell types. **(A)** Voltage responses of representative cells of the investigated cell types to 3 s long sinusoidal current inputs at 2, 5 and 15 Hz at a holding potential of -80 mV under control conditions and in the presence of the I_h-blocker ZD7288 (10 μM). **(B, C)** The magnitude and phase of the impedance as a function of input frequency of the same cells measured at -80 mV in control conditions (black) and in the presence of 10 μM ZD7288 (grey). Note that after blocking I_h both the magnitude and phase profile of the impedance profiles changed substantially in PCs, O-Rs and OLM cells; however, ZD7288 had no apparent effect on the shape of the impedance profiles in FS PTIs. **(D)** Statistical comparison of the five investigated parameters in the different cell types under control conditions and in the presence of 10 μM ZD7288. Since ZD7288 had a similar effect at all investigated membrane potentials, data measured at different potentials were pooled in this figure. Note that ZD7288 significantly changed all properties of the impedance

curves in cell types expressing a sag, but had no significant effect in FS PTIs. *, p< 0.05; **, p< 0.01; ***, p<0.001. (See also Table 3).

These results suggest that I_h is essential for subthreshold resonance in pyramidal cells, O-Rs and OLM cells, and that it contributes substantially to the shape of the impedance profile even in some cells without a clear resonance, e.g. in some of the OLM cells. We also found that the shape of the impedance profile varied substantially between different cell types. Therefore, we set out to investigate whether the observed differences in the impedance curves among cell types might be due to distinct properties of I_h.

6.1.6. The properties of I_h in the different cell types

To examine the differences in the properties of I_h between the cell types (excluding FS PTIs since their impedance curve was not substantially affected by ZD7288 application), whole-cell voltage-clamp experiments were performed (Fig. 10A). First, the voltage-dependent activation of I_h was measured based on the instantaneous tail current at the end of 800 ms steps to different potentials (see Methods). We found that I_h was significantly more activated in PCs than in interneurons at all potentials between -60 and -100 mV; there was no significant difference between O-Rs and OLM cells at any membrane potential (Fig. 10B). Based on sigmoidal fits to activation values, the potential of half-maximal I_h activation ($V_{1/2}$) was -82.9 ± 4.9 mV in pyramidal cells (n=6), -97.3 ± 4.7 mV in O-Rs (n=7) and -97.7 ± 5.0 mV in OLM cells (n=7, Fig. 10B). The slope of the activation function was similar in all cell types: the parameter m was -12.4 ± 1.9 mV in PCs, -10.2 ± 2.7 mV in O-Rs and -8.9 ± 4.0 mV in OLM cells. No significant difference was found in the I_h reversal potential – measured using the instantaneous I-V plot, see Methods – between the different cell types (-33.0 ± 13.4 mV in PCs (n=3), -38.8 ± 2.9 mV in O-Rs (n=4), and -37.0 ± 5.9 mV in OLM cells (n=4)). Therefore, reversal potential values from all cells were pooled and averaged to arrive at a single figure (-36.6 mV) that was used in all subsequent calculations and models (Fig. 10H, I). Next, we determined the maximal I_h conductance in each cell based on the steady-state current (Fig. 10C). We found no significant difference between the cell types, and a substantial variation within any given class (4.1±1.9 nS in PCs, 5.9±2.8 nS in O-Rs, and 4.6±1.8 nS in OLM cells (data presented here as mean ± S.D.) (Fig. 10J).

Finally, we analyzed the kinetics of I_h by fitting either single or double exponential functions to the time course of I_h activation at different membrane potentials. Although the time course could be described fairly accurately using a single exponential function (Fig. 10D), better fit was seen when a double exponential function was used, and the two components could be clearly identified in essentially all cells, with little variation within a given cell type (Fig. 10E, F). The single exponential fit indicated that activation of I_h was significantly faster at all membrane potentials between -80 and -120 mV in PCs than in O-Rs ($p<0.001$ between -80 mV and -100 mV, and $p<0.01$ at -110 and -120 mV) and OLM cells ($p<0.001$ at all voltages in this range). The double exponential fit clearly identified a fast (time constant, 20-50 ms) and a slower (100-500 ms) component of I_h activation in all cell types. Both components tended to be slower in interneurons than in PCs, a difference that reached significance at some (more hyperpolarized) membrane potentials. However, the most substantial difference was in the relative weight of the two components: the activation of I_h was dominated by the fast component at all membrane potentials in PCs, while the two components contributed almost equally in interneurons (Fig. 10G). No significant difference was seen in the kinetics of I_h activation between O-Rs and OLM cells. The activation kinetics were found to be voltage dependent in all cell types investigated, approximated either with single or double exponential functions (Fig. 10D-F).

In summary, differences in the properties of I_h – specifically, the voltage-dependence of steady-state activation and the kinetics of activation – between PCs and the two classes of interneuron with subthreshold resonance suggest that PCs and investigated interneuron types may express distinct subunit compositions of HCN channels, and that this may account for some of the differences in the impedance profiles between different cell types. On the other hand, the lack of any such difference in I_h characteristics between O-Rs and OLM cells, two cell types with distinct impedance profiles, indicates that factors other than the magnitude and kinetic properties of I_h are responsible for the observed variation in their impedance properties.

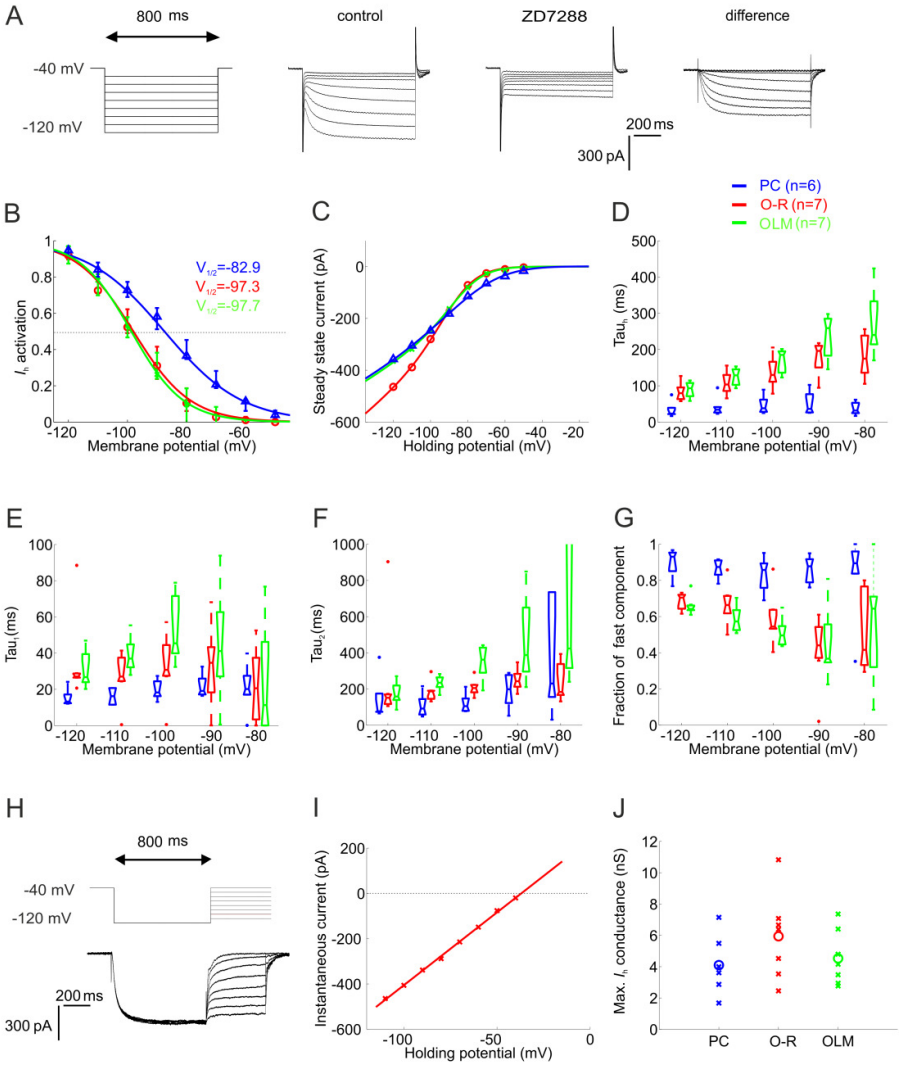

Figue 10. The properties of I_h in the different cell types**. (A)** I_h was elicited by 800 ms-long-hyperpolarizing voltage steps from a holding potential of -40 mV to the range of -50 to -120 mV, in 10 mV steps. Current traces recorded before and after the application of 10 μM ZD7288. The ZD7288-sensitive current was obtained by digital subtraction. **(B)** The activation curves of I_h in the investigated cell types, calculated from tail current amplitudes. **(C)** The current-voltage (I-V) relation of I_h in the different cell types obtained by plotting steady-state currents. Note that at physiologically relevant potentials (positive to -90 mV), a significantly larger amplitude of I_h was activated in PCs than in INs. **(D)** The activation kinetics (Tau_h) of I_h plotted against membrane potential for PCs, O-Rs and OLM cells obtained from single exponential fits. The time course of activation was generally more rapid in PCs than in interneurons over the entire voltage range. **(E, F)** Two components of the activation kinetics could be clearly identified with double exponential fits in all cell types. Fast (Tau_1, E) and slow time constant (Tau_2, F) of I_h activation as a function of voltage for PCs, O-Rs and OLM cells. In each cell type the fast time constant was about 5 to 8 times more rapid than the slow time constant of activation at a given potential. **(G)** The fraction of the fast exponential component (Tau_1) as a function of voltage. Note that in PCs the fraction of Tau_1 was predominant over the entire voltage range, while in interneurons the fast component becomes predominant only at hyperpolarized potentials (below -100 mV) but even at –120 mV it represents only 70 % of the total current amplitude. **(H)** To

determine the reversal potential of the current, I_h was fully activated with a voltage pulse to -120 mV and this was followed by steps to different test potentials (from -110 mV to -40 mV in 10 mV increments). **(I)** The open-channel I-V plot was constructed from the tail current amplitudes measured at each test potential and the reversal potential of I_h was extrapolated from these plots. **(J)** The estimated maximal conductance values of I_h for each cell of the different cell types (crosses). Circles indicate median values. There was no significant difference in the maximal conductance of I_h between the investigated cell types. In all plots PCs are shown in blue, O-Rs in red and OLM cells in green.

6.1.7. Computational model

To provide a quantitative account of the observed differences in the impedance profiles and resonance properties between the different cell types, we fitted the impedance profiles of single-compartment, conductance-based model neurons to those measured experimentally. The simpler model contained a membrane capacitance and a leak conductance, while the more complex I_h-model also included a voltage-gated conductance (see Methods for details).

We determined and compared the best fits to individual impedance profiles using the passive model and the I_h-model; examples of the fits for each cell type are shown in Fig. 11A-C (where amplitude, phase, and complex impedance are displayed separately). The passive model has only three free parameters (the input resistance, the total capacitance of the cell, and an additive serial resistance), while the I_h-model has five effective free parameters. (It has a total of seven parameters: the capacitance, the leak conductance, the maximal I_h conductance, the value of the activation variable at the baseline potential, the derivative of the activation variable with respect to voltage at the baseline potential, the time constant of the activation of I_h, and the series resistance, but these quantities appear only in certain combinations in the expression for the impedance, Equation (5), which reduces the number of actual free parameters to five.) We used the Bayesian information criterion (BIC, which takes into account the number of free parameters, see Methods) to compare the quality of the best fit in the two models (Fig. 11D). We found that the I_h-model described the control impedance curves of PCs, O-Rs and OLM cells better than the passive model (median $r^2 = 0.991$ vs. 0.904 in PCs;

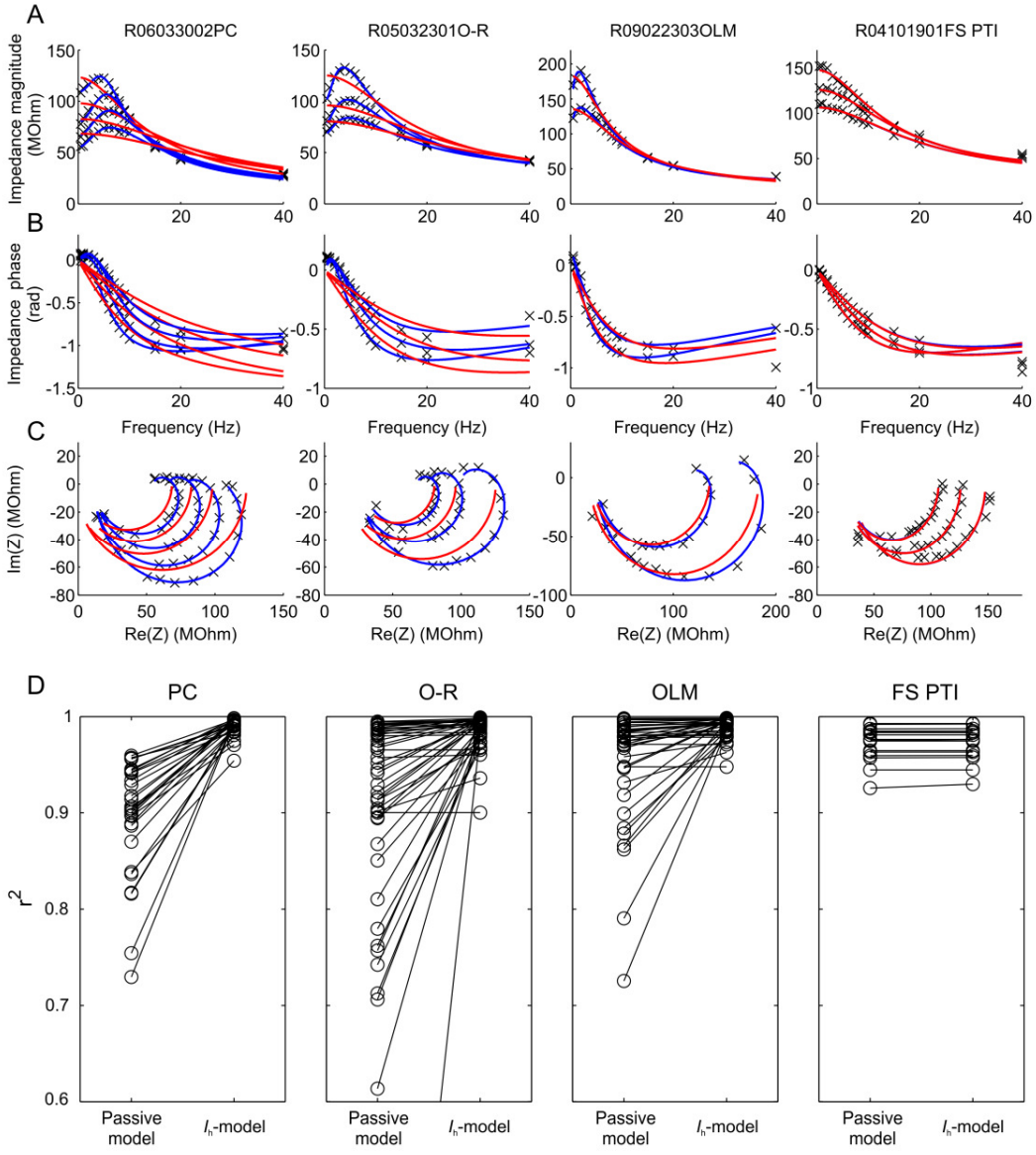

Figure 11. Comparison of fits using a passive and an active model (I_h-model) in various hippocampal cell types. **(A-C)** Examples of the impedance profiles (measured at multiple membrane potentials in each cell) for a single cell of each type in the study are indicated by the crosses; the red lines show best fits to each individual curve based on a passive (three-parameter) cell model; the blue lines are best fits based on the (effectively five-parameter) I_h-model (see Methods for details). Part A displays the absolute value (magnitude) of the impedance and part B the phase of the impedance as a function of input frequency, while in part C the complex impedance values (as defined by the magnitude and the phase) are plotted in the complex plane (in this plot, known as a Nyquist plot, frequency is not explicitly represented). **(D)** Comparison of fit quality between the passive and the I_h-model as measured by the r-square statistic for all impedance profiles recorded under control conditions.

r^2 = 0.992 vs. 0.949 in O-Rs; r^2 = 0.993 vs. 0.978 in OLM cells), and the value of the BIC was lower for the I_h-model in these cell types, indicating that the I_h-model is better even when we take into account the difference in the number of free parameters. On the other hand, the two models were about equally good at describing single control curves in FS PTIs (median r^2 = 0.976 for both models), and the BIC in this case favoured the passive model. In contrast, for the impedance curves measured in the presence of ZD7288, the I_h-model did not perform significantly better than the passive model for any cell type (median r^2 = 0.992 for both models in PCs; r^2 = 0.983 for both models in O-Rs; r^2 = 0.977 vs. 0.976 in OLM cells; r^2 = 0.955 vs. 0.954 in FS PTIs); in fact, the simpler passive model was found to be better in all cell types according to the BIC. These results suggest that I_h makes an essential contribution to the shape of the impedance profile in PCs, O-Rs and OLM cells, converting a basically passive impedance curve into one that is more adequately described by assuming voltage-dependent mechanisms.

Next, we wanted to determine whether the presence of I_h in itself (in combination with appropriate passive characteristics) is sufficient to explain the observed impedance profiles of hippocampal neurons. We also wished to understand to what extent the observed differences in impedance curves between the different cell types could be due to differences in the properties of I_h itself, as described in the previous section. Thus, for each individual neuron, we simultaneously fitted all the available impedance curves (measured under control conditions at different baseline membrane potentials) using the I_h-model, with the properties of I_h (the value and the slope of the steady-state activation and the time constant, all at the appropriate membrane potentials) set according to our voltage-clamp data for the given cell type, and only four free parameters (capacitance, leak conductance and maximal I_h conductance of the neuron, and an additional series resistance) to fit for each cell. This is a much more heavily constrained fit than the ones considered above (which had 3-5 free parameters for every impedance curve, and thus up to 20 for each cell); here, the four fit parameters are assumed to be the same at all membrane potentials in a given cell, and we constrain the voltage-gated conductance to have the cell-type-specific characteristics that we measured for I_h. Typical examples of the fit attained in different cell types are shown in Fig. 12A-C in the form of frequency-amplitude, frequency-

phase, and complex (Nyquist) plots. The quality of the fit was fairly good in all cell types (median $r^2 = 0.941$ in PCs; $r^2 = 0.931$ in O-Rs; $r^2 = 0.959$ OLM cells), especially considering the small number of free parameters, indicating that I_h (in combination with passive membrane properties) is the main determinant of the subthreshold impedance profile in these cells. Importantly, the range of parameters determined through the fitting procedure (in particular, the total capacitance and the maximal I_h conductance) was in good agreement with the values measured in the experimental current-clamp and voltage-clamp protocols (Fig. 12D; cf. Fig. 7 and Fig. 10). Notably, our resonance fits predicted a significantly larger membrane capacitance in the OLM cell population than in the population of O-Rs ($p<0.01$; Wilcoxon rank sum test), while there was no significant difference in the maximal conductance of I_h between the two cell types. Both of these conclusions are in agreement with our experimental measurements, and suggest that the observed differences between the impedance profiles of OLM cells and O-Rs are primarily due to a difference in passive properties rather than a difference in the kinetics or magnitude of a voltage-gated conductance (i.e. I_h).

However, it has to be noted that some systematic deviations between the data and the fitted curves were also evident. These were quantified by computing for the fitted curves the five summary statistics we had defined for the characterization of impedance profiles, and comparing them with the same statistics computed from the actual data (Fig. 12E). We found that the I_h-model was able to capture the overall shape of the impedance profiles as measured by the input resistance and the cutoff frequency quite accurately. On the other hand, the degree of resonance (as measured by Q and Φ_{total}), and the resonant frequency were less well predicted. In particular, the fits consistently predicted a larger degree of resonance (a higher Q value) in interneurons (but not in PCs) than the value determined directly from the data. Thus, the single-compartment I_h-model provides a fairly good but still incomplete account of the impedance profiles of the neurons in our study, and factors not included in this model (such as dendritic morphology, the subcellular localization of I_h, or additional voltage-gated conductances) might also contribute to the measured impedance characteristics.

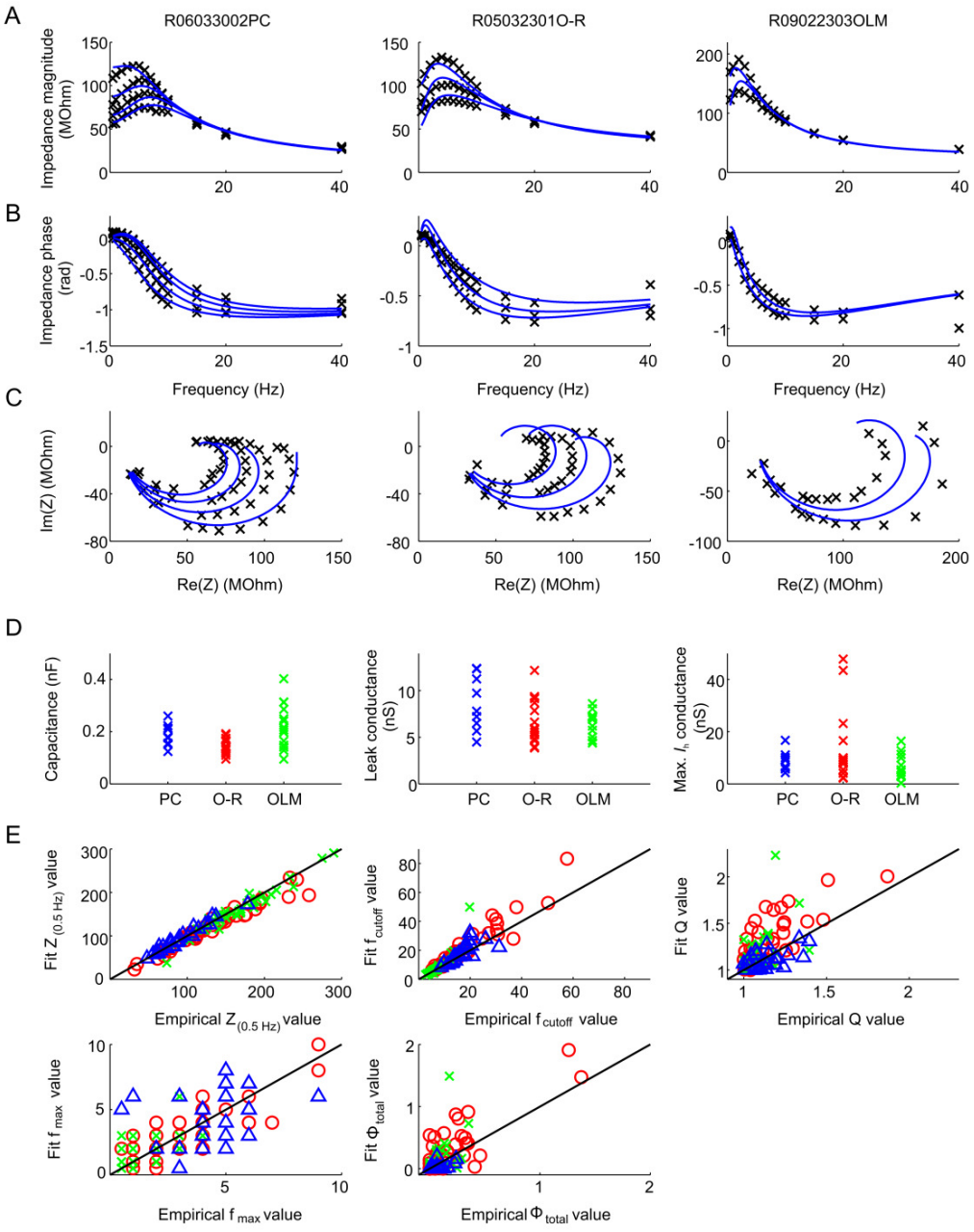

Figure 12. (A-C) Examples of model fits to experimentally measured impedance curves when the characteristics of I_h (voltage of half-activation, slope at half-activation, time constant) were fixed to their empirically determined values (as appropriate for each cell type), and only the capacitance, the leak conductance, and the maximal I_h conductance (as well as an additional series resistance) were allowed to vary. The types of plots in parts A-C are similar to those in Fig. 6. **(D)** Values of the capacitance, the leak conductance, and the maximal I_h conductance as determined by the best fit to the measured impedance curves for each cell (with values from the three I_h-containing cell types shown separately for comparison). **(E)** Empirically determined summary statistics (i.e., $Z_{(0.5\ Hz)}$, f_{cutoff}, Q, f_{max}, and Φ_L) versus the values of the same statistics predicted by the best-fitting I_h-model (with fixed I_h characteristics). Pyramidal cells are indicated by blue triangles, O-Rs by red circles, and OLM cells by green crosses.

6.2. Part II. Network resonances of hippocampal CA1 produced by synaptic synchronization

In the previous chapter we could see that many neurons in the hippocampal CA1 show intrinsic properties that endow them with the capability of entraining oscillations in the theta frequency range. However, this does not necessarily mean that these neurons cannot be involved in higher frequency oscillations. Theoretically there are more possibilities to induce oscillation within a network (see Introduction for a detailed description of these models). There is growing evidence in the literature on the importance of synaptic synchronization in the genesis of gamma frequency oscillations of the hippocampus (Whittington et al., 1995; Fisahn et al., 1998; Traub et al., 2000; Mann et al., 2005), however the relative weight of the excitatory and inhibitory inputs in the synchronization of the neurons is still unclear. *In vitro* models have provided some insights into the mechanisms of gamma oscillogenesis in the CA3 region of the hippocampus, however, very little is known about the properties of gamma oscillations in CA1.

During the CCh-induced gamma oscillation model the rhythmic and synchronous field potential changes are generated within the CA3 by a recurrent mechanism, that involves a monosynaptic feedback connection between CA3 pyramidal cells and perisomatic targeting interneurons of the local CA3 network (Hájos et al., 2004; Mann et al., 2005; Oren et al., 2006 Gulyás et al., 2010). This intrinsic gamma generator also appears to operate in behaving animals (Csicsvári et al., 2003; Bragin et al., 1995). Both *in vivo* and *in vitro* data suggest that in the case of intrinsic hippocampal gamma oscillations, the rhythmic activity of the CA3 network drives the synchronous activities in CA1 (Bragin et al., 1995; Fisahn et al., 1998; Csicsvári et al., 2003), however, the exact cellular mechanisms remain elusive.

This chapter is aimed to explore how the rhythmic excitatory output of CA3 pyramidal cells generates fast oscillations in CA1. To distinguish between the two possible mechanisms ("feed-forward excitation or inhibition") we investigated the firing properties and synaptic inputs of different types of anatomically-identified hippocampal neurons in CA1 during cholinergically-induced gamma oscillations.

6.2.1. Methodological requirements for recording high frequency oscillations under submerged conditions

In order to be able to investigate *in vitro* oscillations under submerged conditions, first of all we had to set the experimental circumstances under which these network events can be consistently induced. Whereas network oscillations can be reliably seen in interface slices (Whittington et al., 1995; Fisahn et al., 1998; Kubota et al., 2003), no such activity persisted in submerged slices using standard flow rate in a commercially available recording chamber. As the metabolic demand may be greater during ongoing network activity (Huchzermeyer et al., 2008), we searched for submerged conditions with improved metabolic supply to allow recording of network activities similar to those observed in interface chambers and the intact brain. We found that increasing the flow rate of the superfusion fluid in a recording chamber modified with an inert plastic insert to optimize laminar flow across the slice allowed us to record cholinergically induced persistent high frequency oscillations in the CA3 area (Hájos et al., 2004). However, these network activities were only rarely seen in CA1, even at high superfusion rates (in 2 out of 9 slices tested).

Since the propagation of the oscillation presumably needs even more intact network than the generation of the oscillation within the circuitry, we used rather thick slices in these experiments (450 μm). However, thicker slices and larger neuronal ensembles involved in the network activity might need even more intense oxygenation and nutrition. Higher flow rates could sustain the higher oxygen demand required for extensive synchronous network events, however, increasing the rate of slice perfusion has its own technical limitations, for instance it can produce mechanical instability of the slices during recordings. The stability of the slices is critical for lasting electrophysiological recordings and high quality optical imaging.

To overcome, or considerably reduce these problems a modified slice chamber with a dual superfusion system was introduced. In this design the slices were placed on a mesh glued between two plastic rings with a thickness of 2 mm. Two separate fluid inlets allowed ACSF to flow separately above and below the slice (Fig. 13A-D). Using this type of chamber, even with a flow rate of 3-3.5 ml/min for each channel, we readily observed prominent cholinergically induced oscillations in CA1 propagated from the CA3 local network (6 out of 8 slices tested). The mechanical stability of the slices were

also greatly improved, while the visibility of the neurons and their processes by the DIC optics were not compromised (Fig. 13E,F). Therefore this type of recording chamber was used in all experiments where the propagation of high frequency oscillations from the CA3 to the CA1 region of the hippocampus was studied.

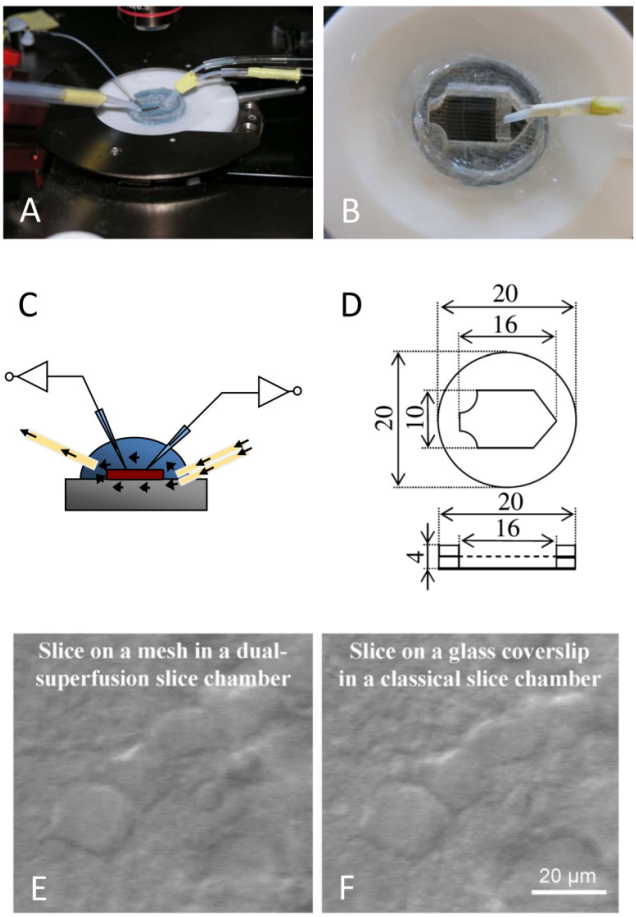

Figure 13. Modified submerged slice chamber with dual superfusion. **(A)** Low magnification picture of a submerged slice chamber with two fluid inlets and one outlet. **(B)** Picture taken at higher magnification of a chamber insert developed for dual-superfusion. **(C)** Schematic drawing of the modified chamber and the fluid stream in the chamber. The slices are placed on a mesh glued between two plastic rings. Two separate fluid inlets allow ACSF to flow both above and below the slice. **(D)** Scaled drawing (in mm) of the insert used for elevating the slice. **(E, F)** DIC images of the same hippocampal slice in a dual-superfusion slice chamber (E) and in a classic-style submerged slice chamber (F). Note that the visibility of the neurons is not compromised by the mesh in the dual-superfusion chamber.

6.2.2. CCh-induced fast network oscillations

Fast network oscillations were induced in horizontal hippocampal slices by bath application of 10 μM CCh. As a first step, network oscillations were monitored by recording the local field potentials using two ACSF filled patch pipettes; one placed in the stratum pyramidale of the CA3b region, and another in the stratum pyramidale of the CA1 region of the hippocampus (Fig. 14A,B). Power spectrum density (PSD) analysis was used to find distinct frequency components of the field potential oscillation recorded in the CA3 and in the CA1 and revealed a peak in the oscillations basically at the same frequency in both regions (mean oscillation frequency was 31.3 ± 0.62 Hz in the CA3 and 31.4 ± 0.6 Hz in the CA1; n=24) (Fig. 14C,D,F). However, the power of the oscillation was usually much smaller in CA1 than in CA3 (the average power was 1360 ± 380 μV in CA3 and 140 ± 26 μV^2 in CA1; n=24) (Fig. 14C,D,E). While a strong correlation was found between the frequency of the oscillations recorded in the CA3 and in the CA1 (R=0.989, p=0, n=24, Pearson's correlation, data not shown), there was no correlation between the power of the oscillation measured in the two hippocampal regions (R=0.290, p=0.168, n=24, Pearson's correlation, data not shown).

6.2.3. Classification of the investigated cell types

Though recordings were made from many different cell types in this study, to make the comparison of the investigated parameters less complicated, the CA1 cells were grouped into four main categories: 1. CA1 pyramidal cells (CA1 PC) (Fig. 15A); 2: oriens-alveus interneurons (OA IN) (Fig. 15C); 3: radiatum interneurons (RAD IN) (Fig. 15D); 4: PV-eGFP positive interneurons (PV+ IN) (Fig. 15B). Cells of the latter type were collected in slices prepared from PV-eGFP mice.

The reasons for this grouping were the following: among perisomatic region targeting interneurons parvalbumin expressing cells have been shown to be key actors in the generation of fast frequency gamma oscillation in the CA3 region (Fuchs et al., 2007; Gulyás et al., 2010), and some studies also indicate that they can be essential also in maintaining the oscillation in CA1 (Fuchs et al., 2007; Tukker et al., 2007). On the other hand CCK-expressing interneurons have been suggested to play a different role in

oscillations (Freund, 2003; Glickfeld and Scanziani, 2006; Freund and Katona, 2007; Tukker et al., 2007; Gulyás et al., 2010). Moreover, it was shown by several studies (Fukudome et al., 2004; Neu et al., 2007; Szabó et al., 2010) that in the presence of CCh the release of GABA from the axon terminals of CCK-expressing interneurons is significantly reduced or even completely abolished, therefore, they are not expected to have a determinant role in the modulation of gamma oscillation under these circumstances (Gulyás et al., 2010).

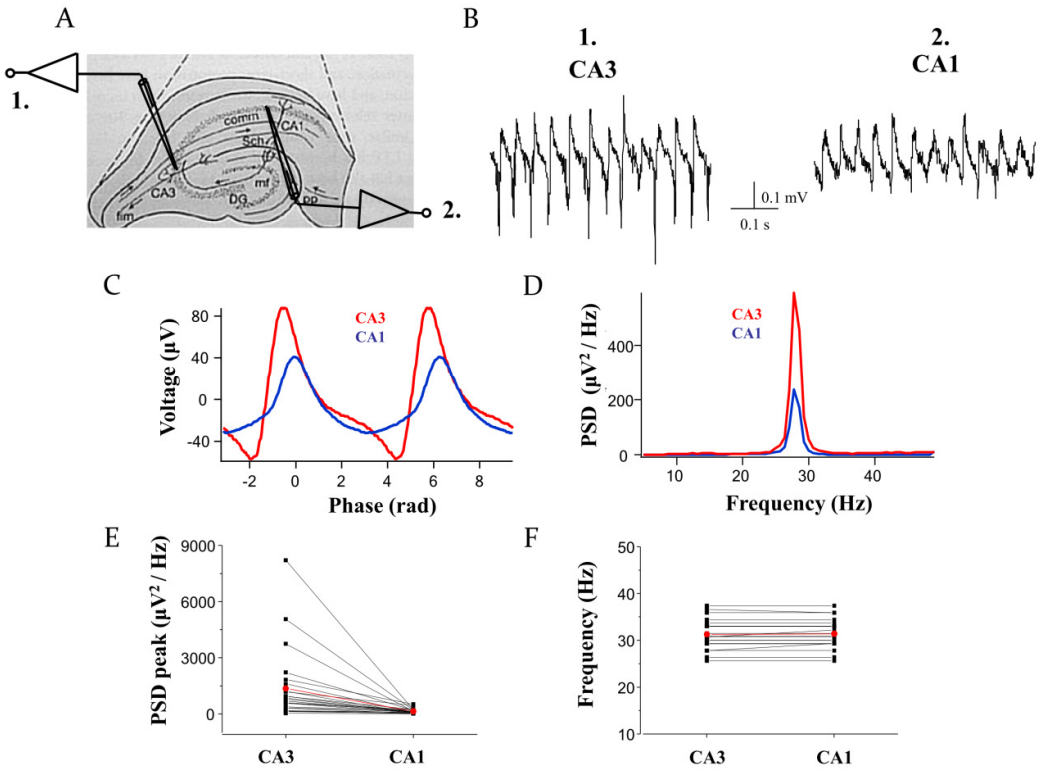

Figure 14. Comparison of field potential oscillations recorded extracellularly from the stratum pyramidale of the CA3 and the CA1 region of the hippocampus after bath application of 10 μM CCh. **(A)** To record field potential oscillations two ACSF filled patch pipettes were positioned to the stratum pyramidale of CA1 and CA3b regions of horizontal hippocampal slices. **(B)** Raw traces recorded simultaneously from CA1 and CA3 stratum pyramidale after bath application of CCh. **(C)** Cycle average of the field potential oscillations showed in part B. Note that the shape of the oscillation was usually also somewhat different in the two areas, and this difference could be observed even on the cycle averaged phases profiles. **(D)** Power spectral density function of the traces in *A* showing gamma frequency peak. **(E, F)** Comparison of power (E) and frequency (F) of oscillations in CA3 and CA1.

The group of PV+ INs included fast spiking basket cells, bistratified cells and axo-axonic cells. These cell types have very similar physiological properties in terms of

firing pattern and the expression of different receptor types (Freund and Buzsáki, 1996), therefore we treated them as a single group, nevertheless we cannot rule out the possibility that these cell types can play different roles in the generation or maintenance of gamma oscillations (see Discussion).

The remaining CA1 INs were categorized into two groups based on the localization of their cell bodies and dendritic arbor. Cells located in the stratum radiatum were included in the group of radiatum interneurons (RAD IN). This group of neurons comprised of several different cell types, such as radiatum-lacunosum-moleculare cells, neurogliaform cells, Schaffer-associated cells, subiculum projecting interneurons, etc.). Though the recorded neuron types formed a very diverse cell population based on their morphological features, they are usually referred as feed-forward inhibitory cells, since their main excitatory intrahippocampal input is formed by the Schaffer collaterals of the CA3 PCs (Tamamaki et al., 1987; Amaral et al., 1991).

Cells with soma and dendrites located mainly in the stratum oriens and alveus formed the group of oriens-alveus interneurons (OA IN). The majority of these cells could be characterized as O-LM cells (n=11 out of 15) (McBain et al., 1994). The remaining cells (n=4) resembled in morphology to the cells that were classified as O-R cells in the previous chapter. They had cell bodies and dendritic arborization in the stratum oriens or alveus of CA1 and their sparsely ramifying axons projected toward the subiculum. The OA INs are usually considered as feedback inhibitory cells, since their main excitatory input originates from CA1 pyramidal cells (Blasco-Ibanez and Freund, 1995).

To be able to compare the behavior of CA1 cells to the CA3 cells during oscillations, we also recorded CA3 pyramidal cells (CA3 PC) and CA3 interneurons (CA3 IN). Here the data of all types of interneurons were pooled, since as it was already shown by previous studies of our research group, interneurons in CA3 all tend to fire at the ascending phase of the oscillation with a monosynaptic delay after the firing of CA3 pyramidal cells (though with different frequency and precision, Hájos et al., 2004).

Only those cells were included in the study that could be unequivocally classified into one of these categories based on their morphological features, except in the group of CA3 pyramidal cells, where data of spiking properties of cells identified by visual inspection only were also included in the analysis.

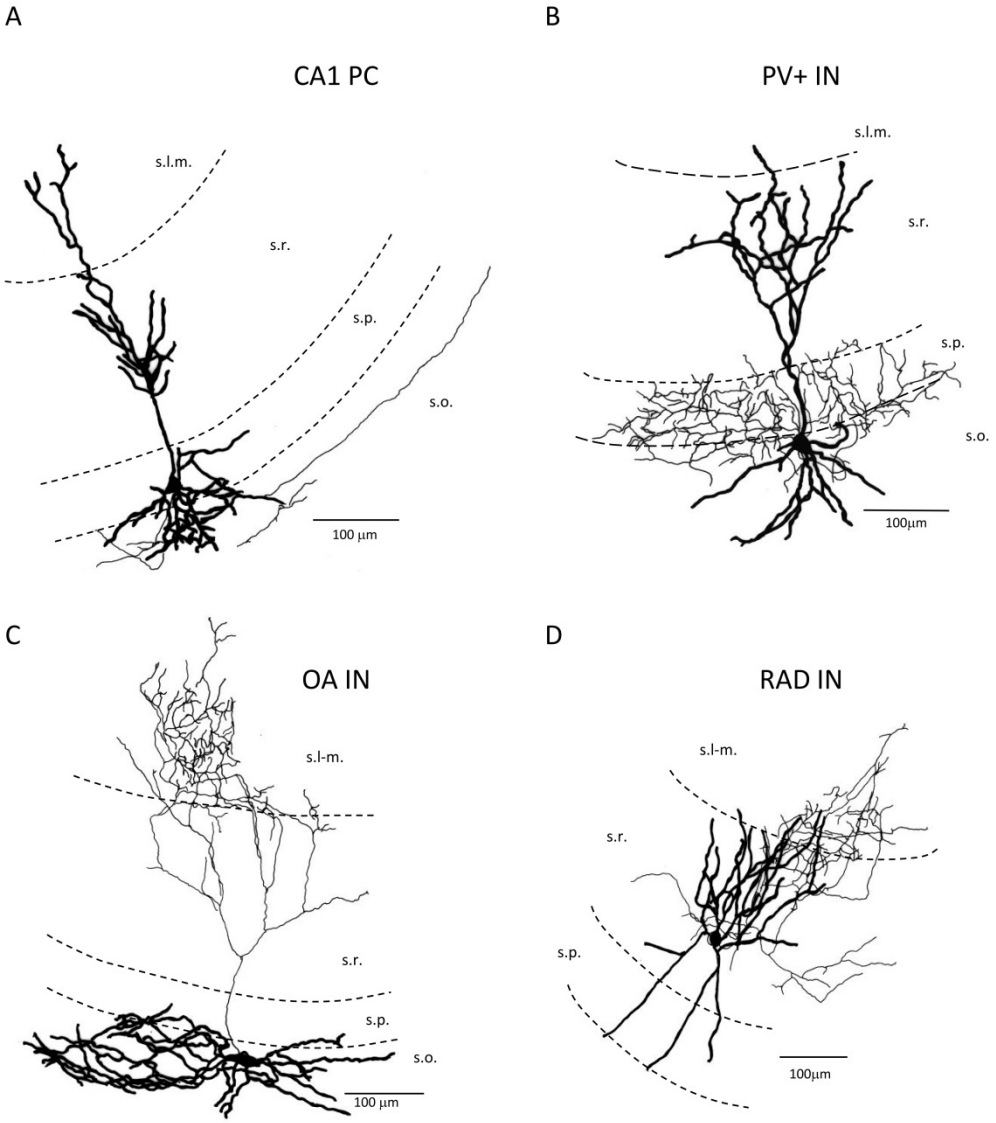

Figure 15. Light microscopic reconstructions of representative cells of the investigated cell groups recorded in the CA1 region of the hippocampus. **(A)** A CA1 pyramidal cell (PC); **(B)** a parvalbumin expressing perisomatic targeting interneuron (PV+ IN); **(C)** an oriens-alveus interneuron (OA IN); **(D)** a radiatum interneuron (RAD IN). Dendrites are represented in black and axons in grey. s.l-m., stratum lacunosum-moleculare; s.r., stratum radiatum; s.p., stratum pyramidale; s.o., stratum oriens.

6.2.4. Firing properties of different cell types during CCh-induced network oscillations in hippocampal slices

To reveal the firing characteristics of CA1 cells in relation to the ongoing network oscillation, the spiking activity of different types of neurons was detected by a

glass pipette filled with ACSF in loose patch mode, while the other pipette used to monitor field oscillations in CA1 was left in the same position in the stratum pyramidale. The Morlet-wavelet based wavelet analysis was applied to reveal the magnitude and phase of the different frequency components (10-45 Hz) of the oscillation. The phase of an event was defined in terms of the dominant wavelet frequency.

To characterize the firing properties of the neurons, we described the following parameters: firing frequency, phase-coupling strength (r_{AP}), phase of firing (Φ_{AP}), and the firing frequency/oscillation frequency in the case of phase-coupled cells. The probability of discharge for each cell type was also calculated. This describes the probability of a cell type to fire at a certain phase of a cycle of the ongoing oscillation (see Methods).

When comparing the firing frequency of the cell types, we observed that CA3 PCs fired at the lowest rates among all the cell types, they fired significantly at lower frequency than CA3 INs ($p<0.01$), PV+ cells in CA1 ($p< 0.01$) and CA1 O-A INs ($p<0.001$). However, there was no significant difference between the firing frequency of CA1 PCs, RAD INs in the CA1 and CA3 PCs (CA3 PC vs. CA1 PC: $p=0.309$; CA3 PC vs. CA1 RAD IN: $p=1$; CA1 PC vs. CA1 RAD IN: $p=1$). Some of the O-A INs were capable of firing doublets during some cycles, which resulted in a quite high mean firing rate of this group on average. RAD INs fired at the lowest rates among interneurons, however, significant differences in the firing rates of different IN types could be shown only between O-A INs and RAD INs ($p<0.001$) (Fig. 16B,E; Fig. 17A,B; Table 4).

Most of the recorded neurons showed gamma-modulated firing according to the Rayleigh test ($Rp < 0.01$), only 6 out of 21 CA1 PC and 3 out of 14 RAD IN were not phase coupled to the ongoing network oscillation. There were no significant differences in the firing rate of phase-coupled and non phase-coupled cells within a cell group. The firing rate was 11.07±1.35 Hz for phase-coupled CA1 PCs (n=15) and 9.26±2.52 Hz for non phase-coupled PCs (n=6, $p=0.624$); and 8.71±1.42 for phase-coupled RAD INs, (n=11) and 8.18±0.83 Hz for non phase-coupled RAD INs (n=3; $p=0.855$).

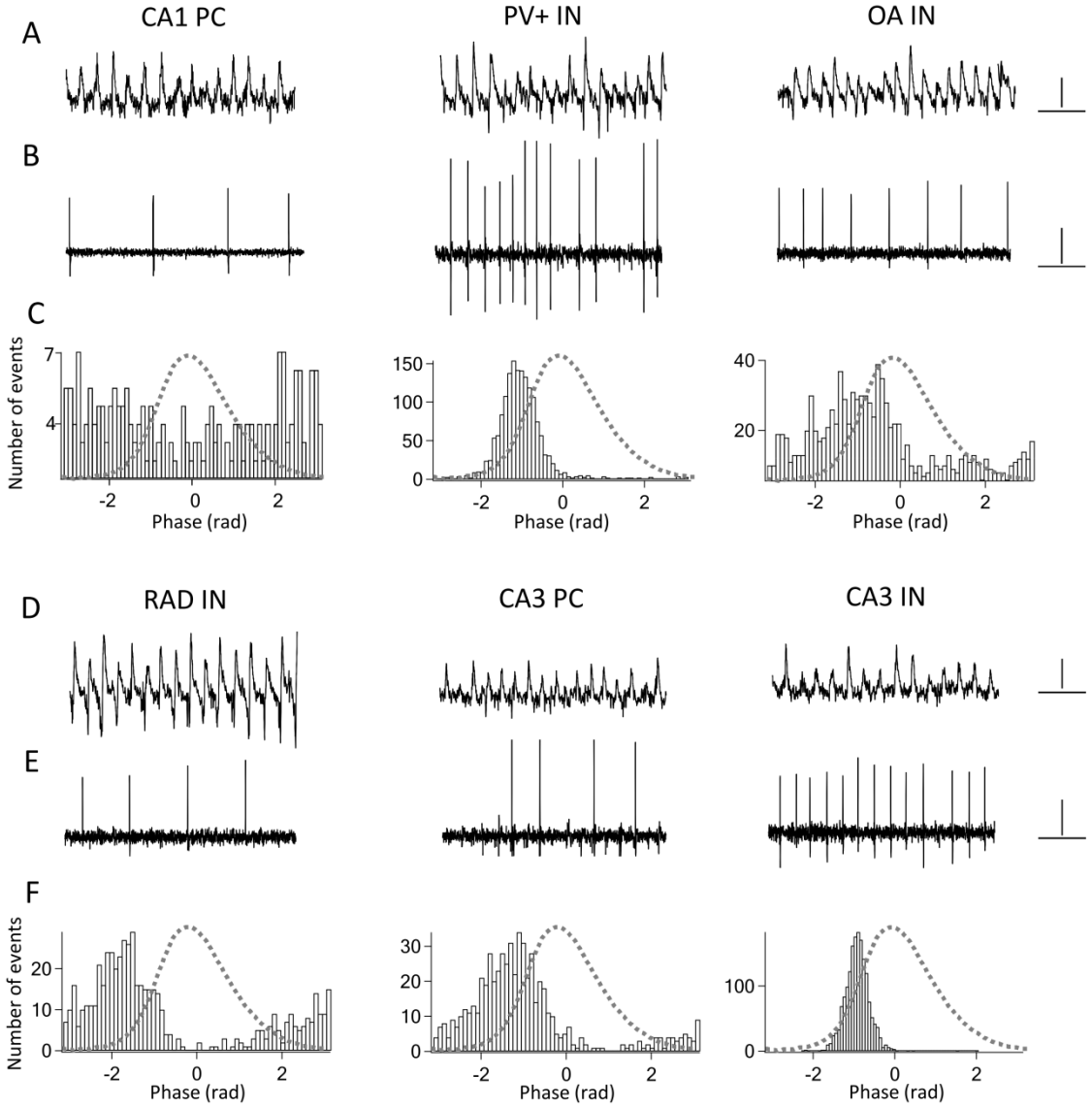

Figure 16. Spiking activity of the different cell types during CCh-induced oscillations. **(A, D)** Extracellular recordings of field potentials in the stratum pyramidale of the CA1. **(B, E)** Simultaneously recorded spike trains from a representative cell of each cell group (loose-patch recordings). **(C, E)** Spike-phase histograms of the same cells showing the number of events vs. the phase of the field potential oscillation during a 60 s long recording epoch. Dotted line: average gamma cycle. Scale bars: 0.1 mV (vertical), and 0.1 s (horizontal).

Though almost all of the recorded cells were modulated by the ongoing field potential oscillation, there were some significant differences among them in the depth of modulation depending on the cell type. CA1 PCs were significantly less phase coupled than PV+ ($p< 0.001$), OA INs ($p<0.01$), CA3 PCs ($p<0.001$), and CA3 INs ($p<0.001$). At the same time, there were no significant differences in r_{AP} between CA1 PCs and CA1 RAD INs ($p=0.714$). Among CA1 cells the firing of PV+ INs was the most

precisely phase coupled to the ongoing field potential oscillation. Beside the mentioned differences in the coupling strength of CA1 PCs and PV+ cells, the r_{AP} of the latter cell type was significantly higher than the r_{AP} of OA INs ($p< 0.01$) and RAD INs ($p<0.001$) as well. However, there were no significant differences between the phase-coupling strength of CA3 PCs, CA3 INs and PV+ INs of the CA1 (CA3 PC vs. CA3 IN: p=0.91; CA3 PC vs. PV+ IN: p=0.051; CA3 IN vs. PV+ IN: p=1) (Fig. 16C,F; Fig. 17C-E; Table 4).

Though most of the recorded neurons fired phase coupled, they did not fire all at the same phase. There were systematic differences in the preferred phase of the different cell types. CA1 PC fired mainly at the trough of the oscillation, while both CA1 and CA3 INs tended to fire at the ascending phase of the oscillation. There were no significant differences in the preferred phase of different interneuron types in the CA1 (PV+ IN vs. O-A IN: p= 0.295; PV+ IN vs. RAD IN: p=0.778; O-A IN vs. RAD IN: p= 0.538) or between CA1 INs and CA3 INs (PV+ INs vs. CA3 INS: p=0.197; O-A INs vs. CA3 INs: p=0.054; RAD INs vs. CA3 INs: p=0.884). CA3 PCs fired also close to the trough, however, somewhat later than CA1 PCs ($p< 0.01$) and somewhat earlier than INs within a cycle (CA1PC vs. PV+ IN: $p<0.001$; CA1 PC vs. O-A IN: $p<0.001$; CA1 PC vs. RAD IN: $p< 0.01$; CA1 PC vs. CA3 IN: $p<0.001$). When translating these phase differences to time differences according to the mean oscillation frequency (31-32 Hz), we could see that CA1 PCs fired 5-6 ms earlier than INs and 1-2 ms earlier than CA3 PCs, while the time difference was approximately 3-4 ms between the discharge of CA3 PCs and INs of both regions (Fig. 16C,F; Fig. 17C-E; Table 4).

The sequence of the discharge of the different cell types suggests that during CCh-induced oscillations CA3 PCs excite both CA3 and CA1 INs that fire at latencies indicative of monosynaptic connections. At the same time, the firing of CA1 PCs was not driven by the discharge of CA3 PCs, i.e. the oscillation presumably propagates from the CA3 to the CA1 region via feed-forward inhibition. In order to prove this hypothesis, we have to reveal what determines the firing properties of the different cell types during oscillations. To investigate this, we recorded the excitatory and inhibitory synaptic currents of the same cells during oscillations and compared them to the firing activity of the neurons.

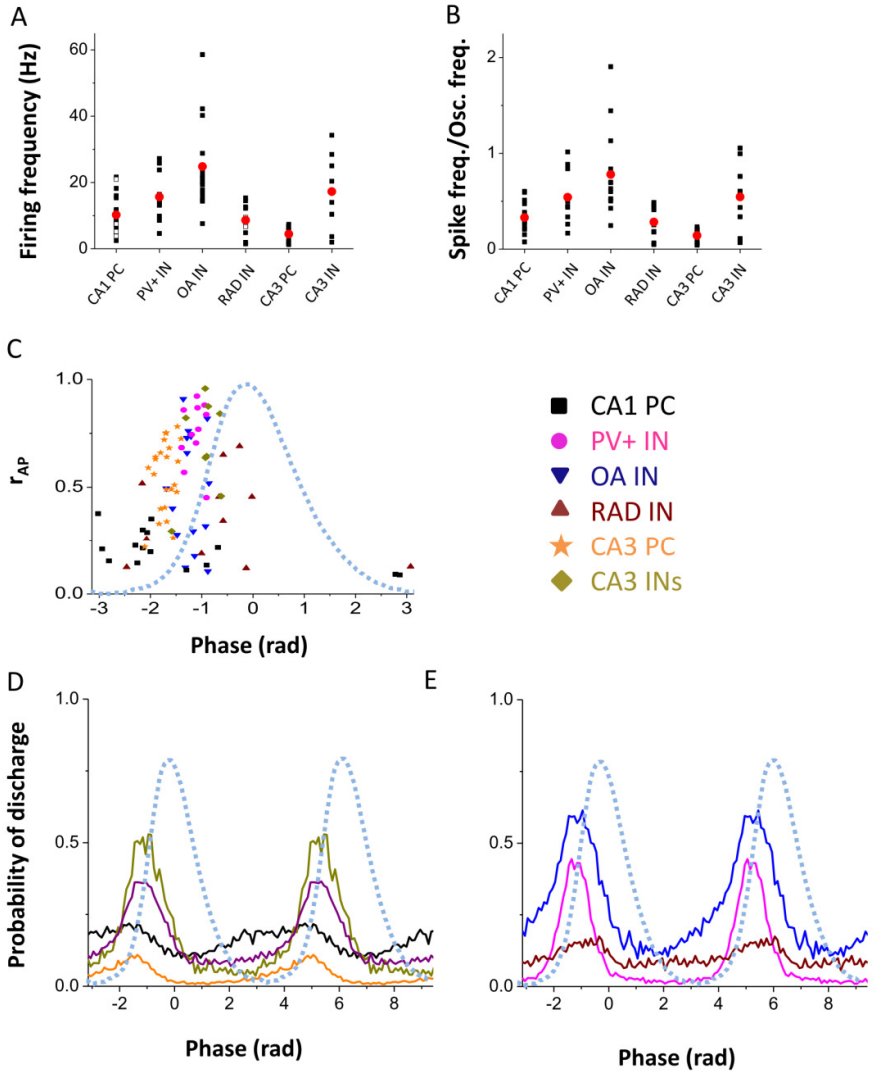

Figure 17. Firing properties of the different cell types during CCh-induced gamma frequency oscillations. **(A)** Firing frequency of the different cell types. Phase-coupled cells (Rp<0.01) are indicated with solid symbols and non-phase-coupled cells with open ones. Means are indicated with red dots. **(B)** The normalized spiking frequency of the phase-coupled cells of the different cell groups. **(C)** The strenght of phase- coupling of firing (r_{AP}) for each phase-coupled cell is plotted as a function of the mean gamma phase. **(D)** The probabilty of discharge for CA1 PCs, CA3 PCs, CA1 INs and CA3 INs as a function of the gamma-cycle. Here the data from all CA1 IN were pooled. Note that CA1 PCs tended to fire at the trough of the oscillation, CA3 PCs fired somewhat later, while both CA3 and CA1 INs fired most likely at the ascending phase of the oscillation. **(E)** As in D, but here the spiking probabilities of distinct CA1 IN types are shown. Different symbols and colors mark different cell types, coding is included in the figure. Dotted blue line shows the averaged field oscillation.

	rate (Hz)	spike freq./osc freq.	r_{AP}	Φ_{AP} (rad)
CA1 PC (n=15)	11.07±1.35	0.33±0.04	0.21±0.02	-2.25±0.23
PV+ IN (n=11)	15.65±2.18	0.54±0.08	0.75±0.04	-1.13±0.06
OA IN (n=15)	24.79±3.37	0.78±0.11	0.49±0.07	-1.22±0.07
RAD IN (n=11)	8.71±1.46	0.28±0.05	0.36±0.06	-1.03±0.37
CA3 PC (n=22)	4.44±0.46	0.14±0.01	0.54±0.03	-1.72±0.04
CA3 IN (n=8)	17.26±4.14	0.76±0.31	0.69±0.08	-0.97±0.13

Table 4. Firing properties of the different cell classes during CCh-induced *in vitro* gamma oscillations. Data are presented as mean±SEM.

6.2.5. The effects of synaptic inputs on the firing properties of the different cell types during CCh-induced gamma frequency oscillations

6.2.5.1. The properties of synaptic currents in the different cell classes

After recording the firing activity of the cells in loose patch mode, the pipette was withdrawn and whole-cell voltage clamp recordings were performed from the same neurons with a new pipette filled with a potassium-gluconate based intrapipette solution. EPSCs were recorded at the estimated reversal potential of IPSCs (~ -70 mV), while IPSCs were recorded at the estimated reversal potential of EPSCs (~ 0 mV). To characterize the synaptic currents of a cell, we determined the phase-coupling strength of EPSCs and IPSCs (r_e and r_i, respectively) as well as the phasic excitatory and inhibitory charge transfer, and correlated these values to the firing properties of the neurons. In order to define the phase-coupling strength of the synaptic currents, the phase of the peak current recorded in each cycle was calculated. Since we were primarily interested in how the gamma-modulation of the spiking of the cells is affected by their synaptic inputs, the comparison of synaptic inputs in the different cell types and the correlation analyses of synaptic inputs and firing properties were carried out only on those cells that showed significant gamma-modulation in their spiking activity.

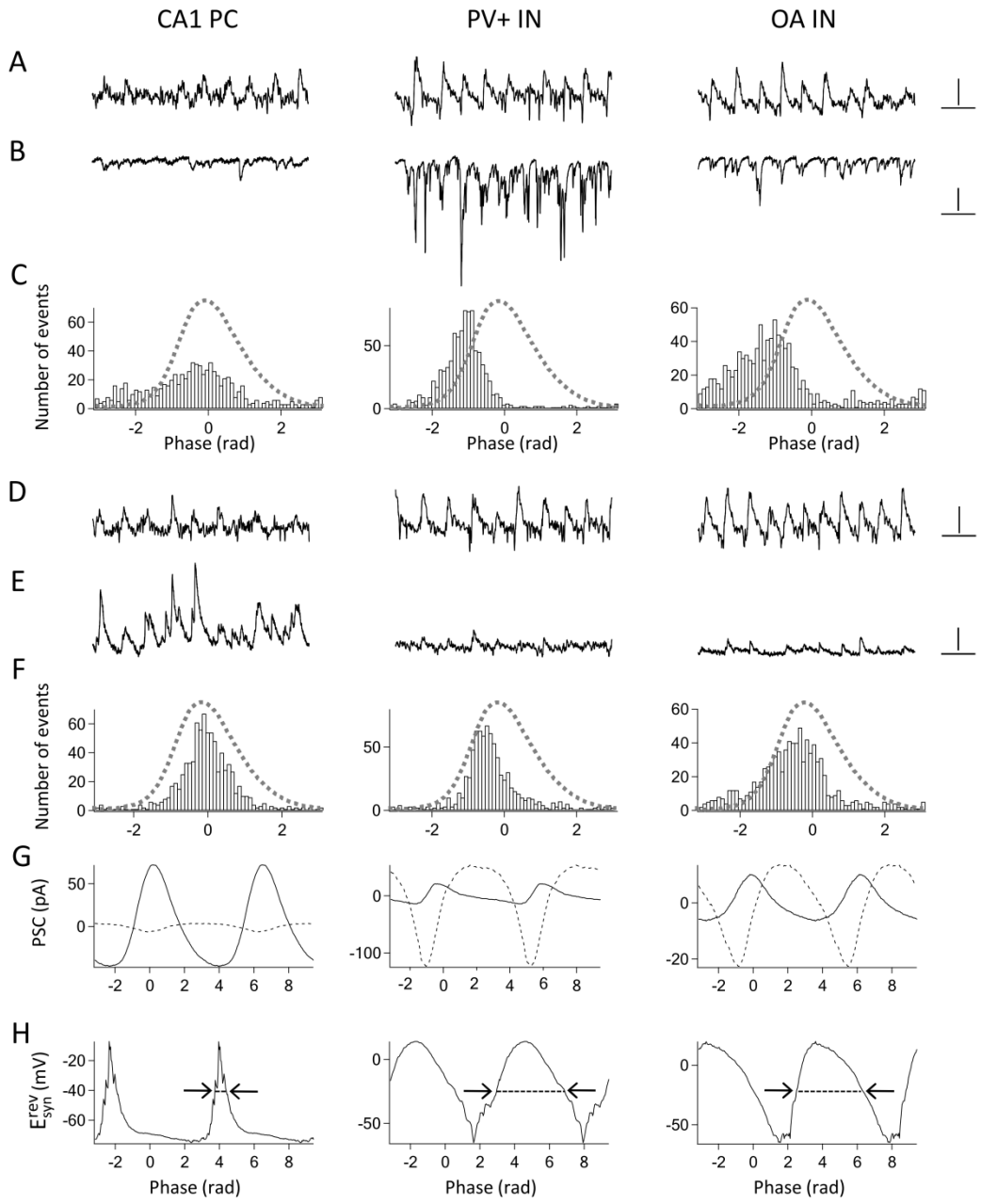

Figure 18/1. Postsynaptic currents of the different cell types during CCh-induced oscillations I. **(A, B)** Simultaneous recordings of field potential oscillations in the stratum pyramidale of the CA1 (A) and excitatory postsynaptic currents (EPSCs) recorded from a representative CA1 PC, PV+ IN and OA IN (B) (the same cells as in Fig. 17). EPSCs were recorded in whole-cell voltage-clamp mode at the estimated reversal potential of inhibitory currents (~ -70 mV). **(C)** The EPSC-phase histogram, of the cells showing the number of peak excitatory currents occurring at a certain phase of the oscillation during a 30-s-long recording epoch. **(D, E, F)**: The same as in A, B and C, but for inhibitory currents. IPSCs were recorded at the estimated reversal potential of EPSCs (~ 0 mV). Dotted line in C and F: average gamma cycle. **(G)** Cycle averaged PSCs in the given CA1 PC, PV+ IN and OA IN. Dotted line: EPSC, solid line: IPSC. **(H)** The net apparent synaptic reversal potential (E_{syn}^{rev}) as a function of the oscillatory cycle. Arrows indicate the half-width of the E_{syn}^{rev} curve. Note the differences in the half-width of E_{syn}^{rev}

curve between PC and most of the INs (see also Figure 18/2). Scale bars: 0.1 mV (vertical), and 0.05 s (horizontal) for field potential traces; and 100 pA (vertical), and 0.05 s (horizontal) for current traces.

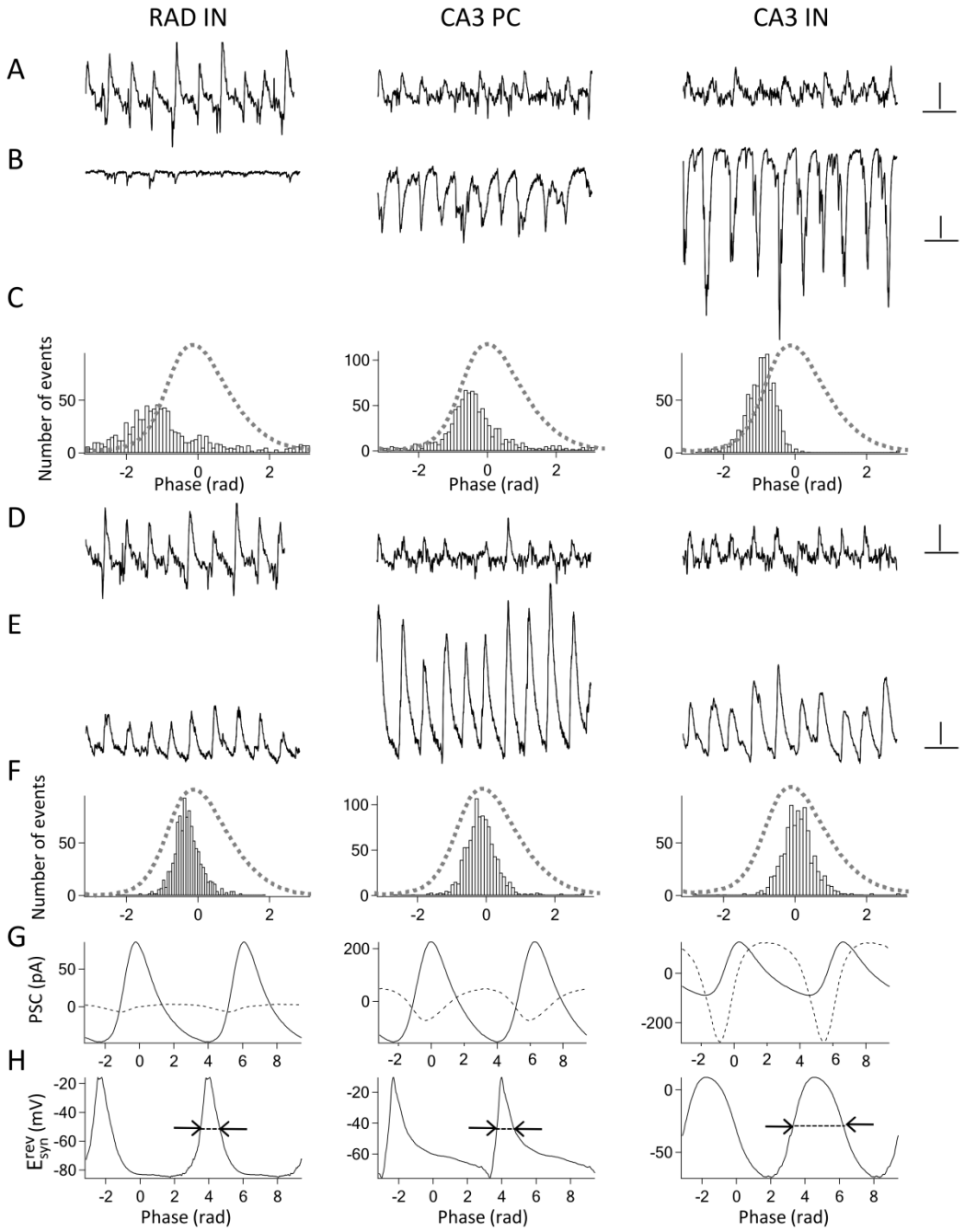

Figure 18/2. Postsynaptic currents of the different cell types during CCh-induced oscillations II. Panels are the same as in Figure 18/1, but from representative cells of the remaining groups: RAD IN, CA3 PC, CA3 IN. Data are from the same cells as in Figure 16. Dotted line in C and F: average gamma cycle. Scale bars: 0.1 mV (vertical), and 0.05 s (horizontal) for field potential traces; and 100 pA (vertical), and 0.05 s (horizontal) for current traces.

Both EPSCs and IPSCs were strongly phase coupled in all cell types, and there were no differences in the strength of phase-coupling of synaptic currents between the different cell types (Fig. 18/1-2 C,F; Fig. 19D,E; Table 5). However, there were significant differences in the amount of phasic charge transfer. CA3 INs got the largest phasic excitatory synaptic input among all cell types, while CA1 PCs the smallest. Among CA1 cells the largest phasic excitatory charge transfer could be measured in PV+ INs. Among CA1 interneurons RAD INs got the smallest phasic excitation. Significant differences in phasic excitatory charge (Q_e) could be detected only between PV+ INs and CA1 PCs ($p<0.001$), CA3 INs and CA1 PCs ($p<0.001$), CA3 INs and RAD INs ($p<0.001$), and CA3 INs and OA INs ($p<0.05$) (Fig. 18/1-2 B,C,G; Fig. 19A; Table 5).

Phasic inhibitory charge transfer was larger in CA3 PCs than in all other cell types ($p<0.001$ between CA3 PCs and all other cell groups in any possible comparisons). There were no differences in the amount of phasic inhibition between the different cell types of CA1 ($p=1$ in all comparisons) or CA1 cells and CA3 INs ($p>0.5$ in all comparisons) (Fig. 18/1-2 E,F,G; Fig. 19B; Table 5).

To see how the amount of synaptic excitation and inhibition related to each other within a cell type, we also calculated the ratio of phasic excitatory to inhibitory charge (Q_e/Q_i). Phasic inhibition exceeded phasic excitation in all pyramidal cells, in both CA1 and CA3 and also in some radiatum interneurons in CA1, whereas the dominant input was excitatory in most of the interneurons in both regions. Q_e/Q_i was significantly smaller in CA1 PCs than PV+ ($p<0.001$), O-A INS ($p<0.05$) and CA3 INs ($p<0.01$), and CA3 PCs and RAD INs of CA1 also had a significantly smaller Q_e/Q_i than PV+ INS in CA1 (CA3 PCs vs. PV+ IN: $p<0.001$, while CA1 RAD INs vs. CA1 PV+INs: $p<0.05$) (Fig. 18/1-2 G; Fig. 19C; Table 5).

In all cells the phase of the peak excitation preceded the phase of the peak inhibition. The peak excitation arrived on the cells between -1.5 and -0.6 radians on the ascending phase of the field oscillation, while the peak inhibition could be detected always somewhat later between -0.6 and -0.2 radians, closer to the peak of the field oscillation. Comparison of the mean phase of the peak current of EPSCs revealed significant differences between PCs and INs; the phase of peak excitation was significantly later in both CA1 PCs and CA3 PCs than in INs of both areas ($p<0.01$ in

all comparisons). On the other hand the mean phase of the peak of inhibitory input was on average somewhat later in PV+ INs and O-A INs in CA1 than in the other cell types ($p < 0.05$ in all cases when comparing these two groups with other cell groups) (Fig. 18/1-2 C,F, Fig. 23; Fig. 24; Table 5).

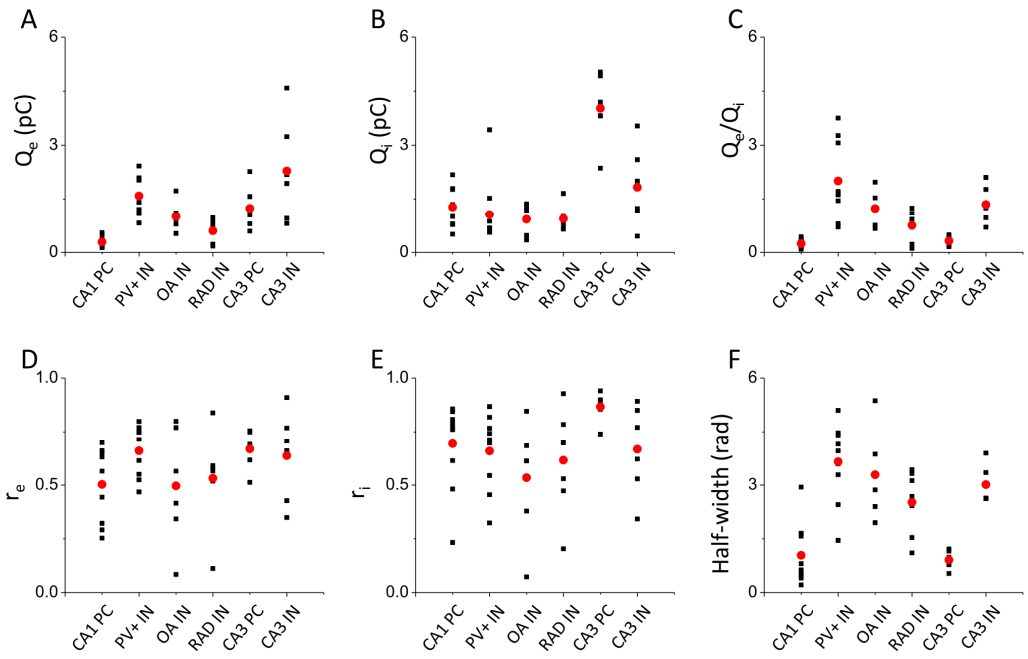

Figure 19. Properties of the synaptic currents measured in the different cell types. **(A, B)** The phasic excitatory (Q_e, A) and inhibitory charge transfer (Q_i, B) in the different cell classes. The differences in Q_e reached significance between CA1 PCs and PV+ INs ($p<0.001$) and CA1 PCs and CA3 INs ($p<0.001$), RAD INs and CA3 INs ($p<0.001$), and OA INs and CA3 INs ($p<0.05$); while CA3 PCs had a larger Q_i than all other cell types ($p<0.001$ in all comparisons between CA3 PCs and other cell types). **(C)** Phasic excitatory/inhibitory charge ratio (Q_e/Q_i) in the different cell types. CA1 PCs had smaller Q_e/Q_i than PV+ IN ($p<0.001$), OA IN ($p<0.05$) and CA3 IN ($p<0.01$), and the difference between Q_e/Q_i also reached significance between PV+ IN and RAD IN($p<0.05$) and PV+ IN and CA3 PC ($p<0.001$). **(D, E)** The phase-coupling strength of the peak EPSCs (r_e, D) and IPSCs (r_i, E) in the different cell types as measured by the phase of the peak time. No significant differences could be detected between these values of the different cell groups. **(F)** The half-width of the E_{syn}^{rev} curve of the different cell groups. The half-width was significantly smaller in both CA1 and CA3 PCs than in the interneurons ($p<0.05$ in all comparisons between PC and IN pairs).

If we are interested in how the synaptic inputs influence the spiking activity of the cells, besides analyzing the timing and magnitude of the excitatory and inhibitory PSCs, we have to be aware of their combined effects, too. To characterize the temporal relationship between inhibitory and excitatory synaptic conductances, the net apparent synaptic reversal potential E_{syn}^{rev} (see Methods) was calculated. E_{syn}^{rev} describes the

effective synaptic conductance during a cycle. There were clear differences in the shape of the E_{syn}^{rev} curve depending on the cell type. To capture these differences, the half-width of the peak of the E_{syn}^{rev} curve was measured. This half-width was significantly narrower in PCs in both CA1 and CA3 than in INs of both regions ($p<0.05$ in all comparisons). This reflects also that the dominant input received by PCs during the oscillation was inhibitory (Fig. 18/1-2 H; Fig. 19F; Table 5).

	r_e	r_i	Q_e (pC)	Q_i (pC)	Q_e/Q_i	Φ_e (rad)	Φ_i (rad)	E_{syn}^{rev}hw (rad)
CA1 PC (n=11)	0.5±0.05	0.69±0.06	0.29±0.04	1.27±0.15	0.24±0.04	-0.64±0.15	-0.18±0.12	1.04±0.25
CA1 PV+ IN (n=9)	0.66±0.04	0.66±0.06	1.59±0.19	1.06±0.31	2.00±0.36	-1.16±0.11	-0.62±0.12	3.65±0.37
CA1 OA IN (n=6)	0.50±0.11	0.53±0.11	1.01±0.16	0.92±0.18	1.23±0.20	-1.52±0.08	-0.54±0.08	3.29±0.5
CA1 RAD IN (n=7)	0.53±0.08	0.62±0.09	0.6±0.11	0.94±0.13	0.75±0.16	-1.23±0.15	-0.19±0.14	2.52±0.34
CA3 PC (n=6)	0.67±0.04	0.86±0.03	1.24±0.25	4.02±0.40	0.32±0.06	-0.66±0.09	-0.23±0.14	0.91±0.11
CA3 IN (n=6)	0.64±0.09	0.67±0.09	2.28±0.59	1.83±0.45	1.35±0.21	-1.21±0.11	-0.17±0.12	3.01±0.21

Table 5. The properties of synaptic inputs of the different cell classes during CCh-induced *in vitro* gamma-oscillations. Data are presented as mean±SEM.

6.2.5.2. Correlations between firing properties and synaptic currents in the different cell types

In order to see how synaptic inputs affect the firing properties of CA1 neurons during oscillations, the firing characteristics of phase-coupled cells were correlated to the properties of the synaptic inputs measured in the same cells.

As PV+ INs and O-A INs fired at higher rates than CA1 PCs and RAD INs and the phasic excitatory charge transfer was also larger in these cells, it was plausible to hypothesize that there is a correlation between excitatory charge and firing rate. Indeed,

when comparing these quantities over all CA1 cells, we found a strong positive correlation between Q_e and the firing frequency of the cells (R=0.495, p<0.01, n=33) (Fig. 20A). The ratio of excitatory and inhibitory charge (Q_e/Q_i) also correlated to firing rate (R=0.401, p<0.05, n=33) (Fig. 20B); however, there was no correlation between phasic inhibitory charge and firing frequency (R=0.063, p=0.728, n=33) (Fig. 20C). These data suggest that the firing rate of the cells is controlled primarily by the excitatory synaptic input.

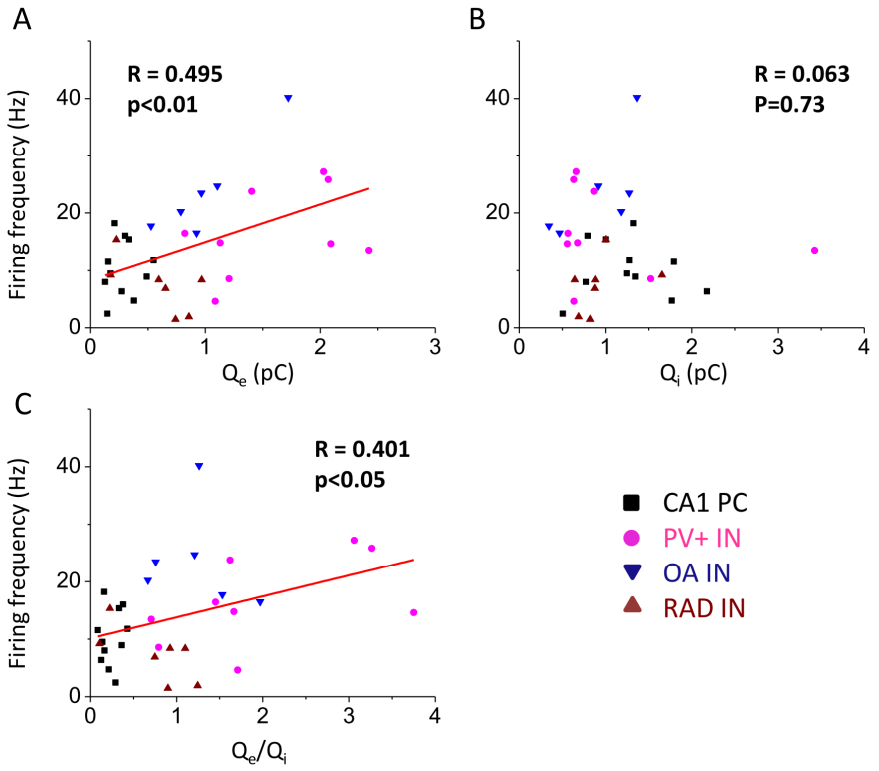

Figure 20. Correlations between the firing frequency and the phasic synaptic charge transfer among CA1 cells. **(A, B, C)** The firing frequency plotted against phasic excitatory (Q_e, A) and inhibitory charge transfer (Q_i, B) and phasic excitatory/ inhibitory charge transfer ratio (Q_e/Q_i, C) for individual CA1 cells. Significant correlations could be shown between the firing rate and Q_e and the firing rate and Q_e/Q_i. Different cell types are marked with different symbols, coding is included in the figure.

Interestingly, no correlation could be found between the excitatory charge transfer and the firing rate when it was tested for CA1 PCs only (data not shown, R=0.284, p=0.371, n=11). However, the correlation between Q_e and firing frequency reached significance, when it was tested on CA1 INs (data not shown, R=0.437, p<0.05, n=22).

In the case of interneurons not only the firing rate, but also the phase-coupling strength tended to depend on excitatory inputs. There was a positive correlation both between r_e and r_{AP} (R=0.675, p<0.001, n=22) and Q_e and r_{AP} among CA1 interneurons (R=0.664, p<0.001, n=22) (Fig. 21A,C). On the other hand no correlation could be observed between r_i and r_{AP} (R=0.326, p=0.138, n=22) or Q_i and r_{AP} (R=0.255, p=0.251, n=22) (Fig. 21B,D). The same correlations were found, when it was tested for all CA1 cells including INs and PCs (r_{AP} and r_e: R= 0.586, p<0.001; r_{AP} and Q_e: R= 0.596; p<0.001; r_{AP} and r_i: R=0.105, p=0.596; r_{AP} and Q_e: R= 0.055, p= 0.762; n=33, data not shown). However; in the case of CA1 PCs, which usually tended to fire less phase coupled than INs, we could not reveal any correlations of r_{AP} and synaptic inputs (r_{AP} and r_e: R= 0.359, p=0.278; r_{AP} and Q_e: R= 0.357; p=0.281; r_{AP} and r_i: R=0.147, p=0.666; r_{AP} and Q_e: R= 0.255, p= 0.251; n=11) (Fig. 21E-H).

To see whether the temporal interaction of phasic excitation and inhibition is important in controlling spike time, the width of E_{syn}^{rev} was correlated to the phase coupling strength of the action potentials. The correlation between these values reached significance only when it was tested for all CA1 neurons, including both PCs and INs. The r_{AP} was usually higher in INs, and this correlated well with the broader E_{syn}^{rev} curve observed in these cell types (R=0.474, p<0.01; n=33) (Fig. 21I).

These correlation analyses show that the more precise and robust excitatory input a CA1 IN receives, the more precisely it will fire during a cycle, while no such correlation could be observed in the case of CA1 PCs.

Similar correlations were found between the phase of firing and the synaptic inputs. The phase of firing correlated well with both the amount of excitation (Q_e) and the excitatory-inhibitory charge ratio (Q_e/Q_i) when tested in all CA1 neurons (Φ_{AP} and Q_e: R=0.503, p<0.05; ΦAP and Q_e/Q_i: R= 0.484, p<0.05, n =33) (Fig. 22A,C), however, no correlation could be observed between Q_i and Φ_{AP} (R=0.308, p>0.05, n=33) (Fig 22B) or r_i and Φ_{AP} (R=0.374, p>0.05, n=33) (data not shown). The phase of firing showed correlation also with the width of the E_{syn}^{rev} curve; cells with broader E_{syn}^{rev} curve tended to fire not only more precisely, but also later in the cycle (R= 0.633, p<0.05, n=33) (Fig. 22D).

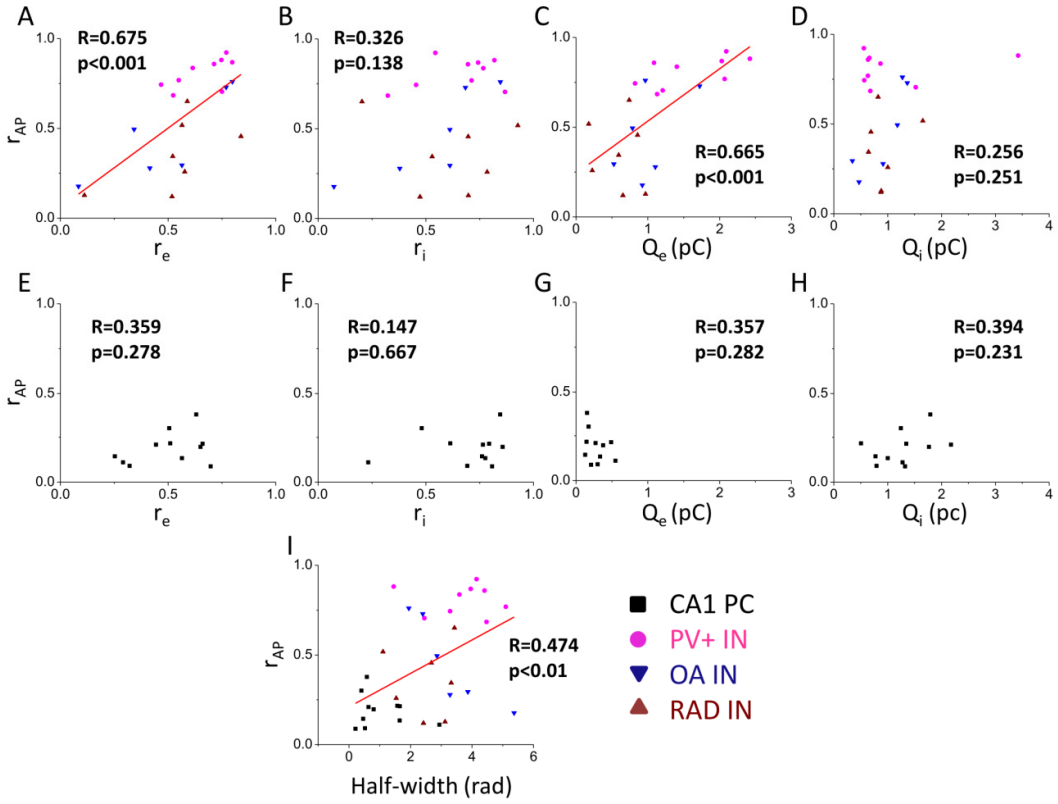

Figure 21. Correlations between the strength of action potential phase coupling (r_{AP}) and the synaptic inputs of the CA1 cells**. (A-H)** The phase coupling strength of the action potentials plotted against the phase coupling strength of excitatory (r_e) and inhibitory inputs (r_i) and phasic excitatory (Q_e) and inhibitory charge transfer (Q_i) for individual CA1 interneurons (A, B, C, D respectively) and pyramidal cells (E, F, G, H respectively). Significant correlations were found only between the properties of excitatory inputs (both r_e and Q_e) and the r_{AP} of interneurons. **(I)** Significant correlations could also be shown between r_{AP} and the half-width of the E_{syn}^{rev} curve when it was tested over all CA1 neurons. Different cell types are marked with different symbols, coding is included in the figure.

Interestingly, correlation between r_e and Φ_{AP} reached statistical significance only in the case of INs (R=0.522, p<0.05, n=22) (Fig. 22F), but failed to show a correlation when tested over all CA1 cells (R=0.310, p>0.05, n=33) (Fig. 22E). These results indicate again that the firing of INs is principally driven by their excitatory synaptic inputs. Although CA1 PCs receive their excitatory input with equally high temporal precision, the amount of excitation is presumably not strong enough to control the spike timing of these cells effectively.

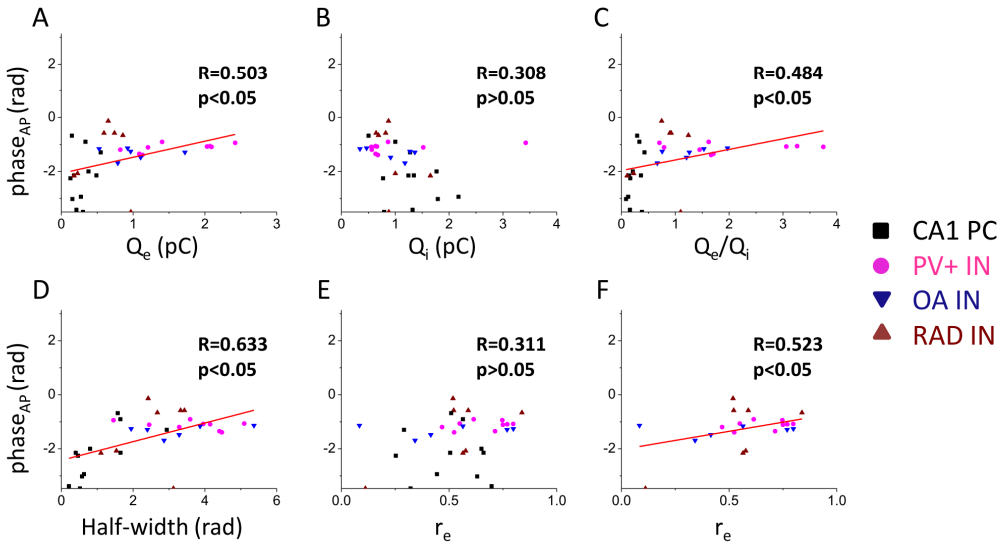

Figure 22. Correlations between the phase of action potentials (Φ_{AP}) and the synaptic inputs of the CA1 cells**. (A-C)** The phase of the action potentials plotted against phasic excitatory (Q_e, A) and inhibitory charge transfer (Q_i, B) and phasic excitatory/ inhibitory charge transfer ratio (Q_e/Q_i, C) for individual CA1 cells. Significant correlations could be shown between the Φ_{AP} and Q_e and Φ_{AP} and Q_e/Q_i when tested over all CA1 neurons. **(D)** The half-width of the E_{syn}^{rev} curve also correlated with Φ_{AP} when it was tested over all CA1 neurons. **(E, F)** The Φ_{AP} plotted against the phase coupling strength of peak excitation for all CA1 neurons (E) and for only INs of the CA1. Interestingly the correlation between r_e and Φ_{AP} reached significance only when it was tested for INs (F), but failed to reach significance when it was tested over all CA1 cells (E). The presented R and p values refer to the linear-angular correlation test (see Methods and Zar, 1999.), a least-squares fit line is shown. Different cell types are marked with different symbols, coding is included in the figure.

6.2.5.3. Phase and time relations between firing and synaptic inputs in the different cell classes

When comparing the phase of the analyzed events (Fig. 23; Table 4; Table 5), we noticed that the phase of peak excitation always preceded the phase of peak inhibition in each cell both in CA3 and CA1; the peak of phasic excitation occurred in the ascending phase of the field potential oscillation, while the peak of phasic inhibition could be observed close to the peak of the field potential oscillation. The phase of action potentials was slightly before or after the phase of the peak EPSC in the case of PV+

INs, O-A INs and most of the RAD INs in CA1 as well as in all CA3 INs (on average these phase differences translate to a time difference of 1-2 ms between the peak excitation and the action potentials of these cells according to a mean oscillation frequency of 31 Hz). However, the phase of action potentials occurred much earlier in CA1 PCs and some CA1 RAD INs than the phase of peak excitation (more than 8 ms earlier). CA3 PCs also fired earlier than their peak excitatory input, but still later in the cycle than CA1 PCs (2-3 ms later). The phase of peak inhibition occurred always later in a cycle then the phase of the action potentials in each recorded cell independently of the cell type or the region (always 2-5 ms later than the peak excitation in a given cell).

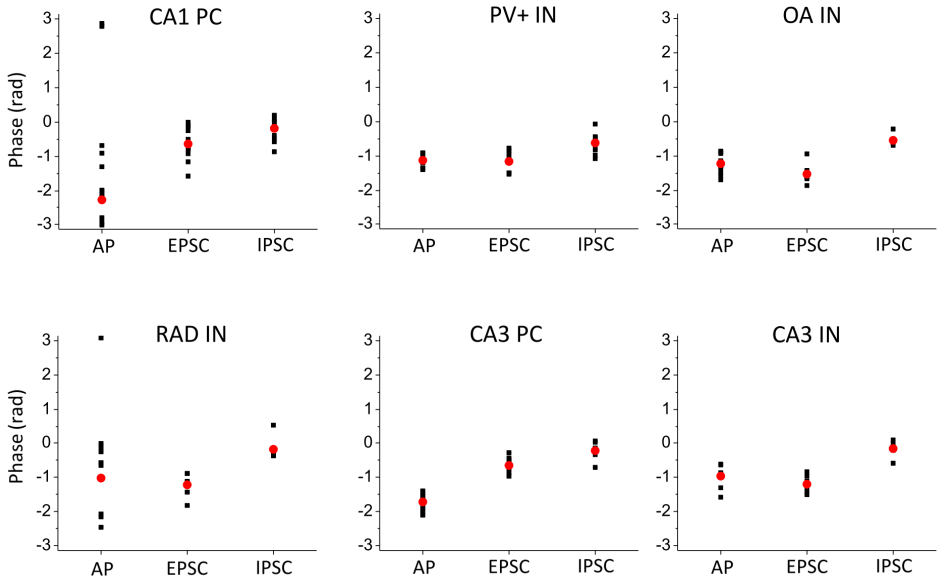

Figure 23. Phase of firing (AP), peak excitation (EPSC) and peak inhibition (IPSC) in phase-coupled ($Rp<0.01$) cells. Note that all neuron types both in CA1 and CA3 received both EPSCs and IPSCs in comparable phases of the oscillation. The action potentials tended to appear right after the peak excitation in the majority of INs, however spiking occurred much earlier than the peak excitation in the case of CA1 PCs, CA3 PCs and some RAD INs. Means are indicated with red dots.

Taken together all the data (Fig. 24), we can conclude that both PCs and INs of the CA1 subfield received the same excitatory input from CA3 PCs via the Schaffer collaterals, however, only the discharge of the CA1 INs was driven by this excitation. These results indicate that the oscillation propagates from the CA3 region to the CA1 via feed-forward inhibition, whereby CA3 PCs excite both CA3 and CA1 INs that fire at latencies indicative of monosynaptic connections. The spiking of CA1 PCs was less

precisely controlled; they probably fired persistently and stopped spiking when they received a strong synaptic inhibition during the oscillation cycle.

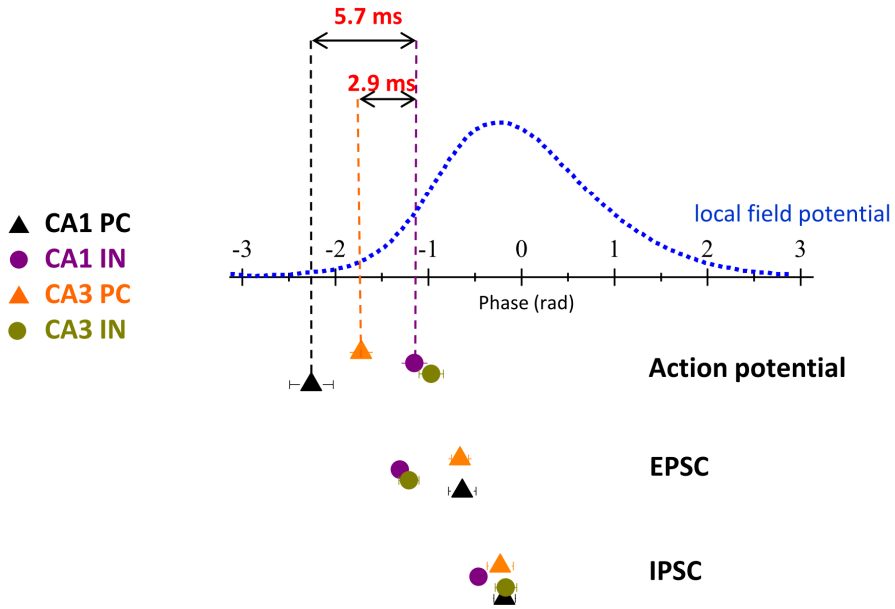

Figure 24. The time differences between the action potentials and the synaptic events recorded in the different cell types indicate that the gamma oscillation propagates from the CA3 to the CA1 region of the hippocampus via feed-forward inhibition. According to our results the average time difference between firing of CA3 PCs and INs of both CA1 and CA3 is 2.9 ms, however the time difference between the firing of CA1 PCs and INs is 5.7 ms on average. The timing of the action potential of the INs correlates well with the timing of their peak excitation and our hitherto presented results also indicate that the timing of the action potentials in INs is mainly controlled by their excitatory input during oscillations. These results indicate that CA1 INs –like CA3 INs -are discharged directly by their excitatory inputs from CA3 PCs. Symbols indicate the mean phases (±SEM) of the action potentials, peak excitation (EPSC) and peak inhibition (IPSC) in the different cell groups. Different symbols and colors mark different cell types, coding is included in the figure. Dotted blue line shows the averaged field oscillation. Bars indicate the mean action potential phase of the four major cell groups. PC: pyramidal cell, IN: interneurons.

7. DISCUSSION

The studies presented in this thesis explored the mechanisms that make the hippocampal network being capable of operating at certain frequencies. The first study addressed the questions what intrinsic properties the different cell types of the CA1 region of the hippocampus have that can be involved in the generation of network oscillations, and which ion channels are involved in forming these properties. The goal of the second study was to elucidate the synaptic mechanisms that underlie gamma frequency oscillations in the CA1 region of the hippocampus.

7.1. Resonance properties of different cell-types of the hippocampal CA1

In the first study we showed that the impedance profiles of neurons calculated from their voltage responses to sinusoidal current inputs differ in pyramidal cells and different classes of interneurons investigated in the CA1 region of the hippocampus. Using electrophysiological measurements combined with computational modeling we demonstrated that these differences arise primarily from differences in the activation properties of I_h, but the passive membrane properties of the cells also made significant contributions.

We found, in agreement with previous results, that the subthreshold resonance at theta frequencies in PCs is dependent on I_h (Hutcheon et al., 1996a; Pape and Driesang, 1998; Dickson et al., 2000; Hu et al., 2002; Fransen et al., 2004; Narayanan and Johnston, 2007). In addition to the I_h-mediated resonance, a so called M-resonance, produced by a depolarization-activated potassium current below the firing threshold has also been described in PCs (Hu et al., 2002; Peters et al., 2005; Hu et al., 2009). According to their findings this type of resonance occurs at about –60 mV, whereas the I_h-mediated resonance they observed was only seen below -70 mV. The apparent lack of M-resonance in our experiments can be explained by the fact that we observed I_h-

mediated resonance at -60 mV, suggesting that M-resonance might only be seen at more depolarized potentials, and possibly only above spike threshold under our conditions.

We found that horizontal interneurons of the stratum oriens were not uniform in their impedance properties. Although both O-R and OLM cells showed some frequency preference due to active membrane conductances, because of their high capacitance and low cutoff frequency the low-pass filter properties still dominated in OLM cells. Our results verify the earlier observations by Pike et al. (2000), in which some interneurons in the stratum oriens were shown to display resonance, and extend it by showing that not all oriens interneurons have the same high-pass characteristics. The finding that O-Rs and OLM cells have distinct impedance properties raises the possibility that similar synaptic input received by these two cell types (Blasco-Ibanez and Freund, 1995) may result in different discharge patterns during specific network events, such as theta and gamma rhythms or sharp-wave-associated ripple oscillations (Klausberger et al., 2003; Gloveli et al., 2005b; Lawrence et al., 2006a; Goldin et al., 2007; Jinno et al., 2007).

Previous studies (Aponte et al., 2006) and our observation that some FS PTI cells (2 out of 7) expressed a minor sag indicate that I_h could also be present in this cell type. However, I_h does not seem to have any effect on the impedance profile of these cells at the investigated potentials. Whereas I_h-mediated subthreshold resonance was negligible in FS PTIs (present study, Hutcheon et al., 1996a), these cells exhibited obvious resonance at gamma frequencies in a study by Pike et al. (2000). This type of resonance is mediated by activation of persistent voltage-dependent sodium channels, opening at membrane potentials positive to -60 mV. Thus, under our conditions this form of resonance would not be expected, since we obtained recordings only at or negative to -60 mV. However, it is apparent already at these subthreshold membrane potentials that their fast membrane time constant and correspondingly high cutoff frequency would allow these cells to be capable of transmitting high frequency inputs.

Since subthreshold resonance seemed to be related to the occurrence of the membrane potential sag, which also showed significant differences among the investigated cell types, our initial supposition was that distinct resonance properties could arise from the differences in I_h-properties among the different cell types. Our data revealed no significant differences between the absolute amounts of I_h-mediated conductance in the investigated cell types. However, as the observed differences in

apparent membrane capacitance probably reflect differences in membrane surface area, the conductance density could still differ substantially. Although it was not possible to directly determine the conductance density from our measurements, we can estimate the cell-type-dependence of this quantity by looking at the ratio of the measured absolute conductance and the average membrane capacitance (as estimated from current clamp experiments) in the different cell types. This comparison suggests that differences in I_h conductance density may indeed be substantial, with O-Rs having an approximately two-fold higher density than PCs and OLM cells, which may explain the stronger resonance observed in O-Rs.

Our experiments also revealed that a significantly larger amount of I_h was activated in PCs than in interneurons at physiologically relevant potentials (above –90 mV), where the resonance properties were investigated. PCs are known to express HCN-channels mainly on their distal dendrites (Magee, 1998; Lőrincz et al., 2002); therefore the differences in I_h activation might be explained by space clamp limitations. However, analysis of the activation kinetics of I_h in the distinct cell types precluded this interpretation, as more distal localization would imply slower apparent kinetics, which is opposite to our findings.

We found a clear difference in the kinetics of I_h between PCs and interneurons. Not only the time course of activation but also the relative proportion of components with a slow and a fast time constant and its change with the membrane potential were different in PCs and interneurons (Fig. 10G). It has been shown that the activation kinetics of HCN channels are predominantly determined by the relative contribution of HCN channel isoforms to the composition of homomeric or heteromeric channels (Santoro et al., 2000); therefore, one possible explanation for these differences in the activation characteristics of I_h in hippocampal neurons is different subunit compositions of HCN channels. Indeed, both immunohistochemical (Brewster et al., 2002; Notomi and Shigemoto, 2004) and *in situ* mRNA hybridization studies (Santoro et al., 2000; Bender et al., 2001; Brewster et al., 2007) suggest that while PCs express mainly HCN1 and HCN2 in their distal dendrites, the proportion of HCN2 and HCN4 (subunits which contribute to slower activation kinetics of I_h; Franz et al., 2000; Santoro et al., 2000; Ishii et al., 2001) is much larger in the stratum oriens, suggesting that they are likely to be expressed in interneurons. Of course we cannot exclude the possibility that various

elements of the neuronal membrane, such as putative auxiliary subunits, scaffolding proteins or cytoskeletal proteins (Wahl-Schott and Biel, 2009) interact with the HCN channels and may also influence the properties of I_h in the distinct hippocampal neurons.

Our computational model strengthened the idea that I_h is the major determinant of the impedance characteristics at subthreshold membrane potentials in hippocampal neurons. However, our result that in stratum oriens interneurons a smaller degree of resonance was observed than that predicted from the model suggests that some other conductances might also be active at these membrane potentials in these particular cell types and dampen the effect of I_h on the impedance profile. The inward rectifier K^+ current might be a good candidate for this effect, as suggested by both theoretical and experimental studies by Hutcheon and colleagues in neocortical neurons (Hutcheon et al., 1996b, a).

7.1.1. Physiological relevance

Several studies have shown that I_h substantially promotes firing when the fluctuation in the membrane potential can activate a sufficient number of HCN channels (Manseau et al., 2008). Importantly, if such fluctuation occurs simultaneously in several PCs even after the activation of a single perisomatic inhibitory cell (Cobb et al., 1995), then a large number of principal neurons could discharge action potentials synchronously, contributing to rhythm generation at theta frequencies. Thus, activation of I_h near or below the spike threshold might indeed be important for oscillatory activities (Kocsis and Li, 2004). This has been directly demonstrated in hippocampal slices, where blocking of I_h diminished the synchronous firing of pyramidal cells at theta frequencies (Cobb et al., 2003). Our voltage-clamp data support these results, since a substantial proportion of HCN channels in pyramidal cells was activated at the resting membrane potential. In contrast, a much lower proportion of HCN channels would be open at resting membrane potential in OLM cells and O-Rs, which is in line with the findings that interneurons in the stratum oriens exhibited less obvious membrane potential oscillations at theta frequencies (Chapman and Lacaille, 1999).

The activation curve of I_h can be profoundly shifted by cyclic nucleotides, which are regulated by G-protein coupled receptor activation (Chen et al., 2001); therefore, subcortical neurotransmitter systems acting on these receptors could significantly affect the opening of HCN channels. Thus, theta frequency membrane potential oscillations as well as the impedance of the interneurons that express HCN channels can be modulated in a state-dependent manner (Maccaferri and McBain, 1996; Gasparini and DiFrancesco, 1999; Placantonakis et al., 2000; Bickmeyer et al., 2002; Rosenkranz and Johnston, 2006), controlling their recruitment into network activity.

I_h has been shown to influence the occurrence of dendritic spikes (Tsay et al., 2007) and the amplitude of EPSPs (George et al., 2009) by interacting with other voltage-gated ion channels, such as N- or T-type Ca^{2+} channels or the so-called M-current mediated by voltage-gated K^+ channels. Therefore the observation that I_h is activated at more hyperpolarized potentials in oriens interneurons than in pyramidal cells might also be important in understanding the differences in dendritic signal-processing mechanisms of these cells.

While several studies have measured the impedance amplitude in various cell types, much less has been known about the phase of the impedance. We determined and compared the impedance phase profiles of four types of hippocampal neuron. In the three "resonant" cell types in our study, positive as well as negative phase shifts could be seen depending on the frequency. Since I_h works effectively as an inductive element in the membrane, it can produce a significant positive phase shift in the voltage response of the cell to an oscillatory input. Both theoretical and experimental studies suggest that this feature of I_h might be important in many processes including control of spike timing (Lengyel et al., 2005; McLelland and Paulsen, 2009) and synaptic plasticity (Narayanan and Johnston, 2007, 2008). Specifically, during oscillations, the phase of the impedance quantifies the phase shift of the cell's membrane potential oscillation relative to the phase of its rhythmic current input. A positive phase shift is especially interesting, since it leads to an apparent paradox whereby the cell's response seems to lead the corresponding change in its input - although this holds in a rigorous sense only for regular sinusoidal oscillations. The fact that distinct classes of hippocampal cells show well-defined, cell-type-specific impedance amplitude and phase-response characteristics may indicate a crucial role of these cellular properties in

the complex dynamics involved in information processing in the central nervous system.

7.2. Gamma-frequency oscillations in the CA1 region of the hippocampus

In the second study the properties of gamma oscillations were investigated in the CA1 region of the hippocampus. We determined that gamma frequency oscillations propagate from the CA3 region, where they are initially generated, to the CA1 region via feed-forward inhibition. By analyzing the synaptic inputs of the different cell types we could prove that the major drive of the oscillation in CA1 is the excitatory input arriving on the local INs via the Schaffer collaterals.

To study the mechanisms underlying the propagation of oscillations from CA3 to CA1 in hippocampal slices we first improved the recording conditions by introducing a novel type of slice chamber with a dual superfusion system. This type of submerged chamber ensures a better metabolic supply for the cells in slice tissues and therefore enables the investigation of high energy consuming neuronal activities, such as network oscillations.

Earlier investigations into the cellular mechanisms underlying network oscillations have been hampered by the transient nature of the induced activity in submerged conditions (McMahon et al., 1998; Kawaguchi, 2001; Gloveli et al., 2005b) as compared to interface conditions (e.g. Whittington et al., 1995; Fisahn et al., 1998; Sanchez-Vives and McCormick, 2000; Kubota et al., 2003). In a recent study of our research group we showed that the local oxygen level is critical for generation and propagation of both spontaneously occurring sharp wave ripple oscillations and cholinergically induced high-frequency oscillations (Hájos et al., 2009). Optimizing the chamber design for laminar flow of superfusion fluid and increasing the flow rate of the fluid enhanced the oxygen supply of the slices and enabled better recording conditions. Superfusing both surfaces of the slice reduces the one sided chemical gradients within the slice and therefore improves the recording conditions even further. These improvements allow studies of neurons under more realistic conditions of network activity, which are essential for a better understanding of neuronal network operation.

By using the double superfusion chamber, we could reliably record network oscillations at gamma frequencies in the CA1 region of hippocampal slices. The frequency of the oscillation induced in our experiments was somewhat lower than the

gamma frequency oscillations observed *in vivo*. However, considering that the frequency of gamma oscillation strongly correlates with the temperature (Dickinson et al., 2003; Gulyás et al., 2010), and our recordings were carried out at 32 °C, it is very likely that the difference between the average oscillation frequencies *in vivo* and *in vitro* arises primarily from the difference in the recording temperature.

In spite of this apparent difference in the frequency profiles of the network activities, the CCh-induced gamma oscillations in the CA1 shared many features of the *in vivo* recorded gamma oscillations in terms of spiking properties of the different cell types. Our data are in agreement with the data presented in a study of Csicsvári et al. (2003), where they recorded unit activity of pyramidal cells and unidentified interneurons of the CA1 and CA3 regions of the hippocampus and correlated it to the ongoing network activity of the behaving animal. First, they also found that both pyramidal cells and interneurons tended to be phase locked to gamma oscillations, but the proportion of gamma-modulated cells was higher for interneurons in both CA1 and CA3 (> 75 %) compared to pyramidal cells (< 43%). Second, a similar sequence of discharge of the different cell types within a gamma cycle was revealed to what we found in our study: the discharge probability of pyramidal cells in the gamma cycle reached a maximum earlier than interneurons in both CA3 and CA1 regions. Third, while both CA1 and CA3 interneurons discharged after CA3 PCs with time lags accounting for monosynaptic delays, the time lag between the discharge of CA1 PCs and CA1 INs was too long to be taken as a monosynaptic excitation, as CA1 PCs fired earlier than CA3 PCs within the cycle.

Another *in vivo* study by Tukker and colleagues (2007) investigated the activity of different anatomically identified cell types of the CA1 region during spontaneously occurring gamma oscillations in the anaesthetized animals. Comparable to our observations, PV+ INs were found to be strongly phase coupled to the ongoing gamma oscillation also under these circumstances.

Fast spiking PV-expressing perisomatic region targeting interneurons have been shown to play a key role in generating gamma frequency oscillations in hippocampal CA3 (Fuchs et al., 2007; Gulyás et al., 2010) and also in other cortical areas (Cardin et al., 2009; Sohal et al., 2009), therefore the strong gamma-modulation of their firing was expected also under our recording conditions. It has to be noted though, that the group

of PV+ interneurons with somata within or close to the stratum pyramidale comprises at least three functionally distinct cell types: fast spiking basket cells, bistratified cells and axo-axonic cells (Freund and Buzsáki, 1996). Under our experimental conditions the population of PV+ cells was found to be rather homogenous in terms of both firing activity and synaptic inputs, therefore we did not make any distinction among these cells. These findings also indicate that not only the perisomatic region targeting PV+ cells, but also the dendritic region targeting bistratified cells showed rather strong phase-coupling, just as it was found by Tukker et al. (2007), which means that not only the somatic, but also the dendritic region of CA1 pyramidal cells receive strong gamma-modulated inhibitory inputs. A periodic fluctuation of the membrane potential at the somatic and concomitantly at the dendritic region could have an important effect on both the integrative properties and the spiking output of the pyramidal cells during special behavioral states that are associated with gamma oscillation in the hippocampus.

We decided to collect data from perisomatic region targeting neurons only from the PV+ eGFP mouse, since we definitely wanted to make a distinction between CCK-expressing and PV-expressing perisomatic region targeting neurons in this study. Therefore, at the moment, we do not have any information about the behavior of CCK-containing basket cells in the CA1 during CCh-induced *in vitro* oscillations. In the *in vivo* experiments of Tukker et al. (2007), most of the CCK-immunopositive cells were phase locked to the gamma oscillation, though less strongly than PV-containing cells, and they tended to fire closer to the trough of the oscillation, similar to pyramidal cells. CCK-containing basket cells express M1/M3 receptors, and therefore their excitability and consequently their firing rate is probably increased upon cholinergic activation (Cea-del Rio et al., 2010; Cea-del Rio et al., 2011). However, in the presence of 10 μM CCh the GABA-release of CCK-expressing cells is significantly reduced (Fukudome et al., 2004; Neu et al., 2007). Therefore, we assume that the contribution of this cell type to the generation of CCh-induced gamma frequency oscillations in hippocampal slices would be negligible (see also Gulyás et al., 2010). Nevertheless, further investigations are required to clarify the exact role of CCK-expressing basket cells in the generation or modulation of hippocampal gamma oscillations.

The group of oriens–alveus interneurons in our study also fired phase locked to the gamma oscillations with a rather high rate. This cell group contained mainly O-LM

cells, and also some other INs that resembled in morphology to those cells that were classified as O-R cells in the first study. Though both of these cell types showed intrinsic frequency-preferences towards the theta frequencies in the first study, during CCh-induced gamma oscillations they fired at relatively high frequencies (~25 Hz on average), and some of them fired even doublets of action potentials. Analogous cell types of CA3 showed similar firing properties during CCh-induced oscillations (Hájos et al., 2004; Oren et al., 2006). On the other hand OLM cells of the hippocampal CA3 fired at somewhat lower frequencies (closer to theta frequencies) during kainate-induced transient gamma oscillations (Gloveli et al., 2005b). In the anaesthetized animal OLM cells showed no tendency of firing phase locked to the spontaneously occurring gamma (Tukker et al., 2007). Since OLM cells express M3 muscarinic ACh receptors (Lawrence et al., 2006a; Lawrence et al., 2006b), it is likely that in the presence of CCh they became depolarized and more excitable, which could account for their relatively higher firing rates under our recording conditions. The observation that OLM cells may show different behavior during different sorts of gamma frequency oscillations, depending on the conditions, suggest that gamma rhythmogenesis might be associated with various underlying physiology.

RAD INs showed large similarity in their behavior to the same cell types found in the CA3 region (Hájos et al., 2004). On average these interneurons showed relatively weak coupling to the oscillation and had the lowest firing rate among interneurons. It has to be noted though that the group of RAD INs showed also the most heterogeneous behavior among the investigated cell types. This heterogeneity might arise from the heterogeneity of the various cell types included in this group and also from their differentially modulated synaptic inputs.

7.2.1. The properties of synaptic inputs of the different cell types during CCh-induced gamma oscillation in CA1

A major advantage of the *in vitro* technique is that it allows to record intracellularly from visually identified neurons and therefore makes it possible to reveal the characteristics of synaptic connections of the functional network that underlies the given network activities. Since our major question regarded the way of propagation of

the oscillation from the CA3 to the CA1 region of the hippocampus, we analyzed our data from this point of view.

The most striking difference could be observed in the amount of synaptic excitation received by the pyramidal cells and the interneurons in CA1. The largest excitatory currents in a given gamma cycle were measured in PV+ INs. This observation is in line with previous results obtained in CA3 (Oren et al., 2006).

The differences found between the cell types were even more robust, when the ratio of excitatory to inhibitory charge (Q_e/Q_i) was compared among them. Since the Q_e/Q_i value is a self normalized value in each cell, it could be used as a more informative measure to compare the actual synaptic drives between the cell groups. In the Q_e/Q_i values the largest difference could be seen again between PV+ INs and PCs; excitation dominated over inhibition in PV+ IN, while inhibitory synaptic currents exceeded excitatory currents in all pyramidal cells.

When analyzing the timing of the events, we could see that excitation always preceded inhibition in all cells; the peak of excitation could be observed at the ascending phase of the oscillation, while the peak of inhibition occurred somewhat later, close to the peak of field potential oscillation. The excitatory inputs arrived in comparable phases to all cells, though the phase of peak excitation occurred slightly later in PCs than in INs. Systematic differences have been reported in the kinetic parameters of the excitatory currents between pyramidal cells and interneurons (Gloveli et al., 2005b), showing that EPSCs in pyramidal cells have slower rise and decay kinetics than in interneurons. Interneurons tend to have larger number of AMPA receptors (Nusser et al., 1998) with different molecular composition (Geiger et al., 1995), which in turn, endows them with faster kinetics (Geiger et al., 1997). It also has to be considered in the interpretation of the data that pyramidal cells receive their excitatory inputs mainly on their distal dendritic spines (Megias et al., 2001) and therefore, space clamp limitations could also influence our measurements. It is striking however, that neither CA1 and CA3 PCs nor CA1 and CA3 INs showed any differences in the phase of their peak excitatory input. We can presume therefore that the slight differences observed in the phases of the excitatory events primarily arise from the above mentioned differences, and both pyramidal cells and interneurons receive their excitatory inputs from a common single phase-coupled source, namely the CA3

pyramidal cells. The time differences between the EPSC peaks in CA1 neurons and the firing of CA3 pyramidal cells and the similarities between the shape of the event phase histogram of the spiking activity of the CA3 PCs and the excitatory events of basically all CA1 cells also supports this conclusion. Finally, the fact that no difference was found in the precision of EPSCs of the investigated cell types also in alignment with this assumption.

Surprisingly, even OA INs appeared to receive their main excitatory input from the same source, i.e. from CA3 PCs. OA INs are usually considered as feedback interneurons, since they receive 60-70% of their glutamatergic inputs from their main target cells: the local pyramidal cells (Blasco-Ibanez and Freund, 1995). However, it seems like that under our recording conditions their phase-locked firing during gamma oscillation is primarily driven by phasic excitatory input originated from CA3 PCs. In a recent study of Croce et al. (2010) the authors revealed that CA3 PC feed-forward and CA1 PC feedback synapses onto OA INs differed in their receptor expression pattern and also in their plasticity properties. These cell type- and afferent-specific rules of synaptic transmission and plasticity suggest that OA INs might be recruited into network activities in various ways depending on the circumstances. It is conceivable for instance that under high cholinergic tone OA INs tend to receive increased CA3 feed-forward and/or suppressed CA1 feedback inputs.

When comparing the inhibitory inputs of the neurons, we found that the absolute inhibitory charge was much larger in CA3 PCs than in any other cell type. This observation is in agreement with the recurrent model of gamma oscillogenesis within the CA3 area uncovered in rat hippocampal slices (Oren et al., 2006). While the amount of phasic inhibitory charge was smaller in CA1 PCs than in CA3 PCs, no significant difference could be found in the ratio of phasic excitatory to inhibitory charge between the two pyramidal cell populations.

Interneurons are likely to receive synaptic inhibition from numerous subpopulations of GABAergic cells, yet the inhibitory inputs were rather homogenous among them in both precision and timing. Though the mean of peak inhibition was somewhat later in OA INs and PV+ INs of CA1 than in the other cell types, these differences could be explained by the diversity of IPSC kinetics of the various types of hippocampal interneurons (Hájos and Mody, 1997). The high synchronicity in the

inhibitory drive of all investigated cell groups could be supported also by the electrical coupling present between GABAergic interneurons (Deans et al., 2001; Hormuzdi et al., 2001; Buhl et al., 2003).

7.2.2. What determines the firing activity of hippocampal CA1 neurons during CCh-induced *in vitro* gamma oscillations?

The correlation analysis of synaptic currents and spiking properties of the cells showed that the firing behavior of interneurons (in terms of firing rate, phase-coupling strength and phase of firing) strongly correlated with the properties of their excitatory inputs, showed no correlation however with their precisely timed inhibitory inputs. These results suggest that the behavior of CA1 INs during CCh-induced oscillations is mainly determined by their excitatory drive arriving from CA3 PCs.

In contrast, neither the excitatory nor the inhibitory input properties correlated with the firing activity in the case of CA1 PCs. Then what determines the firing properties of CA1 pyramidal cells during gamma oscillations?

Though both EPSCs and IPSCs of CA1 PCs were strongly phase locked to the ongoing oscillation and the ratio of excitatory to inhibitory charge was very similar in CA1 and CA3 PCs, pyramidal cells in the two hippocampal regions showed clearly different firing properties. While CA3 PCs fired phase locked close to the trough, but at the early ascending phase of the oscillation, CA1 PCs fired only weakly phase coupled and significantly earlier within an oscillation cycle. Moreover, many CA1 PCs did not show any gamma modulation at all.

The precise phase-coupled firing of CA3 PCs is determined by their dominant inhibitory input (Oren et al., 2006). Though no direct correlation could be shown between the firing properties of CA1 PCs and their synaptic currents, CA1 PCs apparently tended to fire when they received no or just minor inhibition during the cycle. (See Fig. 23 or compare the event phase histograms of the individual cells in Fig. 15 and Fig. 18/1-2).

The firing properties showed significant correlations with both Q_e and Q_e/Q_i when tested over all CA1 neurons, and both the precision and the phase of firing depended on the half width of the E_{syn}^{rev} curve of the cells. These results suggest that the

firing activity of a given cell during CCh-induced gamma oscillations is primarily determined by the relations and combined effects of its synaptic inputs.

Although there were no differences in the strength of phase coupling of the synaptic inputs of the different cell types, because of the differences in the amount of phasic excitatory and inhibitory charge transfer, the concomitantly arriving excitatory and inhibitory inputs were different in the case of PCs and INs in CA1. These differences are reflected in the differences of the width of the E_{syn}^{rev} curve and very likely to form a different time window for firing for PCs and INs. The firing properties of the interneurons are primarily driven by their strong and precisely timed excitatory inputs, while PCs could fire only when they receive reduced inhibition. As a result PCs fire earlier and less phase-coupled than interneurons.

While the enormous inhibitory input of CA3 PCs provides a precisely controlled output of this cell group (Oren et al., 2006), the inhibitory input in CA1 PCs is apparently not so effective, and therefore CA1 PCs fire in a less regulated way. The high cholinergic tone probably increases the excitability of all pyramidal cells in the hippocampus (Storm, 1989; Madison et al., 1987; Gulledge and Kawaguchi, 2007). The larger mean firing frequency of CA1 PCs, however, indicates that CA1 PCs might be more susceptible of firing spontaneously due to the cholinergic receptor activation (see also Dasari and Gulledge, 2011).

The firing behavior of a cell predicted the shape of the E_{syn}^{rev} curve with high precision and vica versa. RAD INs having similar E_{syn}^{rev} curves as CA1 PCs showed also similar firing patterns. This observation raises the issue though, whether the suppressed excitatory input observed in these cells is the result of the increased cholinergic tone and can have physiological relevance or just an *artefact* of the acute slice preparation.

Certainly, we cannot rule out the possibility that some connections within the network are more likely to get injured during the preparation than others. However, it has been reported in several studies that the glutamatergic transmission at Schaffer collateral-CA1 PC synapses is significantly reduced in the presence of CCh (Hasselmo and Schnell, 1994; Scanziani et al., 1995; Shirey et al., 2008; Dasari and Gulledge, 2011), therefore it is more likely that the relatively small absolute excitatory charge recorded in CA1 PCs is primarily due to the increased cholinergic tone in the slice. The suppression of glutamate release at these synapses is predominantly mediated by

presynaptic M4 receptors of the Schaffer collaterals (Shirey et al., 2008; Dasari and Gulledge, 2011). Since M4 receptors are present in high densities in the stratum radiatum of CA1 (Levey et al., 1995), it could be expected that at least some type of the radiatum interneurons also receive suppressed glutamatergic inputs in the presence of CCh.

7.2.3. Physiological relevance

Several lines of studies have demonstrated that the increased cholinergic tone play a crucial role in the encoding of new memories. The effects of ACh on memory-formation have been investigated in rats, monkeys and even in human subjects in different learning tasks (Atri et al., 2004; Tang et al., 1997; Winters and Bussey, 2005). The blockade of muscarinic cholinergic receptors appears to impair the encoding of new memories, but not the retrieval of previously stored memories (Atri et al., 2004), and also tend to impair working memory for some stimuli (Green et al., 2005). On the other hand, increasing the level of hippocampal ACh impairs long term memory (Bunce et al., 2004; Gais and Born, 2004), possibly by interfering with consolidation.

Both pharmacological and modeling studies indicate that ACh may facilitate the learning of new information by enhancement of the influence of afferent input relative to excitatory feedback (Hasselmo and McGaughy, 2004). For instance, in hippocampal CA3 ACh enhances the afferent excitatory inputs from the EC and from the DG through nicotinic receptors (Giocomo and Hasselmo, 2005; Radcliffe et al., 1999), but suppresses the feedback recurrent excitation through muscarinic receptors (Hasselmo et al., 1995; Vogt and Regehr, 2001). The muscarinic receptor activation also suppresses excitatory transmission of the Schaffer collaterals in stratum radiatum of CA1 (Fernandez de Sevilla and Buno, 2003; Hasselmo and Schnell, 1994; Dasari and Gulledge, 2011), but not as much in stratum lacunosum moleculare, where the EC layer III input terminates (Hasselmo and Schnell, 1994). These data are in agreement with behavioral studies showing that high cholinergic tones during waking reduce the influence of hippocampus on the EC and provides dominant feed-forward effects appropriate for encoding (Chrobak and Buzsáki, 1994), while low ACh level during slow wave sleep is critical for declarative memory consolidation (Gais and Born, 2004).

In addition, ACh also activates intrinsic mechanisms that will increase the excitability of the pyramidal cells. The persistent spiking of neurons in the absence of synaptic transmission might be important in allowing maintenance of novel information without prior synaptic modification (Klink and Alonso, 1997; Fransen et al., 2006; Tahvildari et al., 2007).

At the same time the timing of the afferent input relative to the gamma cycle might be important in determining the amplitude, timing and precision of the evoked responses of PCs (Cardin et al., 2009). The synchronized inhibitory postsynaptic potentials evoked by PV+ INs innervating the perisomatic and dendritic regions of the PCs could provide a framework for gating the information processing in a temporally specific manner. It is important therefore to synchronize the firing of PV+ INs very precisely. The precise firing of PV+ INs is regulated by their massive excitatory drive during oscillations (present study, Oren et al., 2006; Fuchs et al., 2007). Unaltered spatial reference memory but impaired spatial working and episodic like memory was reported in behavioral studies from genetically modified mice, where the excitatory drive was selectively reduced on PV+ INs. These mice also showed reduced exploratory activity in response to novel environmental stimuli and impaired novel object recognition (Fuchs et al., 2007). In another genetically modified mice, where the synaptic output of PV+ INs was specifically blocked in hippocampal CA1 the authors also found impaired spatial working, but intact spatial reference memory (Murray et al., 2011). These data indicate that the precisely timed firing of PV+ INs might be essential in the implementation of special learning tasks.

By a detailed analysis of the firing properties and synaptic inputs of CA1 neurons, we showed that at least in the *in vitro* model of intrinsically generated hippocampal gamma oscillation: i, the excitatory drive from CA3 PCs to CA1 PCs is suppressed; ii, CA1 PCs are capable of weakly phase-coupled persistent firing; iii, while the excitatory input on PV+ IN and consequently their inhibitory input on CA1 PCs is increased. These results are in line with modeling studies of memory formation (Hasselmo and Schnell, 1994) and suggest that during CA3 driven gamma oscillations under high cholinergic tone the hippocampal network might be rather suited for encoding of novel information, than for retrieval of the old ones.

Altogether the similarities between the *in vivo* data and the data from our *in vitro* model are convincing and suggest that basically the same functional networks can be involved in CCh-induced persistent oscillations in acute slices and in hippocampal gamma-oscillations of the behaving animal. Hence, this model could be a useful tool for addressing further questions regarding to the properties of intrinsically generated gamma oscillations in the hippocampus. However, it is important to bear in mind that the CCh-induced *in vitro* oscillations presumably mimic only one type of physiologically occurring gamma oscillations of the intact brain.

7.3. General Discussion

Considering that gamma oscillations are often nested within the theta rhythm in the behaving animal (Buzsáki et al., 2003), it would be an interesting issue to examine how these different rhythm generating mechanisms interact with each other.

Cunningham and colleagues reported that during kainate-induced persistent gamma oscillations the amplitude of field gamma activity in the layer II/III of the EC was strongly modulated at theta frequencies. This theta frequency modulation of the field gamma oscillation was temporally correlated with the I_h mediated subthreshold membrane potential oscillations of the stellate cells. The application of the I_h blocker ZD7288 disrupted both the intrinsic theta rhythms of the stellate cells and the theta modulation of the field gamma amplitude (Cunningham et al., 2003).

Both experimental and computational modeling studies suggest that OLM cells could play a crucial role in the generation of theta oscillations in the hippocampus (Gloveli et al., 2005a,b; Rotstein et al., 2005). For instance, during kainate-induced transient gamma oscillations OLM cells tend to fire at theta frequencies (Gloveli et al., 2005b), and the capability of the hippocampal CA1 region of showing theta frequency oscillations depends on the angle of cut during slice preparation, which determines how well the OLM neuronal processes are preserved in the slice (Hájos and Mody, 1997; Gloveli et al., 2005a). We also found that OLM cells are predisposed by their intrinsic membrane properties to operate at relatively low frequencies that could overlap with the theta range. These data suggest that the built-in frequency preferences of the cells can directly contribute to the field potential oscillations.

It has to be considered though that neuromodulators, such as ACh might modulate the impedance properties of the neurons. The cholinergic receptor activation has been shown to influence various types of ion channels in the cells (e.g. M-type K+ channels, Ca^{2+} activated K^+ channels, I_{CAT}) (Colino and Halliwell, 1993; Lawrence et al., 2006b), therefore it can have a substantial impact on the intrinsic membrane properties of the neurons. There are contradictory results in the literature on the effect of ACh on I_h. In voltage clamp experiments from CA1 PCs I_h was found to be enhanced by CCh (Colino and Halliwell, 1993), while in the EC I_h was suppressed under high cholinergic tone (Heys et al., 2010). It also has to be noted that due to the activation of M1/M3 receptors both PCs and OLM cells are depolarized (Dasari and Gulledge, 2011; Lawrence et al., 2006b; Young et al., 2005), which would probably decrease their I_h-mediated frequency tuning properties. In addition to its aptitude to play a key role in rhythm generating processes, I_h was also shown to influence dendritic integration properties of PCs (Johnston, 2005) and even learning abilities of the behaving animal (Nolan et al., 2003; Nolan et al., 2004). Therefore, the cholinergic modulation of I_h activation is a very exciting field of research.

8. CONCLUSION

The main issue of this thesis was to reveal particular mechanisms in the hippocampus that are able to tune the network to operate at certain frequencies. In the first part of the dissertation we could see that some hippocampal CA1 neurons are set to operate at theta frequencies by their intrinsic membrane characteristics, while the second part showed how the circuitry of hippocampal CA1 can be synchronized by synaptic mechanisms to produce gamma frequency oscillations. These results imply that the frequency of the network oscillations could be affected by both the cellular and the synaptic dynamics of single neurons. The resonance properties of single cells might promote synchronized membrane potential oscillations in certain elements of the network, which could produce a field potential oscillation in the extracellular space. However, even though most of the neurons in hippocampal CA1 are prompted to operate at relatively low frequencies by their intrinsic membrane properties, the whole network at a population level can be tuned to produce higher frequency oscillations simply by shifting the balance between synaptic excitation and inhibition on the different elements of the circuitry.

9. SUMMARY

The hippocampal circuitry exhibits a wide variety of behavior related rhythmic activities; however, the exact role of these complex activity patterns in different operations of the brain remains elusive. In order to understand the involvement of rhythmic oscillations occurring at different frequencies in certain brain functions the underlying cellular mechanisms have to be uncovered.

One goal of this thesis was to identify intrinsic membrane properties of different cell types in hippocampal CA1 that can be involved in the generation of network oscillations. To this end, we investigated the impedance profiles and resonance properties of distinct types of anatomically identified neurons in the CA1 region of rat hippocampal slices. We also examined the influence of the hyperpolarization-activated cyclic nucleotide gated current ($I_{h)}$ on the impedance profile of the neurons. We found that pyramidal cells and different types of interneurons in the stratum oriens tended to show subthreshold resonance mainly in the theta frequency range (2-6 Hz), albeit with distinct features. Experimental data and computational modeling indicated that the cell-type specificity of the impedance profiles can largely be explained by the kinetic properties of I_h in combination with the passive membrane characteristics of the neurons.

A second goal of the thesis was to elucidate synaptic mechanisms that may underlie oscillatory activity in hippocampal CA1, particularly in the gamma frequency range (30-100 Hz). To achieve this, we recorded both spiking activity and synaptic inputs of different cell types of the CA1 and CA3 area during cholinergically induced oscillations in mouse hippocampal slices. We found that while the spiking activity of CA1 interneurons was driven mainly by their strongly phase-coupled excitatory inputs presumably arriving from CA3 pyramidal cells, the dominant input of CA1 pyramidal cells was inhibitory and their firing activity was less precisely synchronized. Our data indicate that the oscillation generated intrinsically in the CA3 area propagated to the CA1 region via feed-forward inhibition, i.e. CA3 pyramidal cells excite CA1 interneurons and their rhythmic, phase-locked firing induces oscillation in CA1.

The findings presented in this thesis may further our understanding of the involvement of particular cell types in various network operations, including oscillatory activity in different frequency bands.

10. ÖSSZEFOGLALÁS

A hippokampusz számos, jól definiált viselkedésfüggő ritmikus aktivitásmintázatot mutat, melyek pontos funkciója mindmáig jórészt tisztázatlan. Ahhoz, hogy megérthessük, milyen szerepet töltenek be a szinkron oszcillatorikus aktivitások az agyműködésben, fontos megismernünk a mögöttük meghúzódó sejtszintű és hálózati mechanizmusokat.

Kutatásaink során egyfelől arra kerestük a választ, hogy milyen frekvenciákat preferálnak a hippokampusz CA1 régiójában található idegsejtek. Patkány hippokampuszból készített akut szeletpreparátumokban vizsgáltuk a különböző sejttípusok impedancia-tulajdonságait, és kimutattuk, hogy a piramissejtek illetve a stratum oriensben található különféle interneuronok a théta frekvencia-tartományban (4-8 Hz) mutatnak rezonanciát a küszöbalatti membránpotenciálokon, ámde eltérő sajátságokkal. A sejtek ionáramainak vizsgálatát számítógépes modellezéssel kombináltuk, és megállapítottuk, hogy az egyes sejttípusok impedancia tulajdonságaiban megfigyelhető eltérések mögött a sejttípusok jellegzetes passzív membrántulajdonságai és a sejtekben található, hiperpolarizációra aktiválódó kation-áram (h-áram) különböző, sejttípus-függő tulajdonságai álltak.

A disszertációban szereplő második kísérletsorozatban azt vizsgáltuk, hogy milyen összehangolt hálózati aktivitás révén alakul ki gamma-frekvenciájú (30-100 Hz) oszcilláció a hippokampusz CA1 régiójában. Egér hippokampusz-szeletekben vizsgáltuk, hogy milyen tüzelési mintázatot mutatnak a CA1 és CA3 régióban található idegsejtek a kolinerg receptorok aktivációjával indukált gamma frekvenciájú oszcilláció alatt. A sejtek szinaptikus áramainak vizsgálatával megállapítottuk, hogy míg a CA1 interneuronok tüzelését elsősorban a CA3 piramissejtektől érkező, erős fáziskapcsolt serkentés határozta meg, a CA1 piramissejteken az oszcilláció alatt a szinaptikus gátlás dominált, és tüzelésük kevésbé volt fáziskapcsolt az oszcillációhoz. Eredményeink azt mutatják, hogy a hippokampusz CA3 régiójában keletkező gamma frekvenciájú oszcilláció a CA1 régióra ún. „feed-forward-gátlás” útján terjed át.

A tézisben bemutatott eredmények hozzájárulhatnak annak megértéséhez, hogy a különféle idegsejt-típusok milyen szerepet játszanak az agyban megfigyelhető, bonyolult ritmikus aktivitásmintázatok kialakulásában.

11. ACKNOWLEDGEMENTS

I wish to thank my supervisor, Dr. Norbert Hájos, for the excellent guidance and methodological training, and also for his invaluable help and support during my work as a student research assistant and subsequently as a PhD-student.

I owe my deepest gratitude to my closest collaborator, Dr. Szabolcs Káli, who performed the computational modeling part of the first study presented in this thesis and did also some part of the data analysis. I would like to thank him for the numerous hours of supervision and encouragement, and also for the inspiring conversations and many good laughs we had while working together. Without him this thesis would not exist at all.

I would also like to thank Judit Veres for performing some of the experiments of the second study in this thesis and for all the joyful moments we shared in the lab.

I wish to express my gratitude to Prof. Ole Paulsen for his useful comments and suggestions regarding both studies and also for helping with the data analysis in study I. I am also very thankful to Dr. Iris Oren for helping with the data analysis in study II.

I would like to thank Prof. Tamás Freund for his continuous support and encouragement during my undergraduate and graduate years.

I am grateful to all members of the Department of Cellular and Network Neurobiology in the Institute of Experimental Medicine, especially to the members of the Hájos Lab, for their everyday help in my work and for the joyful and inspiring working atmosphere in the Institute. Special thanks to Katalin Lengyel and Erzsébet Gregori for their excellent technical assistance.

I would like to thank my current supervisor, Prof. Thomas Nevian, for his support and understanding while I've written up my thesis, and express my special thanks to Sigrid Blom and Sarah Moyle for all their help and encouragement.

Finally, I thank my family and my dearest friends in Hungary for their love, faith and support during all times.

12. REFERENCES

Acsády L, Arabadzisz D, Freund TF (1996a) Correlated morphological and neurochemical features identify different subsets of vasoactive intestinal polypeptide-immunoreactive interneurons in rat hippocampus. Neuroscience 73:299-315.

Acsády L, Görcs TJ, Freund TF (1996b) Different populations of vasoactive intestinal polypeptide- immunoreactive interneurons are specialized to control pyramidal cells or interneurons in the hippocampus. Neuroscience 73:317-334.

Adey WR (1967) Hippocampal states and functional relations with corticosubcortical systems in attention and learning. Prog Brain Res 27:228-245.

Amaral DG (1978) A Golgi study of cell types in the hilar region of the hippocampus in the rat. J Comp Neurol 182:851-914.

Amaral DG, Dolorfo C, Alvarez-Royo P (1991) Organization of CA1 projections to the subiculum: a PHA-L analysis in the rat. Hippocampus 1:415-435.

Andersen P, Morris R, Amaral D, Bliss T, O'Keefe J, eds (2007) The Hippocampus Book: Oxford University Press, New York

Aponte Y, Lien CC, Reisinger E, Jonas P (2006) Hyperpolarization-activated cation channels in fast-spiking interneurons of rat hippocampus. J Physiol 574:229-243.

Atri A, Sherman S, Norman KA, Kirchhoff BA, Nicolas MM, Greicius MD, Cramer SC, Breiter HC, Hasselmo ME, Stern CE (2004) Blockade of central cholinergic receptors impairs new learning and increases proactive interference in a word paired-associate memory task. Behav Neurosci 118:223-236.

Baude A, Nusser Z, David J, Roberts B, Mulvihill E, McIlhinney RAJ, Somogyi P (1993) The metabotropic glutamate receptor (mGluR1Ó) is concentrated at perisynaptic membrane of neuronal subpopulations as detected by immunogold reaction. Neuron 11:771-787.

Behrens CJ, van den Boom LP, de Hoz L, Friedman A, Heinemann U (2005) Induction of sharp wave-ripple complexes *in vitro* and reorganization of hippocampal networks. Nat Neurosci 8:1560-1567.

Bender RA, Brewster A, Santoro B, Ludwig A, Hofmann F, Biel M, Baram TZ (2001) Differential and age-dependent expression of hyperpolarization-activated, cyclic nucleotide-gated cation channel isoforms 1-4 suggests evolving roles in the developing rat hippocampus. Neuroscience 106:689-698.

Bickmeyer U, Heine M, Manzke T, Richter DW (2002) Differential modulation of I(h) by 5-HT receptors in mouse CA1 hippocampal neurons. Eur J Neurosci 16:209-218.

Bishop CM (2006) Pattern Recognition and Machine Learning: Springer, Singapore

Blasco-Ibanez JM, Freund TF (1995) Synaptic input of horizontal interneurons in stratum oriens of the hippocampal CA1 subfield:srtructural basis of feed-back activation. Eur J neurosci 7:2170-2180.

Bliss TV, Lomo T (1973) Long-lasting potentiation of synaptic transmission in the dentate area of the anaesthetized rabbit following stimulation of the perforant path. J Physiol 232:331-356.

Boddeke HW, Best R, Boeijinga PH (1997) Synchronous 20 Hz rhythmic activity in hippocampal networks induced by activation of metabotropic glutamate receptors *in vitro*. Neuroscience 76:653-658.

Borhegyi Z, Freund TF (1998) Dual projection from the medial septum to the supramammillary nucleus in the rat. Brain Res Bull 46:453-459.

Borhegyi Z, Maglóczky Z, Acsády L, Freund TF (1998) The supramammillary nucleus innervates cholinergic and GABAergic neurons in the medial septum-diagonal band of Broca complex. Neuroscience 82:1053-1065.

Bragin A, Jando G, Nadasdy Z, Hetke J, Wise K, Buzsáki G (1995) Gamma (40-100 Hz) oscillation in the hippocampus of the behaving rat. J Neurosci 15:47-60.

Brewster A, Bender RA, Chen Y, Dube C, Eghbal-Ahmadi M, Baram TZ (2002) Developmental febrile seizures modulate hippocampal gene expression of hyperpolarization-activated channels in an isoform- and cell-specific manner. J Neurosci 22:4591-4599.

Brewster AL, Chen Y, Bender RA, Yeh A, Shigemoto R, Baram TZ (2007) Quantitative analysis and subcellular distribution of mRNA and protein expression of the hyperpolarization-activated cyclic nucleotide-gated channels throughout development in rat hippocampus. Cereb Cortex 17:702-712.

Buhl DL, Harris KD, Hormuzdi SG, Monyer H, Buzsáki G (2003) Selective impairment of hippocampal gamma oscillations in connexin-36 knock-out mouse *in vivo*. J Neurosci 23:1013-1018.

Buhl EH, Halasy K, Somogyi P (1994) Diverse sources of hippocampal unitary inhibitory postsynaptic potentials and the number of synaptic release sites. Nature 368:823-828.

Buhl EH, Tamás G, Fisahn A (1998) Cholinergic activation and tonic excitation induce persistent gamma oscillations in mouse somatosensory cortex *in vitro*. J Physiol 513 (Pt 1):117-126.

Buhl EH, Szilagyi T, Halasy K, Somogyi P (1996) Physiological properties of anatomically identified basket and bistratified cells in the CA1 area of the rat hippocampus *in vitro*. Hippocampus 6:294-305.

Bunce JG, Sabolek HR, Chrobak JJ (2004) Intraseptal infusion of the cholinergic agonist carbachol impairs delayed-non-match-to-sample radial arm maze performance in the rat. Hippocampus 14:450-459.

Buzsáki G (2002) Theta oscillations in the hippocampus. Neuron 33:325-340.

Buzsáki G, Eidelberg E (1983) Phase relations of hippocampal projection cells and interneurons to theta activity in the anesthetized rat. Brain Res 266:334-339.

Buzsáki G, Leung LW, Vanderwolf CH (1983) Cellular bases of hippocampal EEG in the behaving rat. Brain Res 287:139-171.

Buzsáki G, Czopf J, Kondakor I, Kellenyi L (1986) Laminar distribution of hippocampal rhythmic slow activity (RSA) in the behaving rat: current-source density analysis, effects of urethane and atropine. Brain Res 365:125-137.

Buzsáki G, Horvath Z, Urioste R, Hetke J, Wise K (1992) High-frequency network oscillation in the hippocampus. Science 256:1025-1027.

Buzsáki G, Buhl DL, Harris KD, Csicsvári J, Czeh B, Morozov A (2003) Hippocampal network patterns of activity in the mouse. Neuroscience 116:201-211.

Buzsáki G (1989) Two-stage model of memory trace formation: A role for 'noisy' brain states. Neuroscience 310:551-570.

Cantrell AR, Ma JY, Scheuer T, Catterall WA (1996) Muscarinic modulation of sodium current by activation of protein kinase C in rat hippocampal neurons. Neuron 16:1019-1026.

Cardin JA, Carlen M, Meletis K, Knoblich U, Zhang F, Deisseroth K, Tsai LH, Moore CI (2009) Driving fast-spiking cells induces gamma rhythm and controls sensory responses. Nature 459:663-667.

Cea-del Rio CA, Lawrence JJ, Erdelyi F, Szabó G, McBain CJ (2011) Cholinergic modulation amplifies the intrinsic oscillatory properties of CA1 hippocampal cholecystokinin-positive interneurons. J Physiol 589:609-627.

Cea-del Rio CA, Lawrence JJ, Tricoire L, Erdélyi F, Szabó G, McBain CJ (2010) M3 muscarinic acetylcholine receptor expression confers differential cholinergic modulation to neurochemically distinct hippocampal basket cell subtypes. J Neurosci 30:6011-6024.

Chapman CA, Lacaille JC (1999) Intrinsic theta-frequency membrane potential oscillations in hippocampal CA1 interneurons of stratum lacunosum-moleculare. J Neurophysiol 81:1296-1307.

Chen S, Wang J, Siegelbaum SA (2001) Properties of hyperpolarization-activated pacemaker current defined by coassembly of HCN1 and HCN2 subunits and basal modulation by cyclic nucleotide. J Gen Physiol 117:491-504.

Chevaleyre V, Siegelbaum SA (2010) Strong CA2 pyramidal neuron synapses define a powerful disynaptic cortico-hippocampal loop. Neuron 66:560-572.

Chrobak JJ, Buzsáki G (1994) Selective activation of deep layer (V-VI) retrohippocampal cortical neurons during hippocampal sharp waves in the behaving rat. J Neurosci 14:6160-6170.

Cobb SR, Buhl EH, Halasy K, Paulsen O, Somogyi P (1995) Synchronization of neuronal activity in hippocampus by individual GABAergic interneurons. Nature 378:75-78.

Cobb SR, Larkman PM, Bulters DO, Oliver L, Gill CH, Davies CH (2003) Activation of Ih is necessary for patterning of mGluR and mAChR induced network activity in the hippocampal CA3 region. Neuropharmacology 44:293-303.

Colgin LL, Denninger T, Fyhn M, Hafting T, Bonnevie T, Jensen O, Moser MB, Moser EI (2009) Frequency of gamma oscillations routes flow of information in the hippocampus. Nature 462:353-357.

Colino A, Halliwell JV (1993) Carbachol potentiates Q current and activates a calcium-dependent non-specific conductance in rat hippocampus *in vitro*. Eur J Neurosci 5:1198-1209.

Cope DW, Maccaferri G, Marton LF, Roberts JD, Cobden PM, Somogyi P (2002) Cholecystokinin-immunopositive basket and Schaffer collateral-associated interneurones target different domains of pyramidal cells in the CA1 area of the rat hippocampus. Neuroscience 109:63-80.

Croce A, Pelletier JG, Tartas M, Lacaille JC (2010) Afferent-specific properties of interneuron synapses underlie selective long-term regulation of feedback inhibitory circuits in CA1 hippocampus. J Physiol 588:2091-2107.

Cunningham MO, Davies CH, Buhl EH, Kopell N, Whittington MA (2003) Gamma oscillations induced by kainate receptor activation in the entorhinal cortex *in vitro*. J Neurosci 23:9761-9769.

Czurkó A, Huxter J, Li Y, Hangya B, Muller RU (2011) Theta phase classification of interneurons in the hippocampal formation of freely moving rats. J Neurosci 31:2938-2947.

Csicsvári J, Jamieson B, Wise KD, Buzsáki G (2003) Mechanisms of gamma oscillations in the hippocampus of the behaving rat. Neuron 37:311-322.

Csicsvári J, Hirase H, Czurkó A, Mamiya A, Buzsáki G (1999) Oscillatory coupling of hippocampal pyramidal cells and interneurons in the behaving Rat. J Neurosci 19:274-287.

Dasari S, Gulledge AT (2011) M1 and M4 receptors modulate hippocampal pyramidal neurons. J Neurophysiol 105:779-792.

Deans MR, Gibson JR, Sellitto C, Connors BW, Paul DL (2001) Synchronous activity of inhibitory networks in neocortex requires electrical synapses containing connexin36. Neuron 31:477-485.

Dickinson R, Awaiz S, Whittington MA, Lieb WR, Franks NP (2003) The effects of general anaesthetics on carbachol-evoked gamma oscillations in the rat hippocampus *in vitro*. Neuropharmacology 44:864-872.

Dickson CT, Magistretti J, Shalinsky MH, Fransen E, Hasselmo ME, Alonso A (2000) Properties and role of I(h) in the pacing of subthreshold oscillations in entorhinal cortex layer II neurons. J Neurophysiol 83:2562-2579.

Draguhn A, Traub RD, Schmitz D, Jefferys JG (1998) Electrical coupling underlies high-frequency oscillations in the hippocampus *in vitro*. Nature 394:189-192.

Ellender TJ, Nissen W, Colgin LL, Mann EO, Paulsen O (2010) Priming of hippocampal population bursts by individual perisomatic-targeting interneurons. J Neurosci 30:5979-5991.

Fabian-Fine R, Skehel P, Errington ML, Davies HA, Sher E, Stewart MG, Fine A (2001) Ultrastructural distribution of the alpha7 nicotinic acetylcholine receptor subunit in rat hippocampus. J Neurosci 21:7993-8003.

Fellous JM, Sejnowski TJ (2000) Cholinergic induction of oscillations in the hippocampal slice in the slow (0.5-2 Hz), theta (5-12 Hz), and gamma (35-70 Hz) bands. Hippocampus 10:187-197.

Fernandez de Sevilla D, Buno W (2003) Presynaptic inhibition of Schaffer collateral synapses by stimulation of hippocampal cholinergic afferent fibres. Eur J Neurosci 17:555-558.

Ferraguti F, Klausberger T, Cobden P, Baude A, Roberts JD, Szucs P, Kinoshita A, Shigemoto R, Somogyi P, Dalezios Y (2005) Metabotropic glutamate receptor 8-expressing nerve terminals target subsets of GABAergic neurons in the hippocampus. J Neurosci 25:10520-10536.

Fisahn A, Pike FG, Buhl EH, Paulsen O (1998) Cholinergic induction of network oscillations at 40 Hz in the hippocampus *in vitro*. Nature 394:186-189.

Fisahn A, Contractor A, Traub RD, Buhl EH, Heinemann SF, McBain CJ (2004) Distinct roles for the kainate receptor subunits GluR5 and GluR6 in kainate-induced hippocampal gamma oscillations. J Neurosci 24:9658-9668.

Fox SE, Wolfson S, Ranck JB, Jr. (1986) Hippocampal theta rhythm and the firing of neurons in walking and urethane anesthetized rats. Exp Brain Res 62:495-508.

Fransen E, Alonso AA, Dickson CT, Magistretti J, Hasselmo ME (2004) Ionic mechanisms in the generation of subthreshold oscillations and action potential clustering in entorhinal layer II stellate neurons. Hippocampus 14:368-384.

Fransen E, Tahvildari B, Egorov AV, Hasselmo ME, Alonso AA (2006) Mechanism of graded persistent cellular activity of entorhinal cortex layer v neurons. Neuron 49:735-746.

Franz O, Liss B, Neu A, Roeper J (2000) Single-cell mRNA expression of HCN1 correlates with a fast gating phenotype of hyperpolarization-activated cyclic nucleotide-gated ion channels (Ih) in central neurons. Eur J Neurosci 12:2685-2693.

Frazier CJ, Rollins YD, Breese CR, Leonard S, Freedman R, Dunwiddie TV (1998) Acetylcholine activates an alpha-bungarotoxin-sensitive nicotinic current in rat hippocampal interneurons, but not pyramidal cells. J Neurosci 18:1187-1195.

Freeman WJ (1968) Relations between unit activity and evoked potentials in prepyriform cortex of cats. J Neurophysiol 31:337-348.

Freund TF (1992) GABAergic septal and serotonergic median raphe afferents preferentially innervate inhibitory interneurons in the hippocampus and dentate gyrus. Epilepsy Res Suppl 7:79-91.

Freund TF (2003) Interneuron Diversity series: Rhythm and mood in perisomatic inhibition. Trends Neurosci 26:489-495.

Freund TF, Antal M (1988) GABA-containing neurons in the septum control inhibitory interneurons in the hippocampus. Nature 336:170-173.

Freund TF, Buzsáki G (1996) Interneurons of the hippocampus. Hippocampus 6:347-470.

Freund TF, Katona I (2007) Perisomatic inhibition. Neuron 56:33-42.

Freund TF, Gulyás AI, Acsády L, Görcs T, Tóth K (1990) Serotonergic control of the hippocampus via local inhibitory interneurons. Proc Natl Acad Sci U S A 87:8501-8505.

Frotscher M, Léránth C (1985) Cholinergic innervation of the rat hippocampus as revealed by choline acetyltransferase immunocytochemistry: a combined light and electron microscopic study. J Comp Neurol 239:237-246.

Frotscher M, Vida I, Bender R (2000) Evidence for the existence of non-GABAergic, cholinergic interneurons in the rodent hippocampus. Neuroscience 96:27-31.

Fuchs EC, Zivkovic AR, Cunningham MO, Middleton S, Lebeau FE, Bannerman DM, Rozov A, Whittington MA, Traub RD, Rawlins JN, Monyer H (2007) Recruitment of parvalbumin-positive interneurons determines hippocampal function and associated behavior. Neuron 53:591-604.

Fuentealba P, Begum R, Capogna M, Jinno S, Marton LF, Csicsvari J, Thomson A, Somogyi P, Klausberger T (2008) Ivy cells: a population of nitric-oxide-producing, slow-spiking GABAergic neurons and their involvement in hippocampal network activity. Neuron 57:917-929.

Fukudome Y, Ohno-Shosaku T, Matsui M, Omori Y, Fukaya M, Tsubokawa H, Taketo MM, Watanabe M, Manabe T, Kano M (2004) Two distinct classes of muscarinic action on hippocampal inhibitory synapses: M2-mediated direct suppression and M1/M3-mediated indirect suppression through endocannabinoid signalling. Eur J Neurosci 19:2682-2692.

Gais S, Born J (2004) Low acetylcholine during slow-wave sleep is critical for declarative memory consolidation. Proc Natl Acad Sci U S A 101:2140-2144.

Gasparini S, DiFrancesco D (1999) Action of serotonin on the hyperpolarization-activated cation current (Ih) in rat CA1 hippocampal neurons. Eur J Neurosci 11:3093-3100.

Gaykema RP, Luiten PG, Nyakas C, Traber J (1990) Cortical projection patterns of the medial septum-diagonal band complex. J Comp Neurol 293:103-124.

Geiger JR, Lubke J, Roth A, Frotscher M, Jonas P (1997) Submillisecond AMPA receptor-mediated signaling at a principal neuron- interneuron synapse. Neuron 18:1009-1023.

Geiger JR, Melcher T, Koh DS, Sakmann B, Seeburg PH, Jonas P, Monyer H (1995) Relative abundance of subunit mRNAs determines gating and Ca2+ permeability of AMPA receptors in principal neurons and interneurons in rat CNS. Neuron 15:193-204.

George MS, Abbott LF, Siegelbaum SA (2009) HCN hyperpolarization-activated cation channels inhibit EPSPs by interactions with M-type K(+) channels. Nat Neurosci 12:577-584.

Gillies MJ, Traub RD, LeBeau FE, Davies CH, Gloveli T, Buhl EH, Whittington MA (2002) A model of atropine-resistant theta oscillations in rat hippocampal area CA1. J Physiol 543:779-793.

Giocomo LM, Hasselmo ME (2005) Nicotinic modulation of glutamatergic synaptic transmission in region CA3 of the hippocampus. Eur J Neurosci 22:1349-1356.

Glickfeld LL, Scanziani M (2006) Distinct timing in the activity of cannabinoid-sensitive and cannabinoid-insensitive basket cells. Nat Neurosci 9:807-815.

Glickfeld LL, Roberts JD, Somogyi P, Scanziani M (2009) Interneurons hyperpolarize pyramidal cells along their entire somatodendritic axis. Nat Neurosci 12:21-23.

Gloveli T, Dugladze T, Rotstein HG, Traub RD, Monyer H, Heinemann U, Whittington MA, Kopell NJ (2005a) Orthogonal arrangement of rhythm-generating microcircuits in the hippocampus. Proc Natl Acad Sci U S A 102:13295-13300.

Gloveli T, Dugladze T, Saha S, Monyer H, Heinemann U, Traub RD, Whittington MA, Buhl EH (2005b) Differential involvement of oriens/pyramidale interneurones in hippocampal network oscillations *in vitro*. J Physiol 562:131-147.

Goldin M, Epsztein J, Jorquera I, Represa A, Ben-Ari Y, Crepel V, Cossart R (2007) Synaptic kainate receptors tune oriens-lacunosum moleculare interneurons to operate at theta frequency. J Neurosci 27:9560-9572.

Goutagny R, Jackson J, Williams S (2009) Self-generated theta oscillations in the hippocampus. Nat Neurosci 12:1491-1493.

Gray CM, Singer W (1989) Stimulus-specific neuronal oscillations in orientation columns of cat visual cortex. Proc Natl Acad Sci U S A 86:1698-1702.

Green A, Ellis KA, Ellis J, Bartholomeusz CF, Ilic S, Croft RJ, Phan KL, Nathan PJ (2005) Muscarinic and nicotinic receptor modulation of object and spatial n-back working memory in humans. Pharmacol Biochem Behav 81:575-584.

Green JD, Arduini AA (1954) Hippocampal electrical activity in arousal. J Neurophysiol 17:533-557.

Guerineau NC, Gahwiler BH, Gerber U (1994) Reduction of resting K+ current by metabotropic glutamate and muscarinic receptors in rat CA3 cells: mediation by G-proteins. J Physiol 474:27-33.

Gulledge AT, Kawaguchi Y (2007) Phasic cholinergic signaling in the hippocampus: functional homology with the neocortex? Hippocampus 17:327-332.

Gulyás AI, Hájos N, Freund TF (1996) Interneurons containing calretinin are specialized to control other interneurons in the rat hippocampus. J Neurosci 16:3397-3411.

Gulyás AI, Hájos N, Katona I, Freund TF (2003) Interneurons are the local targets of hippocampal inhibitory cells which project to the medial septum. Eur J Neurosci 17:1861-1872.

Gulyás AI, Szabó GG, Ulbert I, Holderith N, Monyer H, Erdélyi F, Szabó G, Freund TF, Hájos N (2010) Parvalbumin-containing fast-spiking basket cells generate the field potential oscillations induced by cholinergic receptor activation in the hippocampus. J Neurosci 30:15134-15145.

Hájos N, Mody I (1997) Synaptic communication among hippocampal interneurons: properties of spontaneous IPSCs in morphologically identified cells. J Neurosci 17:8427-8442.

Hájos N, Paulsen O (2009) Network mechanisms of gamma oscillations in the CA3 region of the hippocampus. Neural Netw 22:1113-1119.

Hájos N, Mody I (2009) Establishing a physiological environment for visualized *in vitro* brain slice recordings by increasing oxygen supply and modifying aCSF content. J Neurosci Methods 183:107-113.

Hájos N, Papp EC, Acsády L, Levey AI, Freund TF (1998) Distinct interneuron types express m2 muscarinic receptor immunoreactivity on their dendrites or axon terminals in the hippocampus. Neuroscience 82:355-376.

Hájos N, Pálhalmi J, Mann EO, Németh B, Paulsen O, Freund TF (2004) Spike timing of distinct types of GABAergic interneuron during hippocampal gamma oscillations *in vitro*. J Neurosci 24:9127-9137.

Hájos N, Ellender TJ, Zemankovics R, Mann EO, Exley R, Cragg SJ, Freund TF, Paulsen O (2009) Maintaining network activity in submerged hippocampal slices: importance of oxygen supply. Eur J Neurosci 29:319-327.

Halasy K, Buhl EH, Lorinczi Z, Tamas G, Somogyi P (1996) Synaptic target selectivity and input of GABAergic basket and bistratified interneurons in the CA1 area of the rat hippocampus. Hippocampus 6:306-329.

Halliwell JV (1990) Physiological mechanisms of cholinergic action in the hippocampus. Prog Brain Res 84:255-272.

Halliwell JV, Adams PR (1982) Voltage-clamp analysis of muscarinic excitation in hippocampal neurons. Brain Res 250:71-92.

Hamlyn LH (1962) The fine structure of the mossy fibre endings in the hippocampus of the rabbit. J Anat 96:112-120.

Han ZS (1994) Electrophysiological and morphological differentiation of chandelier and basket cells in the rat hippocampal formation: a study combining intracellular recording and intracellular staining with biocytin. Neurosci Res 19:101-110.

Harris NC, Constanti A (1995) Mechanism of block by ZD 7288 of the hyperpolarization-activated inward rectifying current in guinea pig substantia nigra neurons *in vitro*. J Neurophysiol 74:2366-2378.

Hasselmo ME (2005) What is the function of hippocampal theta rhythm?--Linking behavioral data to phasic properties of field potential and unit recording data. Hippocampus 15:936-949.

Hasselmo ME, Schnell E (1994) Laminar selectivity of the cholinergic suppression of synaptic transmission in rat hippocampal region CA1: computational modeling and brain slice physiology. J Neurosci 14:3898-3914.

Hasselmo ME, McGaughy J (2004) High acetylcholine levels set circuit dynamics for attention and encoding and low acetylcholine levels set dynamics for consolidation. Prog Brain Res 145:207-231.

Hasselmo ME, Schnell E, Barkai E (1995) Dynamics of learning and recall at excitatory recurrent synapses and cholinergic modulation in rat hippocampal region CA3. J Neurosci 15:5249-5262.

Heys JG, Giocomo LM, Hasselmo ME (2010) Cholinergic modulation of the resonance properties of stellate cells in layer II of medial entorhinal cortex. J Neurophysiol 104:258-270.

Hormuzdi SG, Pais I, LeBeau FE, Towers SK, Rozov A, Buhl EH, Whittington MA, Monyer H (2001) Impaired electrical signaling disrupts gamma frequency oscillations in connexin 36-deficient mice. Neuron 31:487-495.

Hu H, Vervaeke K, Storm JF (2002) Two forms of electrical resonance at theta frequencies, generated by M-current, h-current and persistent Na+ current in rat hippocampal pyramidal cells. J Physiol 545:783-805.

Hu H, Vervaeke K, Graham LJ, Storm JF (2009) Complementary theta resonance filtering by two spatially segregated mechanisms in CA1 hippocampal pyramidal neurons. J Neurosci 29:14472-14483.

Huchzermeyer C, Albus K, Gabriel HJ, Otahal J, Taubenberger N, Heinemann U, Kovacs R, Kann O (2008) Gamma oscillations and spontaneous network activity in the hippocampus are highly sensitive to decreases in pO2 and concomitant changes in mitochondrial redox state. J Neurosci 28:1153-1162.

Hutcheon B, Yarom Y (2000) Resonance, oscillation and the intrinsic frequency preferences of neurons. Trends Neurosci 23:216-222.

Hutcheon B, Miura RM, Puil E (1996a) Subthreshold membrane resonance in neocortical neurons. J Neurophysiol 76:683-697.

Hutcheon B, Miura RM, Puil E (1996b) Models of subthreshold membrane resonance in neocortical neurons. J Neurophysiol 76:698-714.

Hutcheon B, Miura RM, Yarom Y, Puil E (1994) Low-threshold calcium current and resonance in thalamic neurons: a model of frequency preference. J Neurophysiol 71:583-594.

Ishii TM, Takano M, Ohmori H (2001) Determinants of activation kinetics in mammalian hyperpolarization-activated cation channels. J Physiol 537:93-100.

Jensen O, Lisman JE (2000) Position reconstruction from an ensemble of hippocampal place cells: contribution of theta phase coding. J Neurophysiol 83:2602-2609.

Jinno S, Klausberger T, Marton LF, Dalezios Y, Roberts JD, Fuentealba P, Bushong EA, Henze D, Buzsáki G, Somogyi P (2007) Neuronal diversity in GABAergic long-range projections from the hippocampus. J Neurosci 27:8790-8804.

Johnston D (2005) Channeling a 'funny' side of memory. Nat Neurosci 8:134-135.

Jones BE, Moore RY (1977) Ascending projections of the locus coeruleus in the rat. II. Autoradiographic study. Brain Res 127:25-53.

Kamondi A, Acsády L, Wang XJ, Buzsáki G (1998) Theta oscillations in somata and dendrites of hippocampal pyramidal cells *in vivo*: activity-dependent phase-precession of action potentials. Hippocampus 8:244-261.

Kawaguchi Y (2001) Distinct firing patterns of neuronal subtypes in cortical synchronized activities. The Journal of neuroscience 21:7261-7272.

Klausberger T (2009) GABAergic interneurons targeting dendrites of pyramidal cells in the CA1 area of the hippocampus. Eur J Neurosci 30:947-957.

Klausberger T, Somogyi P (2008) Neuronal diversity and temporal dynamics: the unity of hippocampal circuit operations. Science 321:53-57.

Klausberger T, Marton LF, Baude A, Roberts JD, Magill PJ, Somogyi P (2004) Spike timing of dendrite-targeting bistratified cells during hippocampal network oscillations *in vivo*. Nat Neurosci 7:41-47.

Klausberger T, Magill PJ, Marton LF, Roberts JD, Cobden PM, Buzsáki G, Somogyi P (2003) Brain-state- and cell-type-specific firing of hippocampal interneurons *in vivo*. Nature 421:844-848.

Klausberger T, Marton LF, O'Neill J, Huck JH, Dalezios Y, Fuentealba P, Suen WY, Papp E, Kaneko T, Watanabe M, Csicsvari J, Somogyi P (2005) Complementary roles of cholecystokinin- and parvalbumin-expressing GABAergic neurons in hippocampal network oscillations. J Neurosci 25:9782-9793.

Klink R, Alonso A (1997) Muscarinic modulation of the oscillatory and repetitive firing properties of entorhinal cortex layer II neurons. J Neurophysiol 77:1813-1828.

Kocsis B, Vertes RP (1992) Dorsal raphe neurons: synchronous discharge with the theta rhythm of the hippocampus in the freely behaving rat. J Neurophysiol 68:1463-1467.

Kocsis B, Vertes RP (1994) Characterization of neurons of the supramammillary nucleus and mammillary body that discharge rhythmically with the hippocampal theta rhythm in the rat. J Neurosci 14:7040-7052.

Kocsis B, Li S (2004) *In vivo* contribution of h-channels in the septal pacemaker to theta rhythm generation. Eur J Neurosci 20:2149-2158.

Kocsis B, Di Prisco GV, Vertes RP (2001) Theta synchronization in the limbic system: the role of Gudden's tegmental nuclei. Eur J Neurosci 13:381-388.

Kramis R, Vanderwolf CH, Bland BH (1975) Two types of hippocampal rhythmical slow activity in both the rabbit and the rat: relations to behavior and effects of atropine, diethyl ether, urethane, and pentobarbital. Exp Neurol 49:58-85.

Krnjevic K, Pumain R, Renaud L (1971) The mechanism of excitation by acetylcholine in the cerebral cortex. J Physiol 215:247-268.

Kubota D, Colgin LL, Casale M, Brucher FA, Lynch G (2003) Endogenous waves in hippocampal slices. J Neurophysiol 89:81-89.

Lacaille JC, Schwartzkroin PA (1988a) Stratum lacunosum-moleculare interneurons of hippocampal CA1 region. I. Intracellular response characteristics, synaptic responses, and morphology. JNeurosci 8:1400-1410.

Lacaille JC, Schwartzkroin PA (1988b) Stratum lacunosum-moleculare interneurons of hippocampal CA1 region. II. Intrasomatic and intradendritic recordings of local circuit synaptic interactions. JNeurosci 8:1411-1424.

Lampl I, Yarom Y (1997) Subthreshold oscillations and resonant behavior: two manifestations of the same mechanism. Neuroscience 78:325-341.

Lawrence JJ, Grinspan ZM, Statland JM, McBain CJ (2006a) Muscarinic receptor activation tunes mouse stratum oriens interneurones to amplify spike reliability. J Physiol 571:555-562.

Lawrence JJ, Statland JM, Grinspan ZM, McBain CJ (2006b) Cell type-specific dependence of muscarinic signalling in mouse hippocampal stratum oriens interneurones. J Physiol 570:595-610.

Le Van Quyen M, Foucher J, Lachaux J, Rodriguez E, Lutz A, Martinerie J, Varela FJ (2001) Comparison of Hilbert transform and wavelet methods for the analysis of neuronal synchrony. J Neurosci Methods 111:83-98.

LeBeau FE, Towers SK, Traub RD, Whittington MA, Buhl EH (2002) Fast network oscillations induced by potassium transients in the rat hippocampus *in vitro*. J Physiol 542:167-179.

Lee MG, Chrobak JJ, Sík A, Wiley RG, Buzsáki G (1994) Hippocampal theta activity following selective lesion of the septal cholinergic system. Neuroscience 62:1033-1047.

Lengyel M, Kwag J, Paulsen O, Dayan P (2005) Matching storage and recall: hippocampal spike timing-dependent plasticity and phase response curves. Nat Neurosci 8:1677-1683.

Léránth C, Frotscher M (1987) Cholinergic innervation of hippocampal GAD- and somatostatin-immunoreactive commissural neurons. J Comp Neurol 261:33-47.

Leung LS (1980) Behavior-dependent evoked potentials in the hippocampal CA1 region of the rat. I.correlation with behavior and EEG. Brain Res 198:95-117.

Leung LS, Yu HW (1998) Theta-frequency resonance in hippocampal CA1 neurons *in vitro* demonstrated by sinusoidal current injection. J Neurophysiol 79:1592-1596.

Leung LS, Martin LA, Stewart DJ (1994) Hippocampal theta rhythm in behaving rats following ibotenic acid lesion of the septum. Hippocampus 4:136-147.

Leung LW (1984) Model of gradual phase shift of theta rhythm in the rat. JNeurophysiol 52:1051-1065.

Leung LW, Borst JG (1987) Electrical activity of the cingulate cortex. I. Generating mechanisms and relations to behavior. Brain Res 407:68-80.

Levey AI, Edmunds SM, Koliatsos V, Wiley RG, Heilman CJ (1995) Expression of m1-m4 muscarinic acetylcholine receptor proteins in rat hippocampus and regulation by cholinergic innervation. J Neurosci 15:4077-4092.

Lewis AS, Estep CM, Chetkovich DM (2010) The fast and slow ups and downs of HCN channel regulation. Channels (Austin) 4:215-231.

Li XG, Somogyi P, Ylinen A, Buzsáki G (1994) The hippocampal ca3 network - an *in vivo* intracellular labeling study. Journal of Comparative Neurology 339:181-208.

Lien CC, Jonas P (2003) Kv3 potassium conductance is necessary and kinetically optimized for high-frequency action potential generation in hippocampal interneurons. J Neurosci 23:2058-2068.

Lorente de Nó R (1934) Studies on the structure of the cerebral cortex. II. Continuation of the study of the ammonic system. JPsycholNeur(Leipzig) 46:113-177.

Lőrincz A, Notomi T, Tamás G, Shigemoto R, Nusser Z (2002) Polarized and compartment-dependent distribution of HCN1 in pyramidal cell dendrites. Nat Neurosci 5:1185-1193.

Lüthi A, McCormick DA (1998) H-current: properties of a neuronal and network pacemaker. Neuron 21:9-12.

Maccaferri G (2005) Stratum oriens horizontal interneurone diversity and hippocampal network dynamics. J Physiol 562:73-80.

Maccaferri G, McBain CJ (1996) The hyperpolarization-activated current (Ih) and its contribution to pacemaker activity in rat CA1 hippocampal stratum oriens-alveus interneurones. J Physiol 497 (Pt 1):119-130.

Madison DV, Lancaster B, Nicoll RA (1987) Voltage clamp analysis of cholinergic action in the hippocampus. J Neurosci 7:733-741.

Magee JC (1998) Dendritic hyperpolarization-activated currents modify the integrative properties of hippocampal CA1 pyramidal neurons. J Neurosci 18:7613-7624.

Magee JC (1999) Dendritic Ih normalizes temporal summation in hippocampal CA1 neurons. Nat Neurosci 2(6):508-14.

Maglóczky Z, Acsády L, Freund TF (1994) Principal cells are the postsynaptic targets of supramammillary afferents in the hippocampus of the rat. Hippocampus 4:322-334.

Mann EO, Paulsen O (2005) Mechanisms underlying gamma ('40 Hz') network oscillations in the hippocampus--a mini-review. Prog Biophys Mol Biol 87:67-76.

Mann EO, Suckling JM, Hájos N, Greenfield SA, Paulsen O (2005) Perisomatic feedback inhibition underlies cholinergically induced fast network oscillations in the rat hippocampus *in vitro*. Neuron 45:105-117.

Manseau F, Goutagny R, Danik M, Williams S (2008) The hippocamposeptal pathway generates rhythmic firing of GABAergic neurons in the medial septum and diagonal bands: an investigation using a complete septohippocampal preparation *in vitro*. J Neurosci 28:4096-4107.

Markram H, Segal M (1990) Long-Lasting Facilitation of Excitatory Postsynaptic Potentials in the Rat Hippocampus by Acetylcholine. JPhysiol 427.

Markram H, Lubke J, Frotscher M, Sakmann B (1997) Regulation of synaptic efficacy by coincidence of postsynaptic APs and EPSPs. Science 275:213-215.

McBain CJ, DiChiara TJ, Kauer JA (1994) Activation of metabotropic glutamate receptors differentially affects two classes of hippocampal interneurons and potentiates excitatory synaptic transmission. J Neurosci 14:4433-4445.

McCormick DA, Pape HC (1990) Properties of a hyperpolarization-activated cation current and its role in rhythmic oscillation in thalamic relay neurones. J Physiol 431:291-318.

McLelland D, Paulsen O (2009) Neuronal oscillations and the rate-to-phase transform: mechanism, model and mutual information. J Physiol 587:769-785.

McMahon LL, Williams JH, Kauer JA (1998) Functionally distinct groups of interneurons identified during rhythmic carbachol oscillations in hippocampus *in vitro*. J Neurosci 18:5640-5651.

McQuiston AR, Madison DV (1999a) Nicotinic receptor activation excites distinct subtypes of interneurons in the rat hippocampus. J Neurosci 19:2887-2896.

McQuiston AR, Madison DV (1999b) Muscarinic receptor activity induces an afterdepolarization in a subpopulation of hippocampal CA1 interneurons. J Neurosci 19:5703-5710.

McQuiston AR, Madison DV (1999c) Muscarinic receptor activity has multiple effects on the resting membrane potentials of CA1 hippocampal interneurons. J Neurosci 19:5693-5702.

Megias M, Emri Z, Freund TF, Gulyás AI (2001) Total number and distribution of inhibitory and excitatory synapses on hippocampal CA1 pyramidal cells. Neuroscience 102:527-540.

Meyer AH, Katona I, Blatow M, Rozov A, Monyer H (2002) *In vivo* labeling of parvalbumin-positive interneurons and analysis of electrical coupling in identified neurons. J Neurosci 22:7055-7064.

Moosmang S, Biel M, Hofmann F, Ludwig A (1999) Differential distribution of four hyperpolarization-activated cation channels in mouse brain. Biol Chem 380:975-980.

Murray AJ, Sauer JF, Riedel G, McClure C, Ansel L, Cheyne L, Bartos M, Wisden W, Wulff P (2011) Parvalbumin-positive CA1 interneurons are required for spatial working but not for reference memory. Nat Neurosci 14:297-299.

Murray EA, Mishkin M (1984) Severe tactual as well as visual memory deficits follow combined removal of the amygdala and hippocampus in monkeys. J Neurosci 4:2565-2580.

Naber PA, Lopes da Silva FH, Witter MP (2001) Reciprocal connections between the entorhinal cortex and hippocampal fields CA1 and the subiculum are in register with the projections from CA1 to the subiculum. Hippocampus 11:99-104.

Nádasdy Z, Hirase H, Czurkó A, Csicsvári J, Buzsáki G (1999) Replay and time compression of recurring spike sequences in the hippocampus. J Neurosci 19:9497-9507.

Nakajima Y, Nakajima S, Leonard RJ, Yamaguchi K (1986) Acetylcholine raises excitability by inhibiting the fast transient potassium current in cultured hippocampal neurons. Proc Natl Acad Sci U S A 83:3022-3026.

Narayanan R, Johnston D (2007) Long-term potentiation in rat hippocampal neurons is accompanied by spatially widespread changes in intrinsic oscillatory dynamics and excitability. Neuron 56:1061-1075.

Narayanan R, Johnston D (2008) The h channel mediates location dependence and plasticity of intrinsic phase response in rat hippocampal neurons. J Neurosci 28:5846-5860.

Neu A, Földy C, Soltész I (2007) Postsynaptic origin of CB1-dependent tonic inhibition of GABA release at cholecystokinin-positive basket cell to pyramidal cell synapses in the CA1 region of the rat hippocampus. J Physiol 578:233-247.

Nolan MF, Malleret G, Lee KH, Gibbs E, Dudman JT, Santoro B, Yin D, Thompson RF, Siegelbaum SA, Kandel ER, Morozov A (2003) The hyperpolarization-activated HCN1 channel is important for motor learning and neuronal integration by cerebellar Purkinje cells. Cell 115:551-564.

Nolan MF, Malleret G, Dudman JT, Buhl DL, Santoro B, Gibbs E, Vronskaya S, Buzsáki G, Siegelbaum SA, Kandel ER, Morozov A (2004) A behavioral role for dendritic integration: HCN1 channels constrain spatial memory and plasticity at inputs to distal dendrites of CA1 pyramidal neurons. Cell 119:719-732.

Noma A, Irisawa H (1976) A time- and voltage-dependent potassium current in the rabbit sinoatrial node cell. Pflugers Arch 366:251-258.

Notomi T, Shigemoto R (2004) Immunohistochemical localization of Ih channel subunits, HCN1-4, in the rat brain. J Comp Neurol 471:241-276.

Nusser Z, Lujan R, Laube G, Roberts JD, Molnár E, Somogyi P (1998) Cell type and pathway dependence of synaptic AMPA receptor number and variability in the hippocampus. Neuron 21:545-559.

Nyakas C, Luiten PGM, Spencer DG, Traber J (1987) Detailed projection patterns of septal and diagonal band efferents to the hippocampus in the rat with emphasis on innervation of CA1 and dentate gyrus. Brain ResBull 18:533-545.

O'Keefe J, Recce ML (1993) Phase relationship between hippocampal place units and the EEG theta rhythm. Hippocampus 3:317-330.

Oren I, Mann EO, Paulsen O, Hájos N (2006) Synaptic currents in anatomically identified CA3 neurons during hippocampal gamma oscillations *in vitro*. The Journal of neuroscience 26:9923-9934.

Pálhalmi J, Paulsen O, Freund TF, Hájos N (2004) Distinct properties of carbachol- and DHPG-induced network oscillations in hippocampal slices. Neuropharmacology 47:381-389.

Panula P, Pirvola U, Auvinen S, Airaksinen MS (1989) Histamine-immunoreactive nerve fibers in the rat brain. Neuroscience 28:585-610.

Pape HC (1996) Queer current and pacemaker: the hyperpolarization-activated cation current in neurons. Annu Rev Physiol 58:299-327.

Pape HC, Mager R (1992) Nitric oxide controls oscillatory activity in thalamocortical neurons. Neuron 9:441-448.

Pape HC, Driesang RB (1998) Ionic mechanisms of intrinsic oscillations in neurons of the basolateral amygdaloid complex. J Neurophysiol 79:217-226.

Pare D, Collins DR (2000) Neuronal correlates of fear in the lateral amygdala: multiple extracellular recordings in conscious cats. J Neurosci 20:2701-2710.

Paulsen O, Moser EI (1998) A model of hippocampal memory encoding and retrieval: GABAergic control of synaptic plasticity. Trends Neurosci 21:273-278.

Pawelzik H, Hughes DI, Thomson AM (2002) Physiological and morphological diversity of immunocytochemically defined parvalbumin- and cholecystokinin-positive interneurones in CA1 of the adult rat hippocampus. J Comp Neurol 443:346-367.

Paxinos G, ed (2004) The Rat Nervous System, 3rd Edition: Elsevier Academic Press, London

Penttonen M, Kamondi A, Acsády L, Buzsáki G (1998) Gamma frequency oscillation in the hippocampus of the rat: intracellular analysis *in vivo*. Eur J Neurosci 10:718-728.

Peters HC, Hu H, Pongs O, Storm JF, Isbrandt D (2005) Conditional transgenic suppression of M channels in mouse brain reveals functions in neuronal excitability, resonance and behavior. Nat Neurosci 8:51-60.

Petsche H, Stumpf C, Gogolak G (1962) [The significance of the rabbit's septum as a relay station between the midbrain and the hippocampus. I. The control of

hippocampus arousal activity by the septum cells]. Electroencephalogr Clin Neurophysiol 14:202-211.

Pian P, Bucchi A, Decostanzo A, Robinson RB, Siegelbaum SA (2007) Modulation of cyclic nucleotide-regulated HCN channels by PIP(2) and receptors coupled to phospholipase C. Pflugers Arch 455:125-145.

Pike FG, Goddard RS, Suckling JM, Ganter P, Kasthuri N, Paulsen O (2000) Distinct frequency preferences of different types of rat hippocampal neurones in response to oscillatory input currents. J Physiol 529 Pt 1:205-213.

Placantonakis DG, Schwarz C, Welsh JP (2000) Serotonin suppresses subthreshold and suprathreshold oscillatory activity of rat inferior olivary neurones *in vitro*. J Physiol 524 Pt 3:833-851.

Pöschel B, Draguhn A, Heinemann U (2002) Glutamate-induced gamma oscillations in the dentate gyrus of rat hippocampal slices. Brain Res 938:22-28.

Pouille F, Scanziani M (2001) Enforcement of temporal fidelity in pyramidal cells by somatic feed-forward inhibition. Science 293:1159-1163.

Price CJ, Scott R, Rusakov DA, Capogna M (2008) GABA(B) receptor modulation of feedforward inhibition through hippocampal neurogliaform cells. J Neurosci 28:6974-6982.

Price CJ, Cauli B, Kovács ER, Kulik A, Lambolez B, Shigemoto R, Capogna M (2005) Neurogliaform neurons form a novel inhibitory network in the hippocampal CA1 area. J Neurosci 25:6775-6786.

Radcliffe KA, Fisher JL, Gray R, Dani JA (1999) Nicotinic modulation of glutamate and GABA synaptic transmission of hippocampal neurons. Ann N Y Acad Sci 868:591-610.

Richardson MJ, Brunel N, Hakim V (2003) From subthreshold to firing-rate resonance. J Neurophysiol 89:2538-2554.

Robinson RB, Siegelbaum SA (2003) Hyperpolarization-activated cation currents: from molecules to physiological function. Annu Rev Physiol 65:453-480.

Ropireddy D, Scorcioni R, Lasher B, Buzsáki G, Ascoli GA (2011) Axonal morphometry of hippocampal pyramidal neurons semi-automatically reconstructed after *in vivo* labeling in different CA3 locations. Brain Struct Funct 216:1-15.

Rosenkranz JA, Johnston D (2006) Dopaminergic regulation of neuronal excitability through modulation of Ih in layer V entorhinal cortex. J Neurosci 26:3229-3244.

Rotstein HG, Pervouchine DD, Acker CD, Gillies MJ, White JA, Buhl EH, Whittington MA, Kopell N (2005) Slow and fast inhibition and an H-current interact to create a theta rhythm in a model of CA1 interneuron network. J Neurophysiol 94:1509-1518.

Salinas E, Sejnowski TJ (2000) Impact of correlated synaptic input on output firing rate and variability in simple neuronal models. J Neurosci 20:6193-6209.

Sanchez-Vives MV, McCormick DA (2000) Cellular and network mechanisms of rhythmic recurrent activity in neocortex. Nature neuroscience 3:1027-1034.

Santoro B, Chen S, Luthi A, Pavlidis P, Shumyatsky GP, Tibbs GR, Siegelbaum SA (2000) Molecular and functional heterogeneity of hyperpolarization-activated pacemaker channels in the mouse CNS. J Neurosci 20:5264-5275.

Scanziani M, Gahwiler BH, Thompson SM (1995) Presynaptic inhibition of excitatory synaptic transmission by muscarinic and metabotropic glutamate receptor activation in the hippocampus: are Ca2+ channels involved? Neuropharmacology 34:1549-1557.

Scatton B, Simon H, Le Moal M, Bischoff S (1980) Origin of dopaminergic innervation of the rat hippocampal formation. Neurosci Lett 18:125-131.

Sejnowski TJ, Paulsen O (2006) Network oscillations: emerging computational principles. J Neurosci 26:1673-1676.

Senior TJ, Huxter JR, Allen K, O'Neill J, Csicsvári J (2008) Gamma oscillatory firing reveals distinct populations of pyramidal cells in the CA1 region of the hippocampus. J Neurosci 28:2274-2286.

Shirey JK, Xiang Z, Orton D, Brady AE, Johnson KA, Williams R, Ayala JE, Rodriguez AL, Wess J, Weaver D, Niswender CM, Conn PJ (2008) An allosteric potentiator of M4 mAChR modulates hippocampal synaptic transmission. Nat Chem Biol 4:42-50.

Siapas AG, Wilson MA (1998) Coordinated interactions between hippocampal ripples and cortical spindles during slow-wave sleep. Neuron 21:1123-1128.

Sík A, Ylinen A, Penttonen M, Buzsáki G (1994) Inhibitory CA1-CA3-hilar region feedback in the hippocampus. Science 265:1722-1724.

Sík A, Penttonen M, Ylinen A, Buzsáki G (1995) Hippocampal CA1 interneurons: An *in vivo* intracellular labeling study. Neurosci 15:6651-6665.

Skaggs WE, McNaughton BL (1996) Replay of neuronal firing sequences in rat hippocampus during sleep following spatial experience. Science 271:1870-1873.

Skaggs WE, McNaughton BL, Wilson MA, Barnes CA (1996) Theta phase precession in hippocampal neuronal populations and the compression of temporal sequences. Hippocampus 6:149-172.

Sohal VS, Zhang F, Yizhar O, Deisseroth K (2009) Parvalbumin neurons and gamma rhythms enhance cortical circuit performance. Nature 459:698-702.

Soltész I, Deschenes M (1993) Low- and high-frequency membrane potential oscillations during theta activity in CA1 and CA3 pyramidal neurons of the rat hippocampus under ketamine-xylazine anesthesia. Journal of Neurophysiology 70:97-116.

Somogyi P, Freund TF, Hodgson AJ, Somogyi J, Beroukas D, Chubb IW (1985) Identfied axo-axonic cells are immunoreactive for GABA in the hippocampus and visual cortex of the cat. Brain Res 332:143-149.

Song S, Miller KD, Abbott LF (2000) Competitive Hebbian learning through spike-timing-dependent synaptic plasticity. Nat Neurosci 3:919-926.

Stewart M, Fox SE (1990) Do septal neurons pace the hippocampal theta rhythm? Trends Neurosci 13:163-168.

Storm JF (1989) An after-hyperpolarization of medium duration in rat hippocampal pyramidal cells. J Physiol 409:171-190.

Swanson LW, Cowan WM (1977) An autoradiographic study of the organization of the efferent connections of the hippocampal formation in the rat. J Comp Neurol 172:49-84.

Swanson LW, Sawchenko PE, Cowan WM (1980) Evidence that the commissural, associational and septal projections of the regio inferior of the hippocampus arise from the same neurons. Brain Res 197:207-212.

Szabadics J, Varga C, Molnár G, Oláh S, Barzó P, Tamás G (2006) Excitatory effect of GABAergic axo-axonic cells in cortical microcircuits. Science 311:233-235.

Szabó GG, Holderith N, Gulyás AI, Freund TF, Hájos N (2010) Distinct synaptic properties of perisomatic inhibitory cell types and their different modulation by

cholinergic receptor activation in the CA3 region of the mouse hippocampus. Eur J Neurosci 31:2234-2246.

Tahvildari B, Fransen E, Alonso AA, Hasselmo ME (2007) Switching between "On" and "Off" states of persistent activity in lateral entorhinal layer III neurons. Hippocampus 17:257-263.

Takács VT, Freund TF, Gulyás AI (2008) Types and synaptic connections of hippocampal inhibitory neurons reciprocally connected with the medial septum. Eur J Neurosci 28:148-164.

Tamamaki N, Nojyo Y (1995) Preservation of topography in the connections between the subiculum, field CA1, and the entorhinal cortex in rats. J Comp Neurol 353:379-390.

Tamamaki N, Abe K, Nojyo Y (1987) Columnar organization in the subiculum formed by axon branches originating from single CA1 pyramidal neurons in the rat hippocampus. Brain Res 412:156-160.

Tang Y, Mishkin M, Aigner TG (1997) Effects of muscarinic blockade in perirhinal cortex during visual recognition. Proc Natl Acad Sci U S A 94:12667-12669.

Torrence C, Compo GP (1998) A practical guide to wavelet analysis. B Am Meteorol Soc 79:61-78.

Toselli M, Lux HD (1989) Opposing effects of acetylcholine on the two classes of voltage-dependent calcium channels in hippocampal neurons. EXS 57:97-103.

Tóth K, Freund TF, Miles R (1997) Disinhibition of rat hippocampal pyramidal cells by GABAergic afferents from the septum. J Physiol 500 (Pt 2):463-474.

Tóth K, Freund TF (1992) Calbindin D28k-containing nonpyramidal cells in the rat hippocampus: their immunoreactivity for GABA and projection to the medial septum. Neuroscience 49:793-805.

Tóth K, Borhegyi Z, Freund TF (1993) Postsynaptic targets of GABAergic hippocampal neurons in the medial septum-diagonal band of broca complex. JNeurosci 13:3712-3724.

Towers SK, LeBeau FE, Gloveli T, Traub RD, Whittington MA, Buhl EH (2002) Fast network oscillations in the rat dentate gyrus *in vitro*. J Neurophysiol 87:1165-1168.

Traub RD, Bibbig A, Fisahn A, LeBeau FE, Whittington MA, Buhl EH (2000) A model of gamma-frequency network oscillations induced in the rat CA3 region by carbachol *in vitro*. Eur J Neurosci 12:4093-4106.

Tsay D, Dudman JT, Siegelbaum SA (2007) HCN1 channels constrain synaptically evoked Ca2+ spikes in distal dendrites of CA1 pyramidal neurons. Neuron 56:1076-1089.

Tukker JJ, Fuentealba P, Hartwich K, Somogyi P, Klausberger T (2007) Cell type-specific tuning of hippocampal interneuron firing during gamma oscillations *in vivo*. J Neurosci 27:8184-8189.

Umbriaco D, Garcia S, Beaulieu C, Descarries L (1995) Relational features of acetylcholine, noradrenaline, serotonin and GABA axon terminals in the stratum radiatum of adult rat hippocampus (CA1). Hippocampus 5:605-620.

Vanderwolf CH (1969) Hippocampal electrical activity and voluntary movement in the rat. Electroencephalogr Clin Neurophysiol 26:407-418.

Vanderwolf CH (2001) The hippocampus as an olfacto-motor mechanism: were the classical anatomists right after all? Behav Brain Res 127:25-47.

Vanderwolf CH, Kramis R, Robinson TE (1977) Hippocampal electrical activity during waking behaviour and sleep: analyses using centrally acting drugs. Ciba Found Symp 58:199-226.

Vertes RP, Albo Z, Viana Di Prisco G (2001) Theta-rhythmically firing neurons in the anterior thalamus: implications for mnemonic functions of Papez's circuit. Neuroscience 104:619-625.

Vizi ES, Kiss JP (1998) Neurochemistry and pharmacology of the major hippocampal transmitter systems: synaptic and nonsynaptic interactions. Hippocampus 8:566-607.

Vogt KE, Regehr WG (2001) Cholinergic modulation of excitatory synaptic transmission in the CA3 area of the hippocampus. J Neurosci 21:75-83.

Wahl-Schott C, Biel M (2009) HCN channels: structure, cellular regulation and physiological function. Cell Mol Life Sci 66:470-494.

Wainger BJ, DeGennaro M, Santoro B, Siegelbaum SA, Tibbs GR (2001) Molecular mechanism of cAMP modulation of HCN pacemaker channels. Nature 411:805-810.

Wang J, Chen S, Siegelbaum SA (2001) Regulation of hyperpolarization-activated HCN channel gating and cAMP modulation due to interactions of COOH terminus and core transmembrane regions. J Gen Physiol 118:237-250.

Wang XJ (2002) Pacemaker neurons for the theta rhythm and their synchronization in the septohippocampal reciprocal loop. J Neurophysiol 87:889-900.

Whittington MA, Traub RD, Jefferys JG (1995) Synchronized oscillations in interneuron networks driven by metabotropic glutamate receptor activation. Nature 373:612-615.

Whittington MA, Stanford IM, Colling SB, Jefferys JG, Traub RD (1997) Spatiotemporal patterns of gamma frequency oscillations tetanically induced in the rat hippocampal slice. J Physiol 502 (Pt 3):591-607.

Wierenga CJ, Wadman WJ (2003a) Functional relation between interneuron input and population activity in the rat hippocampal cornu ammonis 1 area. Neuroscience 118:1129-1139.

Wierenga CJ, Wadman WJ (2003b) Excitatory inputs to CA1 interneurons show selective synaptic dynamics. J Neurophysiol 90:811-821.

Wilson M, Bower JM (1992) Cortical oscillations and temporal interactions in a computer simulation of piriform cortex. J Neurophysiol 67:981-995.

Winson J (1974) Patterns of hippocampal theta rhythm in the freely moving rat. Electroencephalogr Clin Neurophysiol 36:291-301.

Winters BD, Bussey TJ (2005) Removal of cholinergic input to perirhinal cortex disrupts object recognition but not spatial working memory in the rat. Eur J Neurosci 21:2263-2270.

Witter MP, Wouterlood FG, Naber PA, Van Haeften T (2000) Anatomical organization of the parahippocampal-hippocampal network. Ann N Y Acad Sci 911:1-24.

Wonnacott S, Barik J, Dickinson J, Jones IW (2006) Nicotinic receptors modulate transmitter cross talk in the CNS: nicotinic modulation of transmitters. J Mol Neurosci 30:137-140.

Wouterlood FG, Saldana E, Witter MP (1990) Projection from the nucleus reuniens thalami to the hippocampal region: light and electron microscopic tracing study in the rat with the anterograde tracer Phaseolus vulgaris-leucoagglutinin. J Comp Neurol 296:179-203.

Ylinen A, Soltész I, Bragin A, Penttonen M, Sík A, Buzsáki G (1995a) Intracellular correlates of hippocampal theta rhythm in identified pyramidal cells, granule cells, and basket cells. Hippocampus 5:78-90.

Ylinen A, Bragin A, Nádasdy Z, Jando G, Szabó I, Sík A, Buzsáki G (1995b) Sharp wave-associated high-frequency oscillation (200 Hz) in the intact hippocampus: network and intracellular mechanisms. J Neurosci 15:30-46.

Young KW, Billups D, Nelson CP, Johnston N, Willets JM, Schell MJ, Challiss RA, Nahorski SR (2005) Muscarinic acetylcholine receptor activation enhances hippocampal neuron excitability and potentiates synaptically evoked Ca(2+) signals via phosphatidylinositol 4,5-bisphosphate depletion. Mol Cell Neurosci 30:48-57.

Yu H, Chang F, Cohen IS (1993) Phosphatase inhibition by calyculin A increases i(f) in canine Purkinje fibers and myocytes. Pflugers Arch 422:614-616.

Zar JH (1999) Biostatistical Analyses, 4th Edition.: Prentice Hall, Upper Saddle River, N.J.

Zolles G, Klocker N, Wenzel D, Weisser-Thomas J, Fleischmann BK, Roeper J, Fakler B (2006) Pacemaking by HCN channels requires interaction with phosphoinositides. Neuron 52:1027-1036.

13. LIST OF PUBLICATIONS

13.1. Publications related to the dissertation

Zemankovics R, Káli S, Paulsen O, Freund TF, Hájos N (2010) Differences in subthreshold resonance of hippocampal pyramidal cells and interneurons: the role of h-current and passive membrane characteristics. J Physiol 588:2109-2132.

Hájos N, Ellender TJ, Zemankovics R, Mann EO, Exley R, Cragg SJ, Freund TF, Paulsen O (2009) Maintaining network activity in submerged hippocampal slices: importance of oxygen supply. Eur J Neurosci 29:319-327.

13.2. Other publications

Varga V, Hangya B, Kránitz K, Ludányi A, Zemankovics R, Katona I, Shigemoto R, Freund TF, Borhegyi Z (2008) The presence of pacemaker HCN channels identifies theta rhythmic GABAergic neurons in the medial septum. J Physiol 586:3893-3915.

Hájos N, Holderith N, Németh B, Papp OI, Szabó GG, Zemankovics R, Freund TF, Haller J (2011) The Effects of an Echinacea Preparation on Synaptic Transmission and the Firing Properties of CA1 Pyramidal Cells in the Hippocampus. Phytother Res. doi: 10.1002/ptr.3556. (*In press*)

14. APPENDIX

14.1. Computational models used in study I

Both neuron-models used in study I were single-compartment, spherical, conductance-based models. The simpler model, which is referred as the *passive-model*, contained only the membrane capacitance and a (voltage-independent) leak conductance. The temporal evolution of the membrane potential (V_m) in this model cell can be described by the following equation:

$$C\frac{dV_m}{dt} = g_l\left(E_l - V_m\right) + I_i \tag{11}$$

where C is the total capacitance of the neuron, g_l is the leak conductance, E_l is the reversal potential of the leak current, and I_i is the external current injection.

The second model (called the I_h-model) also contained, in addition to the membrane capacitance and the leak conductance, a voltage-gated hyperpolarization-activated conductance, which was described by a Hodgkin-Huxley-type formalism with a single gating variable, and whose parameters matched the properties of I_h in different cell types as determined in our experiments. This model is defined by the following set of equations:

$$C\frac{dV_m}{dt} = g_l\left(E_l - V_m\right) + \bar{g}_h m_h\left(E_h - V_m\right) + I_i \tag{12}$$

and

$$\frac{dm_h}{dt} = \frac{m_\infty^{(h)}\left(V_m\right) - m_h}{\tau_h\left(V_m\right)} \tag{13}$$

where $\bar{g}_h$ is the maximal conductance of I_h, m_h is the gating variable for the activation of I_h, E_h is the I_h reversal potential, while $m_\infty^{(h)}(V_m)$ is the steady-state value and $\tau_h(V_m)$ is the time constant for changes in m_h as a function of V_m.

For both of the above models, the impedance profile (the amplitude and phase of the voltage response to small-amplitude sinusoidal current injection as a function of input frequency) could be determined analytically by linearizing all the defining

equations in the vicinity of a given baseline potential. The explicit formulae derived in this manner allowed us to explore how the various parameters affect impedance, and vastly simplified the task of finding the optimal set of parameters to fit experimental data. Linearization involved neglecting terms of second and higher order in the difference between the current membrane potential and the baseline potential in both the membrane voltage equation and the expressions for steady state activation of conductances, and neglecting the voltage dependence of the time constant of all voltage-gated conductances. The rationale for and further details of this procedure may be found in (Hutcheon et al., 1994)). For the passive model, this approach is exact (since the model is linear to begin with), and results in the following expression for the impedance of the membrane:

$$Z = \frac{1}{g_l + i\omega C} \tag{4}$$

where $\omega = 2\pi f$, and f is the frequency of the oscillating input. Taking the absolute value of the complex impedance reproduces the well-known expression $|Z| = \left(g_l^2 + \omega^2 C^2\right)^{-1/2}$ for the impedance magnitude.

In the I_h-model, linearization involved approximating the steady-state activation of I_h as $m_\infty^{(h)}(V_m) \approx m_\infty^{(h)}(V_0) + b(V_m - V_0)$ (where V_0 is the membrane potential in the absence of the oscillating input, b is the slope of the function $m_\infty^{(h)}(V_m)$ at V_0), and taking a voltage-independent value for τ_h. This allowed us to assume that, in response to a sinusoidal current injection, both V_m and m_h have a sinusoidal time dependence at the input frequency, and the amplitude and phase of these oscillations (relative to the input current) can be determined from Equations (12) and (13), producing the following formula for the (complex) impedance of the I_h-model:

$$Z = \frac{1}{g_l + i\omega C + \bar{g}_h m_\infty^{(h)}(V_0) + \dfrac{\bar{g}_h b(V_0 - E_h)}{1 + i\omega\tau_h}} \tag{5}$$

.